UNIVERSITÀ DEGLI STUDI DI TRENTO
DIPARTIMENTO DI FISICA

Static and dynamic properties of spin-orbit-coupled Bose-Einstein condensates

Ph.D. thesis

Supervisor:
Prof. Sandro Stringari

Candidate:
Giovanni Italo Martone

Trento, December 12th, 2014

DOTTORATO DI RICERCA IN FISICA, XXVII CICLO

Ai miei genitori

Acknowledgments

The preparation for the Ph.D. is always one of the most intense experiences in a person's life. Here I would like to spend a few words to thank all the people who helped and supported me throughout such a delicate period.

First of all, I would like to acknowledge my supervisor, prof. Sandro Stringari, for his guidance during the last three years. I confess that it is very hard for me to find the proper words to express all my gratitude. I will never forget all the support and the encouragement he has provided me, both from the scientific and the personal point of view, the strong determination with which he helped me each time a new problem appeared, his patience and, above all, his trust in me. I consider having worked with him as one of the greatest privileges I ever had in my life.

I am also grateful to prof. Lev P. Pitaevskii, with whom I had the honor to collaborate during a significant part of my doctoral studies in Trento. I learned a lot from him in every single discussion we had. His kindness, his rigorous scientific mind and his outstanding knowledge of physical problems have represented an important source of inspiration for my research work.

I would like to express my very sincere thanks to Yun Li, the postdoc in the BEC group who followed my first steps as a doctoral student. The support and the friendship of such a pleasant, generous person have helped me a lot in countless difficult situations, even after her departure from Trento. I will never forget my Chinese "little boss".

I am also indebted towards the permanent members of the experimental team of the BEC Center, Gabriele Ferrari and Giacomo Lamporesi, for patiently providing me much valuable advice on the experimental issues related to the detection of the stripe phase in spin-orbit-coupled Bose gases.

The BEC Center is much more than a research group. Since my very first impact with it, I realized that it is a very special place, with very special people. And I strongly wish to thank all of them for the nice time we spent together during the last three years. Besides those I already mentioned, it has been really an honor to be side-to-side with such brilliant scientists as Franco Dalfovo, Stefano Giorgini, Iacopo Carusotto, Chiara Menotti and Alessio Recati. And with the younger people as well: David Papoular, who has taught me a lot about the value of true friendship, and even more about how the attitude of a young scientist must be; Nicola Bartolo and Luis Peña Ardila, the best mates I could have in the 27th Ph.D. cycle dream team; Onur Umucalılar, a really trusted friend, who helped me survive in the longest and most exciting journey of my life (Singapore); and moreover, Marta Abad, Giulia De Rosi, Simone Donadello, Stefano Finazzi, Yan-Hua Hou, Marco Larcher, Pierre-Élie Larré, Natalia Matveeva, Tomoki Ozawa, Hannah Price, Riccardo Rota, Grazia Salerno, Alberto Sartori, Robin Scott, Simone Serafini, Marek Tylutki, Zeng-Qiang Yu and Peng Zou. Not to mention

the many young visitors of the BEC group who have joined our team, and shared so many nice experiences with us. I also acknowledge the support and the availability of the secretaries, Beatrice Ricci (CNR), Flavia Zanon and Rachele Zanchetta (ERC) and Micaela Paoli (Ph.D. School), and of the technician Giuseppe Froner, who helped me solve all the bureaucratic and technical problems related to my activity at the University of Trento.

Very special thanks are due to my old friend and colleague Leonardo Carcagnì, the person who introduced me for the first time into the fascinating world of ultracold gases. His advice of applying for a Ph.D. position in the BEC Center represents one of the most relevant contributions to this thesis work.

Un altro grazie molto speciale vorrei rivolgerlo, con tutto il cuore, alle ragazze dell'open space, Giovanna, Mary e Roberta. A loro assocerò per sempre uno dei ricordi più belli non solo del mio dottorato, ma di tutta la mia vita. E così, dopo aver passato tre anni a lamentarmi del nostro ufficio, adesso so che ne sentirò la mancanza...

Non posso non ringraziare il trentino doc Andrea, che mi ha dato un grandissimo sostegno nei momenti più difficili della mia lunga fase di ambientamento a Trento. E non voglio dimenticare i conterranei Daniel, Giuseppe e Matteo, la cui presenza qui è stata di grande aiuto ad alleviare la nostalgia di casa. Un grazie anche a Fabrizio e Giulio, per la loro amicizia e tutte le stimolanti discussioni che hanno animato i miei rientri a Brindisi.

Lascio per ultimo il ringraziamento più importante. Lo rivolgo alle persone che hanno sostenuto i miei sforzi da sempre, non facendomi mai mancare nulla. Che hanno patito più di me per le mie sconfitte, e gioito più di me per i miei successi. Che hanno sofferto la mia lontananza da casa, più di quanto l'abbia sofferta io stesso. Questa tesi, e tutto ciò che essa rappresenta, è dedicata a loro. Grazie mamma, grazie papà.

Contents

Introduction

A large variety of exotic phenomena in solid-state systems can take place when their constituent electrons are coupled to an external gauge field, or in the presence of strong spin-orbit coupling. For example, magnetic fields influencing the motion of the electrons are at the base of the well-known quantum Hall effect [1], whereas spin-orbit coupling, i. e. the coupling between an electron's spin and its momentum, is crucial for topological insulators [2, 3], Majorana fermions [4], spintronic devices [5], etc.

Ultracold atomic gases are good candidates to investigate these interesting quantum phenomena. Since the first realization of Bose-Einstein condensation in a dilute atomic gas [6, 7, 8], the experimental techniques aiming at creating and manipulating these systems have undergone remarkable improvements. Nowadays one is able to work with both bosonic and fermionic gases, and to realize mixtures of different species [9]. The interparticle interactions can be tailored practically at will through Feshbach resonances [10]. By using laser light it is possible to achieve a large variety of energy landscapes, including harmonic, periodic, quasiperiodic, and disordered potentials. The dimensionality of the system can also be controlled by using a tight optical confinement of the atomic cloud along one or two directions. This has paved the way to the study of the one-dimensional Tonks-Girardeau gas [11, 12] and the two-dimensional Berezinskii-Kosterlitz-Thouless transition [13].

The main difficulty in employing ultracold gases to simulate condensed-matter phenomena like those listed above stems from the fact that atoms are neutral particles, and consequently they cannot be coupled to a gauge field. In addition, they do not exhibit any coupling between their spin and their center-of-mass motion.

In the last few years there have been several proposal to realize artificial gauge fields for quantum gases, thus overcoming the problem of their neutrality [14]. In particular, approaches based on the analogy between the Coriolis and Lorentz forces have been successfully implemented to realize synthetic gauge fields in rotating neutral fluids, proving to be very efficient for the observation of quantized vortices [15, 16, 17]. An alternative scheme relies on the notion of geometric phase [18], which emerges when the motion of a particle with some internal level structure is slow enough, so that the particle follows adiabatically one of these levels. In such conditions, the particle experiences an effective vector potential. In ultracold atomic gases, several methods to implement these ideas exploit the space-dependent coupling of the atoms with a properly designed configuration of laser beams; the synthetic gauge field arises when the system follows adiabatically one of the local eigenstates of the light-atom interaction Hamiltonian (dressed states) [19, 20, 21, 22]. Other approaches are also possible, such as the periodic shaking of an optical lattice with special frequencies, which couples different Bloch bands [23].

Since 2009, several experiments have been successful in realizing ultracold atomic gases

coupled to artificial gauge fields [24, 25, 26, 27, 28]. For instance, in the experiment of Ref. [25] a space-dependent atom-light coupling was employed to simulate an effective magnetic field exerting a Lorentz-like force on neutral bosons; this procedure has been used to generate quantized vortices in Bose-Einstein condensates.

Another interesting situation occurs when the local dressed states are degenerate, giving rise to spin-orbit-coupled configurations. In particular, by using a suitable arrangement of Raman lasers, the authors of [29] managed to engineer a one-dimensional spin-orbit coupling, characterized by equal Rashba [30] and Dresselhaus [31] strengths, on a neutral atomic BEC. The same scheme has been subsequently extended to realize spin-orbit-coupled Fermi gases [32, 33].

These first experimental achievements have stimulated a growing interest in this field of research, resulting in a wide number of papers devoted to artificial gauge fields and, more specifically, to spin-orbit-coupled quantum gases, both from the theoretical and the experimental side. In this thesis we will focus on the properties of Bose-Einstein condensates with the kind of spin-orbit coupling first realized by the NIST team [29], which at present is the only one available experimentally. However, it must be pointed out that several other kinds of configurations have been considered theoretically, including pure Rashba and spin-orbit-coupled spin-1 systems. Readers who are interested in a broader overview about spin-orbit-coupled quantum gases and, more generally, about artificial gauge fields on neutral atoms, are referred to some recent reviews [14, 34, 35, 36] and references therein.

Outline. This thesis is organized as follows:

- in Chapter 1 we review some of the main theoretical tools for the investigation of the static and dynamic properties of Bose-Einstein condensed gases. In particular, we first consider the mean-field approach yielding the Gross-Pitaevskii equation, and then we describe the Bogoliubov theory and the hydrodynamic approach for the study of the collective modes. We also give a brief overview on the formalism of linear response functions, which will be widely employed throughout all this thesis;

- in Chapter 2 we illustrate the zero-temperature phase diagram of a spin-orbit-coupled Bose-Einstein condensate. This phase diagram turns out to be very rich, and includes novel quantum phases, such as a spin-polarized plane-wave phase and a stripe phase exhibiting periodic modulations in the density profile. We also study the properties of the various kinds of phase transition that can take place in the system as one varies the spin-orbit and the interaction parameters;

- in Chapter 3 we study the dynamic behavior of the gas in the two phases with a uniform ground-state density. In particular, we calculate the density response function of the system, which in turn allows to evaluate the excitation spectrum and the contributions of each excited state to the various sum rules. The excitation spectrum is found to exhibit interesting features both in the phonon (suppression of the sound velocity at the transition between the plane-wave and the

single-minimum phases) and in the large-momenta regime (appearance of a roton minimum in the plane-wave phase);

- in Chapter 4 we deal with the collective excitations of the system in the presence of harmonic trapping. A special emphasis is put on the center-of-mass oscillation, whose properties are studied with a sum-rule approach. Its frequency turns out to be deeply affected by the coupling with the spin degree of freedom, and experiences a strong reduction close to the transition between the plane-wave and the single-minimum phases. By resorting to the hydrodynamic formalism we prove that an analogous behavior is shared by all the modes involving a motion of the gas along the direction of the spin-orbit coupling;

- in Chapter 5 we investigate in detail the properties of the stripe phase. Due to the simultaneous presence of superfluidity and crystalline order, this phase shares interesting analogies with supersolids. This is also confirmed by the calculation of the excitation spectrum, which exhibits a double gapless band structure. In the last part of the chapter we present a procedure to enhance the visibility of the fringes and the stability of the striped configurations, thus making the experimental detection of the modulations in the density profile a realistic perspective.

Notations and conventions. In all this thesis, with the exception of Chapter 1, the Planck constant $\hbar$ and the atomic mass m will be set equal to 1.

Vectors will be typeset in bold math characters: $\boldsymbol{r}$, $\boldsymbol{p}$, ...

The unit vector along the x direction will be denoted by $\hat{\boldsymbol{e}}_x$.

The subscripts x and $\perp$ will be used to denote the components of a vector along the x direction and in the y-z plane, respectively.

When necessary, we will use hats on top of the operators to distinguish them from the numerical quantities: $\hat{n}(\boldsymbol{r})$, $\hat{\boldsymbol{j}}(\boldsymbol{r})$, ...

Abbreviations. The following abbreviations will sometimes be used:

BEC: Bose-Einstein condensation;

GP: Gross-Pitaevskii;

1D, 2D and 3D: one, two and three dimensions.

1. Theory of standard weakly-interacting Bose gases

The theory of Bose-Einstein condensation has been the subject of a huge literature since much time before its experimental achievement. This chapter is devoted to the presentation of some of the main theoretical tools used to study the properties of standard atomic Bose gases. The same tools will be employed in the next chapters to study the physics of spin-orbit-coupled Bose-Einstein condensates. In particular, we review the Gross-Pitaevskii mean-field approach and its conditions of applicability (Section 1.1), and we discuss several methods to investigate the elementary excitations of these systems (Section 1.2). A special emphasis is put on the illustration of the formalism of the linear response theory (Section 1.3). An exhaustive treatment of these concepts is however out of the aims of this thesis; readers interested in more extended discussions can see Refs. [37, 38, 9, 39], on which this chapter is based.

1.1. Order parameter. Gross-Pitaevskii theory

1.1.1. Diluteness criterion

Let us consider an atomic Bose gas of N particles enclosed in a volume V. The position and momentum of each particle will be denoted by $\boldsymbol{r}_j$ and $\boldsymbol{p}_j$, respectively, with $j \in \{1, 2, \ldots, N\}$ being the particle index. Each couple of atoms interacts through some interatomic potential $\mathcal{V}(\boldsymbol{r}_j - \boldsymbol{r}_k)$ depending on their relative position. For neutral atoms, any realistic interatomic potential is typically isotropic and short-range. Isotropic means that $\mathcal{V}$ only depends on the relative distance $r_{jk} = |\boldsymbol{r}_j - \boldsymbol{r}_k|$ of the atoms and not on their orientation in space, while short-range implies that there exists a distance r_0, also called the range of the potential, beyond which the interaction is negligible.

In a rarefied atomic gas the mean interparticle distance $d = \bar{n}^{-1/3}$, fixed by the average density $\bar{n} = N/V$, is much larger than the range of the potential r_0, i.e. the inequality

$$\bar{n} r_0^3 \ll 1 \tag{1.1}$$

holds. Condition (1.1) implies that the probability of finding three or more particles simultaneously within a sphere of radius r_0 is much smaller than the probability of finding only two atoms within this distance. As a consequence, one is allowed to consider only configurations involving pairs of interacting particles, i.e. to take only binary collisions into account.

Another consequence of inequality (1.1) is that the distance between two particles is always large enough to allow for the use of the asymptotic expression for the wave function of their relative motion, which is fixed by the scattering amplitude. Therefore all the properties of the system will depend solely on this latter quantity, while the specific details of the two-body potential will not matter. In addition, in the case of a Bose gas at a temperature smaller than the critical temperature for Bose-Einstein condensation, the relevant values of momenta are those satisfying the inequality

$$\frac{pr_0}{\hbar} \ll 1 \,. \tag{1.2}$$

At such small values of p the scattering amplitude becomes independent of energy as well as of the scattering angle, and can be safely replaced with its low-energy value. The latter, according to standard scattering theory, is determined by the so-called s-wave scattering length a (see, for example, [38, Sect. 9.2]). In conclusion, one expects that all the effects of the interactions on the physical properties of the gas are determined by one single parameters, which is exactly the s-wave scattering length a. In particular, the diluteness condition, which has to be fulfilled in order to apply the theory of dilute gases, can be written as $|a| \ll \bar{n}^{-1/3}$, that is,

$$\bar{n}|a|^3 \ll 1 \,. \tag{1.3}$$

The quantity $\bar{n}|a|^3$ is usually called the gas parameter. Before going on, we notice that, near a Feshbach resonance, the inequality (1.2) is still satisfied, while the diluteness condition (1.3) does not generally hold [38, Sect. 9.2].

1.1.2. Gross-Pitaevskii equation

The many-body Hamiltonian of an atomic Bose gas of N particles can be written as

$$\hat{H} = \sum_{j=1}^{N} \left(\frac{\hat{\boldsymbol{p}}_j^2}{2m} + V_{\text{ext}}(\hat{\boldsymbol{r}}_j) \right) + \frac{1}{2} \sum_{\substack{j,\,k=1 \\ j \neq k}}^{N} \mathcal{V}(\hat{\boldsymbol{r}}_j - \hat{\boldsymbol{r}}_k) \,. \tag{1.4}$$

where $\hat{\boldsymbol{p}}_j = -\mathrm{i}\hbar\nabla_j$ denotes the momentum operator of the j-th particle, m is the atomic mass, and we have introduced an external field $V_{\text{ext}}(\hat{\boldsymbol{r}})$. Let us now rewrite $\hat{H}$ in the formalism of second quantization, introducing the atomic field operator $\hat{\psi}$; one has

$$\begin{aligned} \hat{H} = & \int \mathrm{d}\boldsymbol{r}\, \hat{\psi}^\dagger(\boldsymbol{r}) \left(-\frac{\hbar^2\nabla^2}{2m} + V_{\text{ext}}(\boldsymbol{r}) \right) \hat{\psi}(\boldsymbol{r}) \\ & + \frac{1}{2} \int \mathrm{d}\boldsymbol{r}'\, \mathrm{d}\boldsymbol{r}\, \hat{\psi}^\dagger(\boldsymbol{r})\, \hat{\psi}^\dagger(\boldsymbol{r}')\, \mathcal{V}(\boldsymbol{r}' - \boldsymbol{r})\, \hat{\psi}(\boldsymbol{r})\, \hat{\psi}(\boldsymbol{r}') \,. \end{aligned} \tag{1.5}$$

The field operator can be conveniently written in the form

$$\hat{\psi}(\boldsymbol{r}) = \sum_J \varphi_J(\boldsymbol{r})\, \hat{a}_J \,, \tag{1.6}$$

where the summation runs over the possible values of a complete set of quantum numbers J, φ_J represent a convenient basis of single-particle wave functions, while $\hat{a}_J$ ($\hat{a}_J^\dagger$) are the annihilation (creation) operators of a particle in the state φ_J. The latter obey the bosonic commutation relations

$$[\hat{a}_J, \hat{a}_{J'}^\dagger] = \delta_{JJ'}, \qquad [\hat{a}_J, \hat{a}_{J'}] = [\hat{a}_J^\dagger, \hat{a}_{J'}^\dagger] = 0\,. \tag{1.7}$$

For example, for a homogeneous system of spinless bosons in a box ($V_{\rm ext} = 0$), the quantum numbers J can be taken to be the quantized values of the momentum $\boldsymbol{p}$ along the three directions in space, and the corresponding wave functions $\varphi_{\boldsymbol{p}}$ would just be plane waves.

Bose-Einstein condensation occurs when one of the single-particle states (hereafter called the condensate, $J = 0$) is occupied in a macroscopic way, i.e. its occupation number N_0 is of the order of N, while the other single-particle states have a microscopic occupation of order 1. In this case, it is useful to rewrite Eq. (1.6) separating the contribution of the condensate term from the other components:

$$\hat{\psi}(\boldsymbol{r}) = \varphi_0(\boldsymbol{r})\,\hat{a}_0 + \sum_{J\neq 0} \varphi_J(\boldsymbol{r})\,\hat{a}_J\,. \tag{1.8}$$

The advantage of the representation (1.8) is that it allows to naturally introduce the so-called Bogoliubov approximation, which consists in replacing the operators $\hat{a}_0$ and $\hat{a}_0^\dagger$ with the c-number $\sqrt{N_0}$. This is equivalent to neglecting the non-commutativity of $\hat{a}_0$ and $\hat{a}_0^\dagger$, which is reasonable when dealing with phenomena related to Bose-Einstein condensation, where the occupation number $N_0 = \langle \hat{a}_0^\dagger \hat{a}_0 \rangle \gg 1$. Indeed, the commutator between $\hat{a}_0$ and $\hat{a}_0^\dagger$ is equal to 1, while the operators themselves are of the order of $\sqrt{N_0}$. Equation (1.8) then becomes

$$\hat{\psi}(\boldsymbol{r}) = \psi_0(\boldsymbol{r}) + \delta\hat{\psi}(\boldsymbol{r})\,, \tag{1.9}$$

where we have defined $\psi_0 = \sqrt{N_0}\varphi_0$ and $\delta\hat{\psi} = \sum_{J\neq 0} \varphi_J \hat{a}_J$. In the case of a dilute Bose gas at very low temperatures the noncondensate component $\delta\hat{\psi}$ is negligible, and the system can be described by means of the classical field ψ_0 only, which hereafter will be referred to as the condensate wave function or the order parameter. The density $n(\boldsymbol{r})$ of the gas then corresponds to the condensate density,

$$n(\boldsymbol{r}) = |\psi_0(\boldsymbol{r})|^2\,, \tag{1.10}$$

and one has the normalization condition $\int \mathrm{d}\boldsymbol{r}\, |\psi_0(\boldsymbol{r})|^2 = N_0 = N$ for the condensate wave function ψ_0.

The order parameter ψ_0 characterizes the Bose-Einstein condensed phase, and vanishes above the critical temperature needed for the condensation to occur.

The Bogoliubov ansatz (1.9) for the field operator can be interpreted by saying that the expectation value $\langle\hat{\psi}\rangle$ of the field operator is different from zero. Of course, this statement is not correct if the states on the left and on the right had exactly the same

number of particles. Its exact meaning can be explained as follows: since the occupation number $N_0 \gg 1$, adding one single particle to the condensate does not affect the physical properties of the system. Therefore, a state $|N\rangle$ containing N particles is in practice physically equivalent to the states $|N+1\rangle \propto a_0^\dagger |N\rangle$ and $|N-1\rangle \propto a_0 |N\rangle$. Thus, it makes sense to write $\psi_0 = \langle\hat{\psi}\rangle$, provided that the states on the left have one less particle in the condensate than the states on the right. This allows to consider the replacement of $\hat{\psi}$ by ψ_0 as a kind of mean-field approximation, which is essentially the analogue of the classical limit of quantum electrodynamics, where the classical electromagnetic field entirely replaces the microscopic description in terms of photons.

One should also recall that the field operator $\hat{\psi}$ is defined only up to a constant phase factor. From its definition (1.8), one can see that the order parameter $\psi_0 = \sqrt{N_0}\varphi_0$ shares the same property. One can always multiply this function by the numerical factor $\mathrm{e}^{\mathrm{i}\alpha}$ leaving all the physical observables unaffected. Making an explicit choice for the value of the order parameter, and hence for its phase, corresponds to a formal breaking of gauge symmetry. The phase of the order parameter, being related to the superfluid velocity (see Eq. (1.36) below), plays a major role in characterizing the superfluid phenomena (for a more in-depth discussion of the relationship between superfluidity and Bose-Einstein condensation see, for example, [38, Sect. 6.2]).

In order to derive the equation governing the field ψ_0, which can also describe time-dependent configurations, one first has to switch to the Heisenberg picture for the time evolution of a quantum system. In this representation the quantities $\hat{\psi}$, ψ_0 and $\delta\hat{\psi}$ have an explicit time dependence. The quantum field $\hat{\psi}(\boldsymbol{r},t)$ fulfills the exact equation

$$\begin{aligned} \mathrm{i}\hbar\frac{\partial}{\partial t}\,\hat{\psi}(\boldsymbol{r},t) &= [\hat{\psi}(\boldsymbol{r},t),\hat{H}] \\ &= \left[-\frac{\hbar^2\nabla^2}{2m} + V_{\mathrm{ext}}(\boldsymbol{r}) + \int \mathrm{d}\boldsymbol{r}'\,\hat{\psi}^\dagger(\boldsymbol{r}',t)\,\mathcal{V}(\boldsymbol{r}'-\boldsymbol{r})\,\hat{\psi}(\boldsymbol{r}',t)\right]\hat{\psi}(\boldsymbol{r},t)\,. \end{aligned} \tag{1.11}$$

One could be tempted to say that, in the conditions where the noncondensate component is negligible, we can directly replace $\hat{\psi}$ by ψ_0 in the previous equation. However, for a realistic interatomic potential $\mathcal{V}$, such a replacement is not generally correct. Indeed, a realistic potential always contains a short-range term which varies rapidly at distances of the order of r_0, thus making quantum correlations important. However, in virtue of the above discussion on the diluteness criteria, we know that the actual form of the two-body potential is not important for describing the macroscopic properties of the gas, the only relevant parameter being the s-wave scattering length. As a consequence, one can replace the bare potential by an effective potential

$$\mathcal{V}_{\mathrm{eff}}(\boldsymbol{r}'-\boldsymbol{r}) = g\delta(\boldsymbol{r}'-\boldsymbol{r})\,, \tag{1.12}$$

where the coupling constant g is related to the s-wave scattering length a through [38, Sect. 4.1]

$$g = \frac{4\pi\hbar^2 a}{m}\,. \tag{1.13}$$

Hence, we can legitimately make the simultaneous replacement of $\hat{\psi}$ by ψ_0 and of $\mathcal{V}$ by $\mathcal{V}_{\text{eff}}$, and Eq. (1.11) becomes

$$\mathrm{i}\hbar\frac{\partial}{\partial t}\,\psi_0(\boldsymbol{r},t) = \left(-\frac{\hbar^2\nabla^2}{2m} + V_{\text{ext}}(\boldsymbol{r}) + g\,|\psi_0(\boldsymbol{r},t)|^2\right)\psi_0(\boldsymbol{r},t)\,. \tag{1.14}$$

Equation (1.14) corresponds to the well-known time-dependent Gross-Pitaevskii equation for the order parameter of the condensate. It was derived independently by Gross [40] and Pitaevskii [41], and is the main theoretical tool for investigating nonuniform dilute Bose gases at low temperatures. The Gross-Pitaevskii equation has the typical form of a mean-field equation, where the order parameter must be calculated in a self-consistent way.

It is worth mentioning that the GP equation (1.14) can also be obtained using a variational procedure. In fact, by imposing the stationarity condition

$$\delta\left[\int \mathrm{d}t\,\mathrm{d}\boldsymbol{r}\left(-\mathrm{i}\hbar\,\psi_0^*\frac{\partial}{\partial t}\,\psi_0\right) + \int \mathrm{d}t\,E\right] = 0 \tag{1.15}$$

to the action, one has the equation

$$\mathrm{i}\hbar\frac{\partial\psi_0}{\partial t} = \frac{\delta E}{\delta\psi_0^*}\,, \tag{1.16}$$

for the order parameter, where the energy functional E is given by

$$E\,[\psi_0] = \int \mathrm{d}\boldsymbol{r}\left[\frac{\hbar^2}{2m}\,|\nabla\psi_0|^2 + V_{\text{ext}}(\boldsymbol{r})\,|\psi_0|^2 + \frac{g}{2}\,|\psi_0|^4\right]\,. \tag{1.17}$$

The ground state of the system can be easily obtained within the formalism of the Gross-Pitaevskii mean-field theory. For this, one should recall that, for stationary states evolving in time according to the law $\mathrm{e}^{-\mathrm{i}Et/\hbar}$, the relation $\psi_0 = \langle\hat{\psi}\rangle$ yields the law

$$\psi_0(\boldsymbol{r},t) = \psi_0(\boldsymbol{r})\,\mathrm{e}^{-\mathrm{i}\mu t/\hbar} \tag{1.18}$$

for the time evolution of the order parameter, with $\mu = E(N) - E(N-1) \sim \partial E/\partial N$ being the chemical potential. From (1.14) one finds that ψ_0 obeys the so-called time-independent Gross-Pitaevskii equation

$$\left(-\frac{\hbar^2\nabla^2}{2m} + V_{\text{ext}}(\boldsymbol{r}) + g\,|\psi_0(\boldsymbol{r})|^2\right)\psi_0(\boldsymbol{r}) = \mu\,\psi_0(\boldsymbol{r})\,. \tag{1.19}$$

This equality has the form of a nonlinear Schrödinger equation, with the nonlinearity coming from the mean-field term, proportional to the particle density (1.10). In the absence of interactions ($g = 0$), this equation reduces to the usual Schrödinger equation for the single-particle Hamiltonian $-\hbar^2\nabla^2/(2m) + V_{\text{ext}}(\boldsymbol{r})$, and the condensate wave function becomes equal, up to a factor $\sqrt{N}$, to the corresponding ground-state wave function.

Before concluding the present section, it is useful to briefly discuss some relevant properties of homogeneous systems, where $V_{\rm ext} = 0$. In this case the solution of the stationary GP equation (1.19) describing the ground state is independent of $\boldsymbol{r}$ and can be chosen to be real; then one has $\psi_0(\boldsymbol{r}) = \sqrt{\bar{n}}$, where $\bar{n} = N/V$ is the average density. This wave function corresponds to a plane-wave state with momentum $\boldsymbol{p} = 0$. From (1.17) one finds the value

$$E = \frac{gN^2}{2V} \tag{1.20}$$

for the ground-state energy. A straightforward calculation yields the results

$$\mu = \left(\frac{\partial E}{\partial N}\right)_V = g\bar{n}\,, \qquad P = -\left(\frac{\partial E}{\partial V}\right)_N = \frac{g\bar{n}^2}{2} \tag{1.21}$$

for the chemical potential[1] μ and the pressure P. Another useful quantity to calculate is the thermodynamic compressibility

$$\kappa_T = \left(\frac{\partial P}{\partial \bar{n}}\right)^{-1} = \frac{1}{g\bar{n}}\,, \tag{1.22}$$

which, as expected, tends to infinity in the ideal gas limit $g \to 0$. Using the hydrodynamic relation

$$\kappa_T = \frac{1}{mc^2} \tag{1.23}$$

for the compressibility one obtains the important result

$$c = \sqrt{\frac{g\bar{n}}{m}} \tag{1.24}$$

for the sound velocity. We will see in Par. 1.2.1 that this result coincides with the value obtained considering the long-wavelength limit of the dispersion relation of the elementary excitations.

The condition of thermodynamic stability implies that the compressibility κ_T must be positive, i.e. $a > 0$. Hence, we conclude that a dilute uniform Bose-Einstein condensed gas can exist only if the value of the s-wave scattering length is positive. However one can prove that, in the presence of external fields, Bose-Einstein condensed gases can exist, in a metastable configuration, also if the scattering length is negative [38, Chap. 11].

1.2. Dynamic properties of Bose-Einstein condensates

1.2.1. Bogoliubov theory and elementary excitations

Elementary excitations play an important role in the description of the dynamic behavior of a many-body quantum system. In the case of Bose fluids, one of the most relevant

[1] The chemical potential could also be inferred by inserting $\psi_0(\boldsymbol{r}) = \sqrt{\bar{n}}$ into the stationary GP equation (1.19).

historical examples has been the study of the excitation spectrum of superfluid ^{4}He. This was the subject of several pioneering works by Landau, Bogoliubov and Feynman (for a more detailed discussion on the dynamic behavior of interacting Bose superfluids see, for example, [42]).

For weakly interacting Bose gases at very low temperatures, Bogoliubov theory represents the main tool for the theoretical investigation of the spectrum of elementary excitations. The starting point of this approach is the time-dependent GP equation (1.14) for the order parameter. We have already seen that the ground state of the system is characterized by a stationary solution of the form (1.18). In the low-temperature limit, where the elementary excitations do not interact with each other, the excited states can be found by linearizing the GP equation and calculating the corresponding eigenfrequencies ω. This can be done by looking at solutions of the form

$$\psi_0(\boldsymbol{r},t) = \mathrm{e}^{-\mathrm{i}\mu t/\hbar}\left[\psi_0(\boldsymbol{r}) + u(\boldsymbol{r})\mathrm{e}^{-\mathrm{i}\omega t} + v^*(\boldsymbol{r})\mathrm{e}^{\mathrm{i}\omega t}\right], \tag{1.25}$$

corresponding to small oscillations of the order parameter around the ground-state value. Inserting (1.25) into (1.14), keeping only the terms linear in the complex functions u and v, and collecting all the terms evolving in time like $\mathrm{e}^{-\mathrm{i}\omega t}$ and $\mathrm{e}^{\mathrm{i}\omega t}$, one finds the coupled differential equations

$$\hbar\omega u(\boldsymbol{r}) = \left[\hat{H}_0 - \mu + 2g\left|\psi_0(\boldsymbol{r})\right|^2\right] u(\boldsymbol{r}) + g\left(\psi_0(\boldsymbol{r})\right)^2 v(\boldsymbol{r}), \tag{1.26a}$$

$$-\hbar\omega v(\boldsymbol{r}) = \left[\hat{H}_0 - \mu + 2g\left|\psi_0(\boldsymbol{r})\right|^2\right] v(\boldsymbol{r}) + g\left(\psi_0^*(\boldsymbol{r})\right)^2 u(\boldsymbol{r}), \tag{1.26b}$$

where $\hat{H}_0 = -\hbar^2\nabla^2/(2m) + V_{\mathrm{ext}}(\boldsymbol{r})$. The solutions of Eqs. (1.26) provide the eigenfrequencies and the amplitudes u and v of the normal modes of the system.

The formalism we have just discussed was developed by Pitaevskii [41] to investigate the excitations of vortex lines in a uniform Bose gas. It is worth mentioning that this procedure is equivalent to the diagonalization of the Hamiltonian in Bogoliubov approximation, in which one expresses the noncondensate component $\delta\hat{\psi}$ of the field operator (1.9) in terms of quasiparticle annihilation ($\hat{b}_J$) and creation ($\hat{b}_J^\dagger$) operators through [43, 44]

$$\delta\hat{\psi}(\boldsymbol{r},t) = \sum_{J\neq 0}\left[u_J(\boldsymbol{r})\hat{b}_J(t) + v_J^*(\boldsymbol{r})\hat{b}_J^\dagger(t)\right]. \tag{1.27}$$

By imposing the Bose commutation rules to $\hat{b}_J$ and $\hat{b}_J^\dagger$, one finds that the quasiparticle amplitudes u and v must obey the normalization condition

$$\int \mathrm{d}\boldsymbol{r}\left[u_J(\boldsymbol{r})u_{J'}^*(\boldsymbol{r}) - v_J(\boldsymbol{r})v_{J'}^*(\boldsymbol{r})\right] = \delta_{JJ'}. \tag{1.28}$$

Equations (1.26) must in general be solved numerically. However, an analytic solution can be found for uniform gases ($V_{\mathrm{ext}} = 0$), where $\mu = g\bar{n}$ (see Eq. (1.21)) and $\psi_0(\boldsymbol{r}) = \sqrt{\bar{n}}$. In this case the amplitudes are plane waves, $u_{\boldsymbol{q}}(\boldsymbol{r}) = u_{\boldsymbol{q}}\mathrm{e}^{\mathrm{i}\boldsymbol{q}\cdot\boldsymbol{r}}$ and $v_{\boldsymbol{q}}(\boldsymbol{r}) = v_{\boldsymbol{q}}\mathrm{e}^{\mathrm{i}\boldsymbol{q}\cdot\boldsymbol{r}}$, and

Eqs. (1.26) reduce to

$$\hbar\omega\, u_{\boldsymbol{q}} = \left(\frac{\hbar^2 q^2}{2m} + g\bar{n}\right) u_{\boldsymbol{q}} + g\bar{n}\, v_{\boldsymbol{q}}\,, \tag{1.29a}$$

$$-\hbar\omega\, v_{\boldsymbol{q}} = \left(\frac{\hbar^2 q^2}{2m} + g\bar{n}\right) v_{\boldsymbol{q}} + g\bar{n}\, u_{\boldsymbol{q}}\,. \tag{1.29b}$$

This eigensystem yields the famous Bogoliubov form [45]

$$(\hbar\omega_B)^2 = \left(\frac{\hbar^2 q^2}{2m}\right)\left(\frac{\hbar^2 q^2}{2m} + 2g\bar{n}\right) \tag{1.30}$$

for the excitation spectrum of a uniform Bose gas. Equation (1.30) coincides with the free-particle energy $\hbar^2 q^2/2m$ at large momenta; at low momenta it instead reduces to the phonon-like dispersion $\omega_B = cq$, where the sound velocity c exactly coincides with the value (1.24) given by hydrodynamic theory. The transition between the two regimes takes place when $\hbar^2 q^2/2m \sim g\bar{n}$. By setting $\hbar^2 q^2/2m = g\bar{n}$ with $q = \xi^{-1}$ one can define the characteristic length $\xi = \hbar/\sqrt{2mg\bar{n}}$; the physical meaning of ξ will be discussed in Par. 1.2.2.

The oscillation amplitudes relative to the spectrum (1.30), which obey the normalization condition $|u_{\boldsymbol{q}}|^2 - |v_{\boldsymbol{q}}|^2 = 1$ (see Eq. (1.28)), are

$$u_{\boldsymbol{q}}, v_{\boldsymbol{q}} = \pm\left(\frac{\hbar^2 q^2/2m + g\bar{n}}{2\varepsilon_B(q)} \pm \frac{1}{2}\right)^{1/2}, \tag{1.31}$$

where $\varepsilon_B(q) = \hbar\omega_B(q)$ is given by the positive solution of (1.30).

A relevant quantity that can be evaluated within Bogoliubov theory is the depletion of the condensate due to quantum and thermal fluctuations. For homogeneous system this can be done by introducing the $\boldsymbol{q}$ component

$$\delta\hat{\psi}_{\boldsymbol{q}} = \int \mathrm{d}\boldsymbol{r}\, \mathrm{e}^{-\mathrm{i}\boldsymbol{q}\cdot\boldsymbol{r}}\delta\hat{\psi}(\boldsymbol{r}) = u_{\boldsymbol{q}}\hat{b}_{\boldsymbol{q}} + v^*_{-\boldsymbol{q}}\hat{b}^\dagger_{-\boldsymbol{q}} \tag{1.32}$$

of the noncondensate term (1.27) of the field operator, which is related to the occupation number $n_{\boldsymbol{q}}$ of particle states with momentum $\hbar\boldsymbol{q} \neq 0$ through the relation

$$n_{\boldsymbol{q}} = \langle\delta\hat{\psi}^\dagger_{\boldsymbol{q}}\delta\hat{\psi}_{\boldsymbol{q}}\rangle = |v_{-\boldsymbol{q}}|^2 + |u_{\boldsymbol{q}}|^2\,\langle\hat{b}^\dagger_{\boldsymbol{q}}\hat{b}_{\boldsymbol{q}}\rangle + |v_{-\boldsymbol{q}}|^2\,\langle\hat{b}^\dagger_{-\boldsymbol{q}}\hat{b}_{-\boldsymbol{q}}\rangle\,. \tag{1.33}$$

In deriving the previous equation, we made use of the bosonic commutation rules for the operators $\hat{b}_{\boldsymbol{q}}$ and $\hat{b}^\dagger_{\boldsymbol{q}}$, as well as of the fact that the averages $\langle\hat{b}_{-\boldsymbol{q}}\hat{b}_{\boldsymbol{q}}\rangle$ and $\langle\hat{b}^\dagger_{\boldsymbol{q}}\hat{b}^\dagger_{-\boldsymbol{q}}\rangle$ vanish identically. The average occupation number $\langle\hat{b}^\dagger_{\boldsymbol{q}}\hat{b}_{\boldsymbol{q}}\rangle$ of quasiparticles is given by a Bose distribution with zero chemical potential, and vanishes at zero temperature. The first term on the right-hand side of Eq. (1.33) accounts for the presence of quantum fluctuations, causing the presence of particles with nonzero momentum even at $T = 0$.

Starting from Eq. (1.33), the number of atoms in the condensate at a given temperature T can be calculated through the relation

$$N_0 = N - \sum_{\boldsymbol{q}\neq 0} n_{\boldsymbol{q}} = N - \frac{V}{(2\pi)^3}\int \mathrm{d}\boldsymbol{q}\left[\,|v_{\boldsymbol{q}}|^2 + \frac{|u_{\boldsymbol{q}}|^2 + |v_{-\boldsymbol{q}}|^2}{\exp\left[\varepsilon_B(q)/k_BT\right]-1}\right]. \tag{1.34}$$

The integral of Eq. (1.34) can be evaluated explicitly at $T = 0$, yielding the following result for the condensate density:

$$\bar{n}_0 \equiv \frac{N_0}{V} = \bar{n}\left[1 - \frac{8}{3\sqrt{\pi}}\left(\bar{n}a^3\right)^{1/2}\right]. \tag{1.35}$$

Hence, the fraction of atoms out of the condensate turns out to be proportional to the square root of the gas parameter $\bar{n}a^3$. This quantity is small because we have assumed that the diluteness condition (1.3) holds. Therefore, result (1.35) represent a justification *a posteriori* of the use of the Bogoliubov prescription for the Bose field operators and the perturbative treatment of the noncondensate component at zero temperature.

The measurement of the excitation spectrum of an ultracold atomic gas represents a direct test of the validity of Bogoliubov theory. In particular, in the experiments of Refs. [46, 47, 48] the authors employed two-photon Bragg spectroscopy to probe the excitations in a BEC, and they found a quite good agreement between their data and the theoretical predictions based on the Bogoliubov dispersion law (1.30) (see [49] for a review on the experimental measurement of Bogoliubov excitations in BECs).

1.2.2. Hydrodynamic formalism and Thomas-Fermi limit

Hydrodynamic theory of superfluids provides an elegant and powerful approach to the study of the low-lying collective modes of Bose-Einstein condensed gases. In order to develop the hydrodynamic formalism, one needs to represent the complex order parameter in terms of two real variables, namely its modulus and phase. We then write $\psi_0(\boldsymbol{r},t) = \sqrt{n(\boldsymbol{r},t)}\,\mathrm{e}^{\mathrm{i}\phi(\boldsymbol{r},t)}$, where n represents the superfluid density, while the phase ϕ is related to the superfluid velocity $\boldsymbol{v}_s$ through the relation [38, Sect. 6.2]

$$\boldsymbol{v}_s = \frac{\hbar}{m}\nabla\phi\,. \tag{1.36}$$

The equations governing the dynamics of n and ϕ can be obtained by rewriting the stationarity condition of the action (1.15) in terms of these two variables,

$$\delta\left[\int \mathrm{d}t\,\mathrm{d}\boldsymbol{r}\,\hbar n\frac{\partial\phi}{\partial t} + \int \mathrm{d}t\,E\right] = 0\,, \tag{1.37}$$

with the energy functional given by (see Eq. (1.17))

$$E\left[n,\phi\right] = \int \mathrm{d}\boldsymbol{r}\,\left[\frac{\hbar^2}{2m}\left|\nabla\sqrt{n}\right|^2 + \frac{\hbar^2}{2m}\,n\left|\nabla\phi\right|^2 + V_{\mathrm{ext}}(\boldsymbol{r})\,n + \frac{g}{2}n^2\right]. \tag{1.38}$$

Condition (1.37) yields the continuity equation

$$\frac{\partial n}{\partial t} + \nabla \cdot \boldsymbol{j} = 0\,, \tag{1.39}$$

where we have defined the current density

$$\boldsymbol{j} = n\frac{\hbar}{m}\nabla\phi\,, \tag{1.40}$$

and the equation for the phase

$$\hbar\frac{\partial\phi}{\partial t} + \left(\frac{\hbar^2}{2m}\left|\nabla\phi\right|^2 + V_{\rm ext} + gn - \frac{\hbar^2}{2m\sqrt{n}}\nabla^2\sqrt{n}\right) = 0\,. \tag{1.41}$$

When written in terms of the superfluid velocity $\boldsymbol{v}_s$, the second term on the left-hand side of Eq. (1.41) reads $m\boldsymbol{v}_s^2/2$, which does not explicitly depend on the Planck constant $\hbar$. The last term on the left-hand side of Eq. (1.41) is instead proportional to $\hbar^2$, and corresponds to the so-called "quantum pressure" term. Its presence is a direct consequence of the Heisenberg uncertainty principle, and reveals that the importance of quantum effects is emphasized in nonuniform gases. However, the quantum pressure can be neglected if the density of the gas changes slowly in space. To make this argument more quantitative, let us indicate by R the typical distance characterizing the density variations taking place in the system. This can be the size of the condensate if we are interested in the ground state, or the wavelength of the density oscillations if we consider time-dependent configurations. Then the quantum pressure term scales as $\nabla^2\sqrt{n}/\sqrt{n} \sim R^{-2}$, and becomes negligible if R is much larger than the characteristic length

$$\xi = \frac{\hbar}{\sqrt{2mgn}}\,, \tag{1.42}$$

also called the "healing length" of the condensate (recall that this quantity was already introduced in Par. 1.2.1 to discuss the transition between the phonon and single-particle regimes in the Bogoliubov excitation spectrum). Under such conditions, to which we will refer as the Thomas-Fermi limit, Eq. (1.41) reduces to the simplified form

$$\hbar\frac{\partial\phi}{\partial t} + \left(\frac{\hbar^2}{2m}\left|\nabla\phi\right|^2 + V_{\rm ext} + gn\right) = 0\,, \tag{1.43}$$

which could also be derived from the stationarity condition (1.37) neglecting the quantum pressure contribution (first term) in the energy functional (1.38).

Equations (1.39) and (1.43) are the two hydrodynamic equations describing a Bose-Einstein condensed gas in the presence of an external potential $V_{\rm ext}$. They play an important role in the study of the ground state as well as of the collective modes of such systems.

The ground-state configuration in the Thomas-Fermi limit takes a particularly simple form. In the hydrodynamic formalism it corresponds to a solution of Eqs. (1.39) and

(1.43) characterized by a time-independent density $n = n_0(\boldsymbol{r})$ and a phase of the form $\phi = -\mu t/\hbar$, with μ the ground-state chemical potential. From Eq. (1.43) one finds

$$g n_0(\boldsymbol{r}) + V_{\rm ext}(\boldsymbol{r}) = \mu \,. \tag{1.44}$$

Equation (1.44) expresses the condition of local equilibrium for a system whose chemical potential, in the absence of the external field, would be given by the Bogoliubov relation $\mu = g\bar{n}$. It also allows to estimate the density profile in the presence of an external potential; for example, if $V_{\rm ext}$ is of harmonic type, the predicted density profile has the characteristic shape of an inverted parabola.

The collective modes can be studied in a similar fashion. To this aim, we consider small fluctuations of the density and the phase above the ground-state configuration, i.e. we write $n = n_0 + \delta n$ and $\phi = -\mu t/\hbar + \delta\phi$, and we linearize the hydrodynamic equations (1.39) and (1.43). This yields

$$\frac{\partial}{\partial t}\delta n + \frac{\hbar}{m}\nabla\cdot(n_0\nabla\delta\phi) = 0\,, \tag{1.45a}$$

$$\hbar\frac{\partial}{\partial t}\delta\phi + g\,\delta n = 0\,. \tag{1.45b}$$

By taking the derivative of Eq. (1.45a) with respect to t and using Eq. (1.45b), one finds the useful relation

$$\frac{\partial^2}{\partial t^2}\delta n = \nabla\cdot\left[c^2(\boldsymbol{r})\nabla\delta n\right] \tag{1.46}$$

for the density fluctuations of the superfluid, where $c(\boldsymbol{r}) = \sqrt{g n_0(\boldsymbol{r})/m}$ has the meaning of a local sound velocity (see Eq. (1.24)).

As we mentioned above, the hydrodynamic theory is expected to correctly describe density oscillations whose wavelength is much larger than the healing length (1.42). In particular, in a uniform system ($V_{\rm ext} = 0$) the solutions of (1.46) are sound waves propagating with the Bogoliubov velocity (1.24). The main advantage of the hydrodynamic formulation is that it allows to simplify the study of collective oscillations also in trapped configurations, where analytic results for the frequencies of the low-lying discretized modes can be obtained [50, 51, 52].

1.3. Linear response functions

1.3.1. Dynamic structure factor and sum rules

Linear response theory is a powerful tool for investigating the dynamic behavior of an interacting many-body quantum system. It basically consists in analyzing how the system reacts when an external perturbation is applied; in the linear regime, which applies when the perturbation is weak enough, the response only depends on the properties of the system in the absence of the external probe. This in turn allows to extrapolate useful information, for example, on its collective modes. In this paragraph we will illustrate some general features of the linear response formalism, while in the next one

we will focus on density excitations, and we will show how to calculate the response in the case of a weakly-interacting Bose gas. For simplicity, we will focus only on systems at zero temperature; however, the results we are going to show can be extended also to finite temperatures, by including the proper Boltzmann factors in all the formulas [38, Chap. 7].

Let us consider a many-body system described by the Hamiltonian H, and let F and G be two linear operators of physical interest[2]. Without loss of generality one can take these operator as having vanishing ground-state expectation values. The system is assumed to be coupled to an external field through the time-dependent Hamiltonian

$$H_{\mathrm{pert}}(t) = -\lambda G \mathrm{e}^{-\mathrm{i}\omega t}\mathrm{e}^{\eta t} - \lambda^* G^\dagger \mathrm{e}^{\mathrm{i}\omega t}\mathrm{e}^{\eta t}\,. \tag{1.47}$$

In Eq. (1.47) λ represents the strength of the external field, which, following the above considerations, will be taken small enough in order to apply linear response theory. The presence of the factor $\mathrm{e}^{\eta t}$, with η positive and small, ensures that at $t = -\infty$ the system is governed by the unperturbed Hamiltonian H. The adiabatic condition implied by this factor is crucial in order to work in the linear regime.

Let us now calculate the fluctuation $\delta\langle F^\dagger\rangle$ induced by the presence of the external field. This fluctuation oscillates in time with the same frequency ω as the external perturbation (1.47), and can be written as

$$\delta\langle F^\dagger\rangle = \lambda \mathrm{e}^{-\mathrm{i}\omega t}\mathrm{e}^{\eta t}\chi_{F^\dagger,G}(\omega) + \lambda^* \mathrm{e}^{\mathrm{i}\omega t}\mathrm{e}^{\eta t}\chi_{F^\dagger,G^\dagger}(-\omega)\,. \tag{1.48}$$

The quantity $\chi_{F^\dagger,G}(\omega)$ is called the "linear response function" or the "dynamic polarizability" of the system. It satisfies the property $\chi^*_{F^\dagger,G}(\omega) = \chi_{F,G^\dagger}(-\omega)$. As we mentioned before, the response function gives information about the properties of the system in the absence of the external perturbation, and can be straightforwardly calculated using perturbation theory. If the system is in its ground state $|0\rangle$ at $t = -\infty$, then one finds the result [53, 54]

$$\chi_{F^\dagger,G}(\omega) = -\frac{1}{\hbar}\sum_n \left[\frac{\langle 0|F^\dagger|n\rangle\langle n|G|0\rangle}{\omega - \omega_{n0} + \mathrm{i}\eta} - \frac{\langle 0|G|n\rangle\langle n|F^\dagger|0\rangle}{\omega + \omega_{n0} + \mathrm{i}\eta}\right], \tag{1.49}$$

where $|n\rangle$ and $\omega_{n0} = (E_n - E_0)/\hbar$ are, respectively, the eigenstates and the excitation frequencies relative to the unperturbed Hamiltonian ($H|n\rangle = E_n|n\rangle$).

A useful quantity is the dynamic structure factor relative to the operator F:

$$S_F(\omega) = \sum_n |\langle n|F|0\rangle|^2\,\delta(\hbar\omega - \hbar\omega_{n0})\,. \tag{1.50}$$

The quantity $|\langle n|F|0\rangle|^2$ is called the strength of the operator F relative to the state $|n\rangle$. Notice that S_F vanishes at $\omega < 0$, since the excitation energies $\hbar\omega_{n0}$ are always positive.

[2] Since now on, in this thesis we will omit the "hats" above the symbols for the operators whenever possible. Hats will be kept when necessary to avoid confusion; for example, we will write the density operator as $\hat{n}(\boldsymbol{r})$ to distinguish it from its expectation value $n(\boldsymbol{r}) = \langle\hat{n}(\boldsymbol{r})\rangle$.

In the simplest case $F = G$, the response function $\chi_F \equiv \chi_{F^\dagger,F}$ can be written in terms of the corresponding dynamic structure factor S_F as

$$\chi_F(\omega) = -\int_{-\infty}^{\infty} \mathrm{d}\omega' \left[\frac{S_F(\omega')}{\omega - \omega' + \mathrm{i}\eta} - \frac{S_{F^\dagger}(\omega')}{\omega + \omega' + \mathrm{i}\eta} \right] . \tag{1.51}$$

Using the Dirac relation

$$\lim_{\eta \to 0} \frac{1}{x - a + \mathrm{i}\eta} = \mathrm{P}\frac{1}{x - a} - \mathrm{i}\pi\delta(x - a) , \tag{1.52}$$

where P is the principal part, the function χ_F can be naturally separated into its real and imaginary parts, which are given by

$$\mathrm{Re}\,\chi_F(\omega) = -\int_{-\infty}^{+\infty} \mathrm{d}\omega' \left[S_F(\omega')\mathrm{P}\frac{1}{\omega - \omega'} - S_{F^\dagger}(\omega')\mathrm{P}\frac{1}{\omega + \omega'} \right] \tag{1.53}$$

and

$$\mathrm{Im}\,\chi_F(\omega) = \pi \left(S_F(\omega) - S_{F^\dagger}(-\omega) \right) , \tag{1.54}$$

respectively. Notice that $\mathrm{Re}\,\chi_F$ is symmetric with respect to ω, while $\mathrm{Im}\,\chi_F$ is antisymmetric. Furthermore, for positive ω one finds that $\mathrm{Im}\,\chi_F$ and S_F are equal, up to a factor π. The latter property actually holds only at zero temperature, while at finite temperature the two functions can significantly differ; in particular, the dynamic structure factor exhibits a much stronger dependence on T with respect to $\mathrm{Im}\,\chi_F$, which consequently represents a more fundamental quantity from the point of view of many-body theory [38, Chap. 7].

In order to determine explicitly the response function or, equivalently, the dynamic structure factor, one generally needs to solve the Schrödinger equation and find the eigenstates and the eigenfrequencies of the system. However, one can obtain useful information on the behavior of the dynamic structure factor by resorting to the method of sum rules, which provides an algebraic way to evaluate the moments of the dynamic structure factor

$$m_p(F) = \hbar^{p+1} \int_{-\infty}^{+\infty} \mathrm{d}\omega\, \omega^p S_F(\omega) = \sum_n (E_n - E_0)^p \left| \langle n|F|0\rangle \right|^2 . \tag{1.55}$$

A major advantage of this method is that it can reduce the calculation of the dynamical properties of the many-body system to the knowledge of a few key parameters relative to the ground state. Indeed, using the completeness relation $\sum_n |n\rangle\langle n| = 1$ and the definition (1.50) for the dynamic structure factor, one easily obtains the following sum rules:

$$m_0(F) + m_0(F^\dagger) = \langle \{F^\dagger, F\} \rangle , \tag{1.56}$$

$$m_0(F) - m_0(F^\dagger) = \langle [F^\dagger, F] \rangle , \tag{1.57}$$

$$m_1(F) + m_1(F^\dagger) = \langle [F^\dagger, [H, F]] \rangle , \tag{1.58}$$

$$m_1(F) - m_1(F^\dagger) = \langle \{F^\dagger, [H, F]\} \rangle , \tag{1.59}$$

where the average is taken on the ground state, and we have considered only the lowest moments. In general, $S_F \neq S_{F^\dagger}$ so that the sum rules (1.57) and (1.59) may also differ from zero. The sum rules (1.57) and (1.58) are related to the high-frequency expansion of the dynamic response function (1.51), which is given by

$$\chi_F(\omega)_{\omega\to\infty} = -\frac{1}{\hbar\omega}\langle[F^\dagger, F]\rangle - \frac{1}{(\hbar\omega)^2}\langle[F^\dagger,[H,F]]\rangle\,. \tag{1.60}$$

Notice that the leading term in the expansion, which behaves like $1/\omega$, vanishes if F commutes with its adjoint, as in the case of the density operator (see next paragraph). Another interesting property is that the sum rules (1.56) and (1.59) containing the anticommutators do not enter the above expansion. In the opposite limit of small ω, the dynamic polarizability approaches its static limit (static polarizability) according to the law

$$\chi_F(0) \equiv \chi_F(\omega)_{\omega\to 0} = m_{-1}(F) + m_{-1}(F^\dagger)\,, \tag{1.61}$$

where m_{-1} is the inverse energy-weighted moment of the dynamic structure factor. In contrast to the moments with $p \geq 0$, the inverse energy-weighted moments cannot be reduced in terms of commutators, and they are usually evaluated through the direct calculation of the static response.

One of the advantages of the formalism of linear response function is that, in the $T = 0$ limit we are considering, where the dynamic structure factor vanishes for $\omega < 0$, it allows to derive rigorous upper bounds for the energy $\hbar\omega_{\rm min}$ of the lowest state excited by the operator F. In particular, for any value of p, the following inequalities hold:

$$\hbar\omega_{\rm min} \leq \frac{m_{p+1}(F)}{m_p(F)} \tag{1.62}$$

and

$$\hbar\omega_{\rm min} \leq \sqrt{\frac{m_{p+1}(F)}{m_{p-1}(F)}}\,. \tag{1.63}$$

Analogously, one can prove that the moments of F satisfy

$$\frac{m_{p+1}(F)}{m_p(F)} \geq \frac{m_p(F)}{m_{p-1}(F)}\,, \tag{1.64}$$

which for $p = 0$ provides an upper bound to the non-energy-weighted moment m_0:

$$m_0(F) \leq \sqrt{m_1(F)m_{-1}(F)}\,. \tag{1.65}$$

All the previous inequalities become identities only if a single excited state of the system exhausts the strength of the operator F or, in other words, if the dynamic structure factor has a delta structure of the form $S_F(\omega) \propto \delta(\hbar\omega - \hbar\bar{\omega})$. In this case $\omega_{\rm min} = \bar{\omega}$, and the quantities on the right-hand side of Eqs. (1.62) and (1.63) coincide with $\hbar\bar{\omega}$ for any value of p. Other useful inequalities involving sum rules will be presented in Sect. 5.1.

1.3.2. Density response function

In this paragraph we will apply the formalism of linear response theory to the most important problem of the density response function.

Let us consider the $\boldsymbol{q}$ component

$$\hat{\rho}_{\boldsymbol{q}} = \sum_{j=1}^{N} \mathrm{e}^{-\mathrm{i}\boldsymbol{q}\cdot\boldsymbol{r}_j} = \int \mathrm{d}\boldsymbol{r}\, \mathrm{e}^{-\mathrm{i}\boldsymbol{q}\cdot\boldsymbol{r}} \hat{n}(\boldsymbol{r}) \tag{1.66}$$

of the density operator

$$\hat{n}(\boldsymbol{r}) = \sum_{j=1}^{N} \delta(\boldsymbol{r} - \boldsymbol{r}_j)\,, \tag{1.67}$$

where $\boldsymbol{r}_j$ is the coordinate operator of the jth particle. The density response function, hereafter called $\chi(\boldsymbol{q},\omega)$, is obtained by making the choice $F = G = \delta\hat{\rho}^\dagger_{\boldsymbol{q}}$, with $\delta\hat{\rho}^\dagger_{\boldsymbol{q}} = \hat{\rho}^\dagger_{\boldsymbol{q}} - \langle\hat{\rho}^\dagger_{\boldsymbol{q}}\rangle$, in Eq. (1.49). Notice that the ground-state expectation value $\langle\hat{\rho}^\dagger_{\boldsymbol{q}}\rangle$ vanishes in uniform systems if $\boldsymbol{q} \neq 0$. One can write

$$\chi(\boldsymbol{q},\omega) = -\frac{1}{\hbar}\sum_n \left[\frac{\left|\langle 0|\delta\hat{\rho}_{\boldsymbol{q}}|n\rangle\right|^2}{\omega - \omega_{n0} + \mathrm{i}\eta} - \frac{\left|\langle 0|\delta\hat{\rho}^\dagger_{\boldsymbol{q}}|n\rangle\right|^2}{\omega + \omega_{n0} + \mathrm{i}\eta}\right]. \tag{1.68}$$

Analogously, the dynamic structure factor takes the form (see Eq. (1.50) with $F = \delta\hat{\rho}^\dagger_{\boldsymbol{q}}$)

$$S(\boldsymbol{q},\omega) = \sum_n \left|\langle 0|\delta\hat{\rho}_{\boldsymbol{q}}|n\rangle\right|^2 \delta(\hbar\omega - \hbar\omega_{n0})\,. \tag{1.69}$$

The relevance of the dynamic structure factor resides in the fact that it characterizes the scattering cross-section of inelastic reactions where the scattering probe transfers momentum $\hbar\boldsymbol{q}$ and energy $\hbar\omega$ to the system, as happens, for example, in neutron scattering from liquid helium.

Let us now discuss the behavior of the moments

$$m_p(\boldsymbol{q}) = \hbar^{p+1}\int_{-\infty}^{+\infty} \mathrm{d}\omega\, \omega^p S(\boldsymbol{q},\omega) \tag{1.70}$$

of the dynamic structure factor. In many cases these can be evaluated explicitly through the method of sum rules. The derivation of sum rules for the density operator can be greatly simplified if the unperturbed configuration is invariant with respect to either parity or time reversal, in which case the following identity holds:

$$S(\boldsymbol{q},\omega) = S(-\boldsymbol{q},\omega)\,. \tag{1.71}$$

An example of configuration which violates equality (1.71) is represented by the plane-wave phase of a spin-orbit-coupled Bose-Einstein condensate, which will be discussed later on in this thesis.

The non-energy-weighted ($p = 0$) moment can be expressed as

$$m_0(\boldsymbol{q}) = \hbar \int_{-\infty}^{+\infty} \mathrm{d}\omega \, S(\boldsymbol{q}, \omega) = N S(\boldsymbol{q}) \,, \tag{1.72}$$

where the quantity

$$S(\boldsymbol{q}) = \frac{1}{N} \left(\langle \hat{\rho}_{\boldsymbol{q}} \hat{\rho}_{-\boldsymbol{q}} \rangle - |\langle \hat{\rho}_{\boldsymbol{q}} \rangle|^2 \right) \tag{1.73}$$

is the so-called static structure factor, which is determined by the fluctuations of the density. Equation (1.73) was derived using Eq. (1.69) and the completeness relation $\sum_n |n\rangle\langle n| = 1$. At small $\boldsymbol{q}$ the static structure factor is sensitive to dynamical correlations. However, at high $\boldsymbol{q}$ only incoherent processes are important, and the sum $\hat{\rho}^\dagger_{\boldsymbol{q}} \hat{\rho}_{\boldsymbol{q}} = \sum_{j,k} \exp\left[\mathrm{i}\boldsymbol{q} \cdot (\boldsymbol{r}_j - \boldsymbol{r}_k)\right]$ is exhausted by the $j = k$ term; as a consequence, one finds the model-independent asymptotic behavior $S(\boldsymbol{q})_{\boldsymbol{q}\to\infty} = 1$. It is worth pointing out that the static structure factor is always symmetric under inversion of $\boldsymbol{q}$ into $-\boldsymbol{q}$, even in the cases where the identity (1.71) does not hold; this general feature follows from the expression (1.73) and the commutation relation involving the density operators:

$$S(\boldsymbol{q}) - S(-\boldsymbol{q}) = \frac{1}{N} \langle [\hat{\rho}_{\boldsymbol{q}}, \hat{\rho}_{-\boldsymbol{q}}] \rangle = 0 \,. \tag{1.74}$$

Another very relevant sum rule is given by the energy-weighted moment

$$m_1(\boldsymbol{q}) = \hbar^2 \int_{-\infty}^{+\infty} \mathrm{d}\omega \, \omega \, S(\boldsymbol{q}, \omega) = \frac{1}{2} \langle [\delta\hat{\rho}^\dagger_{\boldsymbol{q}}, [H, \delta\hat{\rho}_{\boldsymbol{q}}]] \rangle \,, \tag{1.75}$$

where we have used the completeness relation and the identity (1.71). To calculate the double commutator of Eq. (1.75), we first notice that, for velocity-independent potentials, only the kinetic energy contributes to the inner commutator $[H, \delta\hat{\rho}_{\boldsymbol{q}}]$, which becomes

$$[H, \delta\hat{\rho}_{\boldsymbol{q}}] = -\hbar \boldsymbol{q} \cdot \hat{\boldsymbol{j}}_{\boldsymbol{q}} \,, \tag{1.76}$$

where

$$\hat{\boldsymbol{j}}_{\boldsymbol{q}} = \frac{1}{2m} \sum_{j=1}^{N} \left(\boldsymbol{p}_j \mathrm{e}^{-\mathrm{i}\boldsymbol{q}\cdot\boldsymbol{r}_j} + \mathrm{e}^{-\mathrm{i}\boldsymbol{q}\cdot\boldsymbol{r}_j} \boldsymbol{p}_j \right) = \int \mathrm{d}\boldsymbol{r} \, \mathrm{e}^{-\mathrm{i}\boldsymbol{q}\cdot\boldsymbol{r}} \hat{\boldsymbol{j}}(\boldsymbol{r}) \tag{1.77}$$

is the $\boldsymbol{q}$ component of the current density operator

$$\hat{\boldsymbol{j}}(\boldsymbol{r}) = \frac{1}{2m} \sum_{j=1}^{N} \left[\boldsymbol{p}_j \delta(\boldsymbol{r} - \boldsymbol{r}_j) + \delta(\boldsymbol{r} - \boldsymbol{r}_j) \boldsymbol{p}_j \right] . \tag{1.78}$$

The double commutator can now be evaluated explicitly, yielding $[\delta\hat{\rho}_{\boldsymbol{q}}, [H, \delta\hat{\rho}_{-\boldsymbol{q}}]] = N\hbar^2 q^2/m$. Then, one finds the model-independent result

$$m_1(\boldsymbol{q}) = \hbar^2 \int_{-\infty}^{+\infty} \mathrm{d}\omega \, \omega \, S(\boldsymbol{q}, \omega) = N \frac{\hbar^2 q^2}{2m} \,, \tag{1.79}$$

also known as the f-sum rule [55, 56]. This is the analogue of the well-known dipole Thomas-Reich-Kuhn sum rule for atomic spectra, and represents a remarkable result in many respects. First, it holds for a wide class of many-body systems, independent of statistics and temperature. Second, as we shall see later, it can be used, together with other moments, to estimate the frequency of the collective excitations. In addition, the f-sum rule is also deeply connected to the equation of continuity. This can be seen by taking the inverse Fourier transform of Eq. (1.76) and switching to the Heisenberg representation, which yields

$$\frac{\partial}{\partial t}\hat{n}(\boldsymbol{r},t) + \nabla \cdot \hat{\boldsymbol{j}}(\boldsymbol{r},t) = 0\,. \tag{1.80}$$

By taking the average of the previous equation over an arbitrary configuration out of equilibrium, one recovers the usual conservation law of the particle number.

The double commutator appearing in Eq. (1.75) also fixes the high-ω behavior of the dynamic response function (recall that the term $1/\omega$ identically vanishes in this case):

$$\chi(\boldsymbol{q},\omega)_{\omega\to\infty} = -\frac{1}{(\hbar\omega)^2}\langle[\delta\hat{\rho}_{\boldsymbol{q}},[H,\delta\hat{\rho}_{-\boldsymbol{q}}]]\rangle = -\frac{Nq^2}{m\omega^2}\,. \tag{1.81}$$

Hence, for systems where the inversion property (1.71) holds, one finds the relation $\chi(\boldsymbol{q},\omega)_{\omega\to\infty} = -2m_1(\boldsymbol{q})/(\hbar\omega)^2$ between the density response function and the energy-weighted moment of $\delta\hat{\rho}_{\boldsymbol{q}}$. However, the validity of Eq. (1.81) is not restricted to this hypothesis.

Finally, let us consider the inverse energy-weighted moment

$$m_{-1}(\boldsymbol{q}) = \int_{-\infty}^{+\infty} \mathrm{d}\omega\, \frac{S(\boldsymbol{q},\omega)}{\omega}\,. \tag{1.82}$$

From Eq. (1.61) one finds that this moment is related to the static response of the system,

$$N\chi(\boldsymbol{q}) \equiv \chi(\boldsymbol{q},0) = 2m_{-1}(\boldsymbol{q})\,, \tag{1.83}$$

where we have again made use of Eq. (1.71). In uniform systems the low-$\boldsymbol{q}$ limit of the static response can be related to the thermodynamic compressibility κ_T. In fact, in this case the deformations induced by the external force can be exactly expressed in terms of the local changes of the pressure, and a simple calculation gives the results

$$\lim_{\boldsymbol{q}\to 0}\int_{-\infty}^{+\infty} \mathrm{d}\omega\, \frac{S(\boldsymbol{q},\omega)}{\omega} = \frac{N\kappa_T}{2} = \frac{N}{2mc^2}\,, \tag{1.84}$$

where we made use of Eq. (1.23) relating the compressibility to the sound velocity c. Equation (1.84) is known as the compressibility sum rule.

The results we have just illustrated can be used to apply the inequalities (1.62)–(1.65) with $p = 0$ to the case of the density operator. Equation (1.62) provides an upper bound

for the energy of the elementary excitations in terms of the static structure factor, which corresponds to the so-called Feynman energy [57]

$$\hbar\omega_F(\boldsymbol{q}) = \frac{m_1(\boldsymbol{q})}{m_0(\boldsymbol{q})} = \frac{\hbar^2 q^2}{2mS(\boldsymbol{q})}\,, \tag{1.85}$$

where we have used the sum rules (1.72) and (1.79). The Feynman estimate has been extensively used to discuss the excitation spectrum of superfluid helium as a function of $\boldsymbol{q}$. Inequality (1.65), in combination with the f-sum rule (1.79) and the relation (1.61), instead connects the static structure factor to the static response function:

$$S(\boldsymbol{q}) \leq \sqrt{\frac{\hbar^2 q^2}{4m}\chi(\boldsymbol{q})}\,. \tag{1.86}$$

In the small-$\boldsymbol{q}$ limit, where $\chi(\boldsymbol{q})$ approaches the compressibility $\kappa_T = 1/mc^2$, one finds the useful result that the static structure factor vanishes linearly as $\boldsymbol{q} \to 0$,

$$S(\boldsymbol{q}) \leq \frac{\hbar q}{2mc}\,. \tag{1.87}$$

Still in the same limit, using Eq. (1.63), one finds that the lowest excitation frequency vanishes like

$$\omega_{\min}(\boldsymbol{q}) \leq cq\,. \tag{1.88}$$

The above results have been derive on a very general basis. No assumption on the exact nature of the system has been made, except for the validity of the f-sum rule and the fact that the compressibility is finite. With this simple assumptions, we proved that the excitation spectrum is gapless (Eq. (1.88)) and that the density fluctuations, given by $S(\boldsymbol{q})$, are vanishingly small in the long-wavelength limit (Eq. (1.87)). In the next paragraph we will prove that, in the special case of a standard weakly-interacting Bose gas, the bounds (1.87) and (1.88) become identities, since all the moments are exhausted by a single excited state. Actually, in the dilute Bose gas this is true for all values of $\boldsymbol{q}$. It is also remarkable that in superfluid helium, a system characterized by strong correlations, the bounds (1.87) and (1.88) become identities in the small-$\boldsymbol{q}$ limit.

1.3.3. Response function of a weakly-interacting Bose gas

In this paragraph we present a method to calculate the density response function of a weakly-interacting Bose gas. This approach is based on the formalism of the Bogoliubov theory, which has already been exploited in Par. 1.2.1 to find the excitation spectrum of this system. An equivalent procedure, which relies on the formalism of quasiparticle operators, is illustrated in [38, Sect. 7.6].

Let us assume that a time-dependent perturbation of the form (1.47), with $G = \delta\hat{\rho}^\dagger_{\boldsymbol{q}}$, is added to the Hamiltonian of the system. The condensate wave function $\psi_\lambda(\boldsymbol{r}, t)$ describing this configuration can be found by solving the time-dependent Gross-Pitaevskii

equation (1.14) with an additional term accounting for the presence of the perturbation,

$$\mathrm{i}\hbar\frac{\partial}{\partial t}\,\psi_\lambda(\boldsymbol{r},t) = \left[H_0 + V_\lambda(\boldsymbol{r},t) + g\,|\psi_\lambda(\boldsymbol{r},t)|^2\right]\psi_\lambda(\boldsymbol{r},t)\,, \tag{1.89}$$

with $H_0 = -\hbar^2\nabla^2/2m + V_{\mathrm{ext}}(\boldsymbol{r})$ and $V_\lambda(\boldsymbol{r},t) = -\lambda \mathrm{e}^{\mathrm{i}(\boldsymbol{q}\cdot\boldsymbol{r}-\omega t)}\mathrm{e}^{\eta t} + \mathrm{H.c.}$ To simplify the notation, in the next steps of the calculation we will omit the small imaginary part η of the oscillation frequency; it will be restored at the end, once the full expression of the density response function will be available.

In the limit of small λ one can look for solutions of Eq. (1.89) corresponding to small-amplitude oscillations around the unperturbed ground-state configuration, namely

$$\psi_\lambda(\boldsymbol{r},t) = \mathrm{e}^{-\mathrm{i}\mu t/\hbar}\left[\psi_0(\boldsymbol{r}) + u_\lambda(\boldsymbol{r})\mathrm{e}^{-\mathrm{i}\omega t} + v_\lambda^*(\boldsymbol{r})\mathrm{e}^{\mathrm{i}\omega t}\right]\,. \tag{1.90}$$

This ansatz is formally equal to the one of Eq. (1.25), but now the small amplitudes u_λ and v_λ are proportional to the perturbation strength λ, and depend on both its wave vector $\boldsymbol{q}$ and frequency ω. In order to calculate these amplitudes, one must insert Eq. (1.90) into (1.89), keep only the linear terms in λ, u_λ and v_λ, and collect separately the terms evolving in time like $\mathrm{e}^{\mathrm{i}\omega t}$ and $\mathrm{e}^{-\mathrm{i}\omega t}$. This procedure yields the following coupled differential equations:

$$\left[\hat{H}_0 - \mu + 2g\,|\psi_0(\boldsymbol{r})|^2 - \hbar\omega\right]u_\lambda(\boldsymbol{r}) + g\,(\psi_0(\boldsymbol{r}))^2\,v_\lambda(\boldsymbol{r}) = \lambda\mathrm{e}^{\mathrm{i}\boldsymbol{q}\cdot\boldsymbol{r}}\,, \tag{1.91a}$$

$$\left[\hat{H}_0 - \mu + 2g\,|\psi_0(\boldsymbol{r})|^2 + \hbar\omega\right]v_\lambda(\boldsymbol{r}) + g\,(\psi_0^*(\boldsymbol{r}))^2\,u_\lambda(\boldsymbol{r}) = \lambda\mathrm{e}^{\mathrm{i}\boldsymbol{q}\cdot\boldsymbol{r}}\,. \tag{1.91b}$$

Once the previous equations have been solved, it is straightforward to calculate, up to linear order in λ, the fluctuation of the density

$$\delta n_\lambda(\boldsymbol{r},t) = |\psi_\lambda(\boldsymbol{r},t)|^2 - |\psi_0(\boldsymbol{r})|^2 = \left[\psi_0^*(\boldsymbol{r})\,u_\lambda(\boldsymbol{r}) + \psi_0(\boldsymbol{r})\,v_\lambda(\boldsymbol{r})\right]\mathrm{e}^{-\mathrm{i}\omega t} + \mathrm{c.c.} \tag{1.92}$$

The $\boldsymbol{q}$ component of δn_λ is then found to exhibit the typical structure, already shown in Eq. (1.48), for the fluctuation of an operator caused by an external perturbation,

$$\delta\rho_{\boldsymbol{q},\lambda}(t) = \int \mathrm{d}\boldsymbol{r}\,\mathrm{e}^{-\mathrm{i}\boldsymbol{q}\cdot\boldsymbol{r}}\,\delta n_\lambda(\boldsymbol{r},t) = \lambda\chi(\boldsymbol{q},\omega)\mathrm{e}^{-\mathrm{i}\omega t} + \lambda^*\tilde{\chi}(\boldsymbol{q},-\omega)\mathrm{e}^{\mathrm{i}\omega t}\,, \tag{1.93}$$

where the density response function, corresponding to the coefficient of the term oscillating in time like $\mathrm{e}^{-\mathrm{i}\omega t}$, is given by

$$\chi(\boldsymbol{q},\omega) = \lambda^{-1}\int \mathrm{d}\boldsymbol{r}\,\mathrm{e}^{-\mathrm{i}\boldsymbol{q}\cdot\boldsymbol{r}}\left[\psi_0^*(\boldsymbol{r})\,u_\lambda(\boldsymbol{r}) + \psi_0(\boldsymbol{r})\,v_\lambda(\boldsymbol{r})\right]\,. \tag{1.94}$$

Equation (1.94) allows to express the density response function in terms of the ground-state wave function and of the small amplitudes $u_\lambda(\boldsymbol{r})$ and $v_\lambda(\boldsymbol{r})$ entering the ansatz (1.90). The latter have to be determined by solving Eqs. (1.91), which in general can be done only numerically, similarly to the case of Eqs. (1.26). However, for homogeneous configurations ($V_{\mathrm{ext}} = 0$) an analytical solution of Eqs. (1.91) can be found of the

form $u_\lambda(\boldsymbol{r}) = u_\lambda e^{i\boldsymbol{q}\cdot\boldsymbol{r}}$ and $v_\lambda(\boldsymbol{r}) = v_\lambda e^{i\boldsymbol{q}\cdot\boldsymbol{r}}$, with u_λ and v_λ satisfying the inhomogeneous equations

$$\left(\frac{\hbar^2 q^2}{2m} + g\bar{n} - \hbar\omega\right) u_\lambda + g\bar{n}\, v_\lambda = \lambda\,, \tag{1.95a}$$

$$\left(\frac{\hbar^2 q^2}{2m} + g\bar{n} + \hbar\omega\right) v_\lambda + g\bar{n}\, u_\lambda = \lambda\,, \tag{1.95b}$$

where we have used the results $\psi_0(\boldsymbol{r}) = \sqrt{\bar{n}}$ and $\mu = g\bar{n}$ for the uniform Bose gas. Solving Eqs. (1.95) one finds that the amplitudes are given by

$$u_\lambda,\, v_\lambda = \mp \frac{1}{\hbar}\frac{\omega \pm \hbar q^2/2m}{\omega^2 - \omega_B^2(q)}\sqrt{\bar{n}}\,\lambda\,, \tag{1.96}$$

where $\omega_B(q)$ is the Bogoliubov dispersion law (1.30). After inserting these results into Eq. (1.94) and carrying out the integration over $\boldsymbol{r}$, we finally obtain the expression of the density response function for a weakly-interacting Bose gas,

$$\chi(\boldsymbol{q},\omega) = -\left[\frac{1}{\omega - \omega_B(q) + i\eta} - \frac{1}{\omega + \omega_B(q) + i\eta}\right]\frac{N\hbar^2 q^2}{2m\varepsilon_B(q)}\,, \tag{1.97}$$

where $\varepsilon_B = \hbar\omega_B$, and we have restored the small imaginary part of the frequency by replacing ω with $\omega + i\eta$ close to the poles. Comparing Eq. (1.97) with the general structure of the density response function given in Eq. (1.68), one finds that in weakly-interacting Bose gases only a single state is excited by a density perturbation, its frequency being given by the Bogoliubov expression (1.30).

The dynamic structure factor can be easily obtained by applying the Dirac relation (1.52) to the response function (1.97) and taking its imaginary part. One finds

$$S(\boldsymbol{q},\omega) = \pi^{-1}\mathrm{Im}\,\chi(\boldsymbol{q},\omega) = N\frac{\hbar^2 q^2}{2m\varepsilon_B(q)}\,\delta\left(\hbar\omega - \varepsilon_B(q)\right) \tag{1.98}$$

for $\omega \geq 0$, while $S(\boldsymbol{q},\omega) = 0$ for $\omega < 0$. Using this expression for the dynamic structure factor, one can immediately see that the f-sum rule (1.79) is satisfied, while the inverse energy-weighted moment reads

$$m_{-1}(\boldsymbol{q}) = N\frac{\hbar^2 q^2}{2m\varepsilon_B^2(q)}\,. \tag{1.99}$$

In the small-$\boldsymbol{q}$ limit one has $\varepsilon_B(q) = \hbar c q$, and therefore Eq. (1.99) approaches the constant value $N/2mc^2$, in agreement with the general result (1.84) for the compressibility sum rule.

The static structure factor is also easily evaluated and takes the nontrivial form

$$S(\boldsymbol{q}) = \frac{\hbar^2 q^2}{2m\varepsilon_B(q)}\,. \tag{1.100}$$

Notice that it vanishes like $\hbar q/2mc$ as $\boldsymbol{q} \to 0$. As already pointed out, this behavior is not peculiar to the dilute Bose gas, but holds in general for interacting superfluids (see the discussion above Eq. (1.87)).

2. Ground state of a spin-orbit-coupled Bose-Einstein condensate

A key feature of spin-orbit-coupled Bose-Einstein condensates is their rich phase diagram. The aim of this chapter is to illustrate some relevant ground-state properties of the quantum phases exhibited by these systems. We first discuss the situation at the single-particle level (Section 2.1), showing how the spin-orbit Hamiltonian is realized experimentally, and highlighting the peculiar features of the single-particle energy spectrum. Then we consider the many-body ground state (Section 2.2), whose properties are investigated within the mean-field Gross-Pitaevskii theory through a variational approach. We point out the occurrence of novel configurations, including a striped and a spin-polarized phase, and we study the properties of the various phase transitions that can take place in the system. Finally, we calculate two important quantities characterizing the system in all its quantum phases, namely the magnetic polarizability and the compressibility (Section 2.3). This chapter is based on Refs. [58, 59, 60].

2.1. Single-particle picture

The experimental setup employed in Ref. [29] to realize spin-orbit coupling consists of a ^{87}Rb Bose-Einstein condensate in the $F = 1$ hyperfine manifold, with a bias magnetic field providing a nonlinear Zeeman splitting between the three levels of the manifold. The BEC is coupled to the field of two Raman lasers having orthogonal linear polarizations, frequencies ω_L and $\omega_L + \Delta\omega_L$, and wave vector difference $\boldsymbol{k}_0 = k_0\hat{\boldsymbol{e}}_x$, with $\hat{\boldsymbol{e}}_x$ the unit vector along the x direction. The laser field induces transitions between the three states characterized by a Rabi frequency Ω fixed by the intensity of the lasers. This Raman process is illustrated schematically in Fig. 2.1. The frequency splitting ω_Z between the states $|F = 1, m_F = 0\rangle$ and $|F = 1, m_F = -1\rangle$ is chosen to be very close to the frequency difference $\Delta\omega_L$ between the two lasers, while the separation $\omega_Z - \omega_q$ between $|F = 1, m_F = 0\rangle$ and $|F = 1, m_F = +1\rangle$ contains a large additional shift from Raman resonance due to the quadratic Zeeman effect. This implies that the state $|m_F = +1\rangle$ can be neglected, and we are left with an effective spin-1/2 system, with the two spin states given by $|\uparrow\rangle = |m_F = 0\rangle$ and $|\downarrow\rangle = |m_F = -1\rangle$. The single-particle Hamiltonian of this system takes the form (we set $\hbar = m = 1$)

$$h_0 = \frac{\boldsymbol{p}^2}{2} + \frac{\Omega}{2}\sigma_x \cos(2k_0 x - \Delta\omega_L t) + \frac{\Omega}{2}\sigma_y \sin(2k_0 x - \Delta\omega_L t) - \frac{\omega_Z}{2}\sigma_z \,, \qquad (2.1)$$

where σ_k with $k = x$, y, z denotes the usual 2×2 Pauli matrices. The Hamiltonian (2.1) is not translationally invariant but exhibits a screwlike symmetry, being invariant with

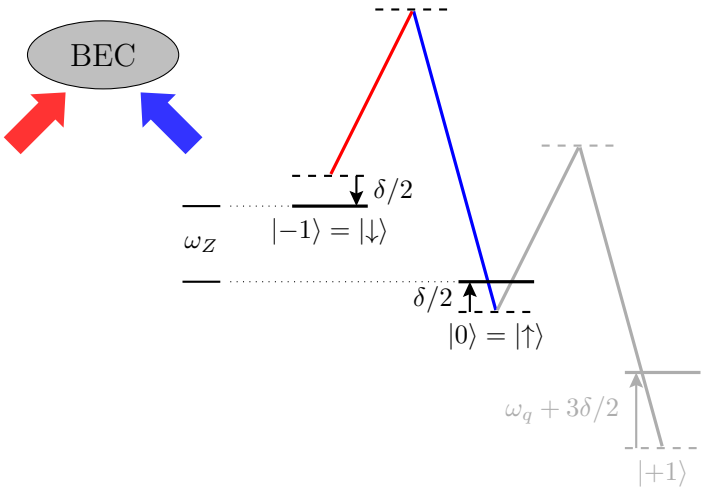

Figure 2.1. Level diagram. Two Raman lasers with orthogonal linear polarizations couple the two states $|\uparrow\rangle = |m_F = 0\rangle$ and $|\downarrow\rangle = |m_F = -1\rangle$ of the $F = 1$ hyperfine manifold of ^{87}Rb, which differ in energy by a Zeeman splitting ω_Z. The lasers have frequency difference $\Delta\omega_L = \omega_Z + \delta$, where δ is a small detuning from the Raman resonance. The state $|m_F = +1\rangle$ can be neglected since it has a much larger detuning, due to the quadratic Zeeman shift ω_q.

respect to helicoidal translations of the form $\mathrm{e}^{\mathrm{i}d(p_x - k_0\sigma_z)}$, consisting of a combination of a rigid translation by distance d and a spin rotation by angle $-dk_0$ around the z axis.

Let us now apply the unitary transformation $\mathrm{e}^{\mathrm{i}\Theta\sigma_z/2}$, corresponding to a position and time-dependent rotation in spin space by the angle $\Theta = 2k_0x - \Delta\omega_L t$, to the wave function obeying the Schrödinger equation. As a consequence of the transformation, the single-particle Hamiltonian (2.1) is transformed into the translationally invariant and time-independent form

$$h_0^{\mathrm{SO}} = \frac{1}{2}\left[(p_x - k_0\sigma_z)^2 + p_\perp^2\right] + \frac{\Omega}{2}\sigma_x + \frac{\delta}{2}\sigma_z\,. \tag{2.2}$$

The spin-orbit nature acquired by the Hamiltonian results from the noncommutation of the kinetic energy and the position-dependent rotation, while the renormalization of the effective magnetic field $\delta = \Delta\omega_L - \omega_Z$ results from the additional time dependence exhibited by the wave function in the rotating frame. The new Hamiltonian is characterized by equal contributions of Rashba [30] and Dresselhaus [31] couplings. It has the peculiar property of violating both parity and time-reversal symmetry. It is worth pointing out that the operator $\boldsymbol{p}$ entering (2.2) is the canonical momentum $-\mathrm{i}\nabla$, with the physical velocity being given by $\boldsymbol{v}_\pm = \boldsymbol{p} \mp k_0\hat{\boldsymbol{e}}_x$ for the spin-up and spin-down particles. In terms of $\boldsymbol{p}$ the eigenvalues of (2.2) are given by

$$\varepsilon_\pm(\boldsymbol{p}) = \frac{p_x^2 + p_\perp^2}{2} + E_r \pm \sqrt{\left(k_0 p_x - \frac{\delta}{2}\right)^2 + \frac{\Omega^2}{4}} \tag{2.3}$$

where $E_r = k_0^2/2$ is the recoil energy. The double-branch structure exhibited by the dispersion (2.3) reflects the spinor nature of the system.

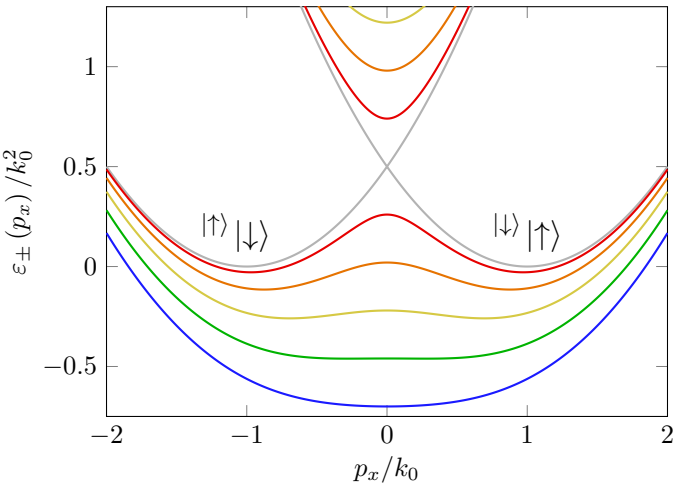

Figure 2.2. Single-particle dispersion (2.3) at $\delta = 0$. Eigenergies calculated for Raman coupling ranging from $\Omega = 0$ (grey) to $\Omega = 2.4\,k_0^2$ (blue). The two minima in the lower branch disappear at $\Omega = 2k_0^2$.

We now focus on the case $\delta = 0$ and $\Omega \geq 0$. In Fig. 2.2 we plot the dispersion (2.3) as a function of p_x, for different values of Ω. The lower branch $\varepsilon_-(\boldsymbol{p})$ exhibits, for $\Omega < 2k_0^2$, two degenerate minima at momenta $\boldsymbol{p} = \pm k_0\sqrt{1-\Omega^2/4k_0^4}\,\hat{\boldsymbol{e}}_x$, both capable to host Bose-Einstein condensation. At larger values of Ω the spectrum has instead a single minimum at $\boldsymbol{p} = 0$. The effective mass of particles moving along x, fixed by the relation $m/m^* = \mathrm{d}^2\varepsilon/\mathrm{d}p_x^2$, also shows a nontrivial Ω dependence. Near the minimum one finds [61]

$$\frac{m}{m^*} = \begin{cases} 1 - \left(\dfrac{\Omega}{2k_0^2}\right)^2 & \text{for} \quad \Omega < 2k_0^2 \\ 1 - \dfrac{2k_0^2}{\Omega} & \text{for} \quad \Omega > 2k_0^2 \end{cases} \tag{2.4}$$

Thus, the effective mass exhibits a divergent behavior at $\Omega = 2k_0^2$, where the double-well structure disappears and the spectrum has a p_x^4 dispersion near the minimum.

Before concluding the present section, it is worth mentioning that a single-particle dispersion similar to (2.3) can also be achieved by trapping the atoms in a shaken optical lattice, as has been recently realized experimentally [28]. In such systems, different Bloch bands coupled through lattice shaking bear several analogies with the spin states involved in the Raman process described above [62].

2.2. Many-body ground state

We shall now illustrate how the peculiar features of the single-particle dispersion (2.3) are at the origin of new interesting phases in the many-body ground state of the BEC. For a gas N particles enclosed in a volume V, in the presence of two-body interactions,

the many-body Hamiltonian takes the form

$$H = \sum_j h_0^{\mathrm{SO}}(j) + \frac{1}{2}\sum_{\sigma,\sigma'}\int \mathrm{d}\boldsymbol{r}\, g_{\sigma\sigma'}\,\hat{n}_\sigma(\boldsymbol{r})\hat{n}_{\sigma'}(\boldsymbol{r}), \tag{2.5}$$

where h_0^{SO} is given by (2.2), $j = 1,\ldots,N$ is the particle index, and σ, σ' are the spin indices ($\uparrow,\downarrow = \pm$) characterizing the two spin states. The spin-up and spin-down density operators entering (2.5) are defined by $\hat{n}_\pm(\boldsymbol{r}) = \sum_j P_{\pm,j}\,\delta(\boldsymbol{r}-\boldsymbol{r}_j)$, where $P_\pm = (1 \pm \sigma_z)/2$ denotes the two spin projection operators. The relevant coupling constants $g_{\sigma\sigma'} = 4\pi a_{\sigma\sigma'}$ in the different spin channels are fixed by the corresponding s-wave scattering lengths $a_{\sigma\sigma'}$. Notice that the two-body interaction terms are not affected by the spin rotation discussed in Sect. 2.1.

2.2.1. Mean-field phase diagram: a variational approach

To investigate the ground state of the system we resort to the Gross-Pitaevskii mean-field approach, which has been discussed in Sect. 1.1. For this, we introduce the two-component wave function $\Psi = (\psi_\uparrow\ \psi_\downarrow)^T$ describing our spin-1/2 condensate, and we write the energy functional associated to Hamiltonian (2.5) as

$$E[\Psi] = \int \mathrm{d}\boldsymbol{r}\left[\Psi^\dagger h_0^{\mathrm{SO}}\Psi + \frac{1}{2}\sum_{\sigma,\sigma'} g_{\sigma\sigma'}\left(\Psi^\dagger P_\sigma\Psi\right)\left(\Psi^\dagger P_{\sigma'}\Psi\right)\right]. \tag{2.6}$$

When written in terms of $\psi_{\uparrow,\downarrow}$, Eq. (2.6) reads

$$\begin{aligned} E[\psi_\uparrow,\psi_\downarrow] = &\int \mathrm{d}\boldsymbol{r}\left[\psi_\uparrow^*(\boldsymbol{r})\frac{(p_x-k_0)^2+p_\perp^2}{2}\,\psi_\uparrow(\boldsymbol{r}) + \psi_\downarrow^*(\boldsymbol{r})\frac{(p_x+k_0)^2+p_\perp^2}{2}\,\psi_\downarrow(\boldsymbol{r})\right] \\ &+ \int \mathrm{d}\boldsymbol{r}\left\{\frac{\Omega}{2}\left[\psi_\uparrow^*(\boldsymbol{r})\psi_\downarrow(\boldsymbol{r}) + \psi_\downarrow^*(\boldsymbol{r})\psi_\uparrow(\boldsymbol{r})\right] + \frac{\delta}{2}\left[|\psi_\uparrow(\boldsymbol{r})|^2 - |\psi_\downarrow(\boldsymbol{r})|^2\right]\right\} \\ &+ \int \mathrm{d}\boldsymbol{r}\left[\frac{g_{\uparrow\uparrow}}{2}|\psi_\uparrow(\boldsymbol{r})|^4 + \frac{g_{\downarrow\downarrow}}{2}|\psi_\downarrow(\boldsymbol{r})|^4 + g_{\uparrow\downarrow}|\psi_\uparrow(\boldsymbol{r})|^2|\psi_\downarrow(\boldsymbol{r})|^2\right]. \end{aligned} \tag{2.7}$$

The use of the mean-field description for a spin-orbit-coupled Bose gas can be justified *a posteriori* by estimating the quantum depletion of the system and proving that it remains small for reasonable values of the spin-orbit coupling parameters; this calculation is postponed to Sect. 3.1.

Since now on, in this thesis we will assume $\delta = 0$ and equal intraspecies interactions $g_{\uparrow\uparrow} = g_{\downarrow\downarrow} \equiv g$, unless otherwise specified; the effects of the presence of a non-vanishing magnetic detuning and of spin-asymmetric interactions on the ground state will be briefly discussed in Par. 2.2.2.

The Gross-Pitaevskii equation for the spinor order parameter can be deduced in the same way as in Sect. 1.1 and reads

$$\mathrm{i}\frac{\partial\Psi}{\partial t} = \left[h_0^{\mathrm{SO}} + +\frac{1}{2}\left(g+g_{\uparrow\downarrow}\right)\left(\Psi^\dagger\Psi\right) + \frac{1}{2}\left(g-g_{\uparrow\downarrow}\right)\left(\Psi^\dagger\sigma_z\Psi\right)\sigma_z\right]\Psi\,, \tag{2.8}$$

where the right-hand side corresponds to the functional derivative $\delta E[\Psi]/\delta\Psi^\dagger$ of the energy (2.6).

The ground-state wave function in uniform matter can in principle be determined by looking for a stationary solution of Eq. (2.8) of the form $\Psi(\boldsymbol{r},t) = \mathrm{e}^{-\mathrm{i}\mu t}\Psi(\boldsymbol{r})$. However, here we will use a different approach, consisting in a variational procedure based on the following ansatz [58]:

$$\Psi(\boldsymbol{r}) = \sqrt{\bar{n}}\left[C_+\begin{pmatrix}\cos\theta\\ -\sin\theta\end{pmatrix}\mathrm{e}^{\mathrm{i}k_1 x} + C_-\begin{pmatrix}\sin\theta\\ -\cos\theta\end{pmatrix}\mathrm{e}^{-\mathrm{i}k_1 x}\right], \tag{2.9}$$

where $\bar{n} = N/V$ is the average density, and k_1 represents the canonical momentum where Bose-Einstein condensation takes place. For a given value of $\bar{n}$, k_0, Ω and of the coupling constants g and $g_{\uparrow\downarrow}$, the variational parameters are C_+, C_-, k_1 and θ. Their values are determined by minimizing the energy (2.7) with the normalization constraint $\int \mathrm{d}\boldsymbol{r}\,\Psi^\dagger\Psi = N$, i. e. $|C_+|^2+|C_-|^2 = 1$. Minimization with respect to θ yields the general relation

$$\theta = \frac{1}{2}\arccos\frac{k_1}{k_0} \quad (0 \le \theta \le \pi/4) \tag{2.10}$$

fixed by the single-particle Hamiltonian (2.2). Once the other variational parameters are determined, it is possible to calculate key physical quantities like, for example, the momentum distribution accounted for by the parameter k_1, the total density

$$n(\boldsymbol{r}) = \Psi^\dagger\Psi = \bar{n}\left[1 + 2|C_+C_-|\frac{\sqrt{k_0^2-k_1^2}}{k_0}\cos\left(2k_1x+\phi\right)\right], \tag{2.11}$$

the longitudinal ($s_z(\boldsymbol{r})$) and transverse ($s_x(\boldsymbol{r})$, $s_y(\boldsymbol{r})$) spin densities

$$s_z(\boldsymbol{r}) = \Psi^\dagger\sigma_z\Psi = \bar{n}\left(|C_+|^2 - |C_-|^2\right)\frac{k_1}{k_0}, \tag{2.12}$$

$$s_x(\boldsymbol{r}) = \Psi^\dagger\sigma_x\Psi = -\bar{n}\left[\frac{\sqrt{k_0^2-k_1^2}}{k_0} + 2|C_+C_-|\cos\left(2k_1x+\phi\right)\right], \tag{2.13}$$

$$s_y(\boldsymbol{r}) = \Psi^\dagger\sigma_y\Psi = \bar{n}\,|C_+C_-|\frac{2k_1}{k_0}\sin\left(2k_1x+\phi\right), \tag{2.14}$$

with ϕ the relative phase between C_+ and C_-, and the corresponding spin polarizations $\langle\sigma_k\rangle = \int \mathrm{d}\boldsymbol{r}\, s_k(\boldsymbol{r})/N$ with $k = x,\, y,\, z$. Before going on, we notice that results (2.13) and (2.14) hold in the spin-rotated frame where the Hamiltonian takes the form (2.5). Since the operators σ_x and σ_y do not commute with σ_z, the transverse spin density along x calculated in the original laboratory frame exhibits an additional oscillatory behavior $s_x(\boldsymbol{r})\cos\left(2k_0x - \Delta\omega_L t\right) - s_y(\boldsymbol{r})\sin\left(2k_0x - \Delta\omega_L t\right)$, with $s_x(\boldsymbol{r})$ and $s_y(\boldsymbol{r})$ given by (2.13) and (2.14), characterizing the laser potential of Eq. (2.1) (an analogous result holds for the transverse spin density along y).

The ansatz (2.9) exactly describes the ground state of the single-particle Hamiltonian h_0^{SO} (ideal Bose gas), reproducing all the features presented in Sect. 2.1, including the

values of the canonical momentum k_1. In this case the energy is independent of $C_\pm$, reflecting the degeneracy of the ground state.

The same ansatz is well suited also for discussing the role of interactions, which crucially affect the explicit values of C_+, C_- and k_1. By inserting (2.9) into (2.7), one finds that the energy per particle $\varepsilon = E/N$ takes the form

$$\varepsilon = \frac{k_0^2}{2} - \frac{\Omega}{2k_0}\sqrt{k_0^2 - k_1^2} - F(\beta)\frac{k_1^2}{2k_0^2} + G_1\,(1+2\beta)\ , \tag{2.15}$$

where we have defined the dimensionless parameter $\beta = |C_+|^2|C_-|^2 \in [0,\, 1/4]$ and the function

$$F(\beta) = \left(k_0^2 - 2G_2\right) + 4\,(G_1 + 2G_2)\,\beta\,, \tag{2.16}$$

with the interaction parameters $G_1 = \bar{n}(g+g_{\uparrow\downarrow})/4$ and $G_2 = \bar{n}(g-g_{\uparrow\downarrow})/4$ (here we assume $G_1 > 0$ to ensure the stability of the system in the absence of external potentials). By minimizing (2.15) with respect to β and k_1 we obtain the mean-field ground state of the system.

Let us first consider minimization with respect to k_1. If $\Omega > 2F(\beta)$ the energy (2.28) is an increasing function of k_1, and the minimum takes place at $k_1 = 0$. If instead $\Omega < 2F(\beta)$ one finds that ε is minimized by the choice

$$k_1(\beta) = k_0\sqrt{1 - \frac{\Omega^2}{4\,[F(\beta)]^2}}\,, \tag{2.17}$$

which generalizes the ideal gas result discussed in Sect. 2.1, where one has $F = k_0^2$. Equations (2.16) and (2.17) explicitly show that the momentum distribution is modified by the interaction. Plugging Eq. (2.17) into (2.15) we find the following result for the energy per particle:

$$\varepsilon = -\frac{\Omega^2}{8F(\beta)} + G_1 + G_2\,(1-4\beta)\ . \tag{2.18}$$

The ground state of the system can be found by looking for the minimum of (2.18) with respect to β. One can easily prove that the second-order derivative of (2.18) with respect to β is negative. This means that the minimum is achieved at one of the limiting values of β, i.e. 0 or 1/4. The ground state is then compatible with three distinct quantum phases, which will be called "stripe phase", "plane-wave phase" and "single-minimum phase" (sometimes in this thesis we will refer to them simply as "phase I", "phase II" and "phase III", respectively). The corresponding phase diagram is shown in Fig. 2.3.

(I) Stripe phase. For small values of the Raman coupling Ω the ground state is a linear combination of the two plane-wave states $\mathrm{e}^{\pm \mathrm{i}k_1 x}$ with equal weights ($|C_+| = |C_-| = 1/\sqrt{2}$), yielding a vanishing longitudinal spin polarization (see Eq. (2.12)). The most striking feature of this phase is the appearance of density modulations in the form of stripes according to the law

$$n(\boldsymbol{r}) = \bar{n}\left[1 + \frac{\Omega}{2\,(k_0^2 + G_1)}\cos\left(2k_1 x + \phi\right)\right]\ . \tag{2.19}$$

The periodicity of the fringes π/k_1 is determined by the wave vector

$$k_1 = k_0\sqrt{1-\frac{\Omega^2}{4\left(k_0^2+G_1\right)^2}} \tag{2.20}$$

and differs from the one of the laser potential, equal to π/k_0 (see Eq. (2.1)). These modulations have a deeply different nature with respect to those exhibited by the density profile in the presence of usual optical lattices. Indeed, they appear as the result of a spontaneous breaking mechanism of translational invariance, with the actual position of the fringes being given by the value of the phase ϕ. Because of the coexistence of BEC and crystalline order, the stripe phase shares important analogies with supersolids [63]. It also shares similarities with the spatial structure of smectic liquid crystals. The contrast in $n(\boldsymbol{r})$ is given by

$$\frac{n_{\max}-n_{\min}}{n_{\max}+n_{\min}} = \frac{\Omega}{2(k_0^2+G_1)} \tag{2.21}$$

and vanishes as $\Omega \to 0$ as a consequence of the orthogonality of the two spin states entering Eq. (2.9) (in this limit $\theta \to 0$ and $k_1 \to k_0$). One must notice that the stripe phase is energetically favorable only provided that $G_2 > 0$, i.e. $g > g_{\uparrow\downarrow}$, a condition which ensures miscibility of the two spin components in the absence of spin-orbit coupling. In the opposite case $G_2 < 0$ the first-order derivative $\partial\varepsilon/\partial\beta$ is always positive and only the plane-wave and the single-minimum phases are available. Finally, it is worth mentioning that the ansatz, Eq. (2.9), for the stripe phase provides only a first approximation, which ignores higher-order harmonics caused by the nonlinear interaction terms in the Hamiltonian. The properties of the stripe phase will be the subject of Chap. 5 of this thesis.

(II) Plane-wave phase. For larger values of the Raman coupling, the system enters a new phase, the so-called plane-wave phase (also called the spin-polarized or demixed phase), where Bose-Einstein condensation takes place in a single plane-wave state with momentum $\boldsymbol{p} = k_1\hat{\boldsymbol{e}}_x$ ($C_- = 0$), lying on the x direction (in the following we choose $k_1 > 0$). In this phase, the density is uniform and the spin polarization is given by

$$\langle\sigma_z\rangle = \frac{k_1}{k_0} \tag{2.22}$$

with

$$k_1 = k_0\sqrt{1-\frac{\Omega^2}{4\left(k_0^2-2G_2\right)^2}}\,. \tag{2.23}$$

An energetically equivalent configuration is obtained by considering the BEC in the single-particle state with $\boldsymbol{p} = -k_1\hat{\boldsymbol{e}}_x$ ($C_+ = 0$). The choice between the two configurations is determined by a mechanism of spontaneous symmetry breaking, typical of ferromagnetic configurations.

(III) Single-minimum phase. At even larger values of Ω, the system enters the single-minimum phase (also called zero momentum phase), where the condensate has

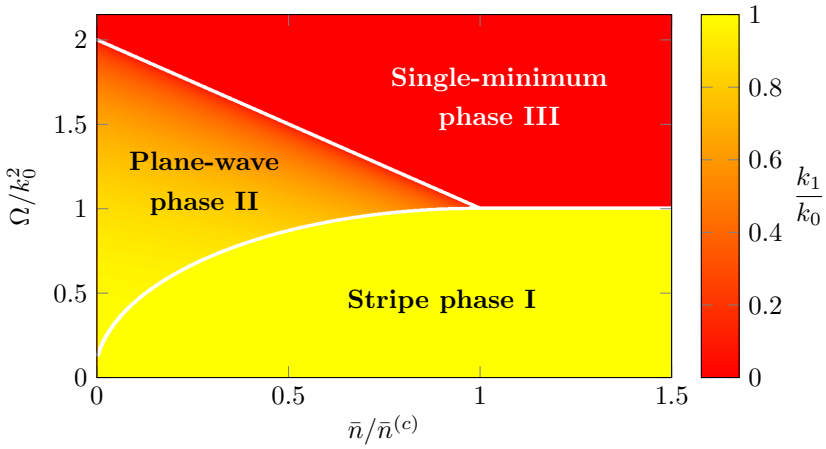

Figure 2.3. Phase diagram of a spin-orbit-coupled BEC. The color represents the value of k_1/k_0. The white solid lines identify the phase transitions (I-II), (II-III) and (I-III). The diagram corresponds to a configuration with $\gamma = (g - g_{\uparrow\downarrow})/(g + g_{\uparrow\downarrow}) = 0.0012$ consistent with the value of [29].

zero momentum ($k_1 = 0$), the density is uniform, and the average spin polarization $\langle\sigma_z\rangle$ identically vanishes, while $\langle\sigma_x\rangle = -1$. Contrary to what one would naively expect, also the single-minimum phase exhibits nontrivial properties, as we will see in Chapts. 3 and 4.

The chemical potential as a function of the average density in the three phases can be calculated from the energy per particle (2.15) through the relation $\mu(\bar{n}) = \partial\left(\bar{n}\varepsilon\right)/\partial\bar{n}$, and takes the form

$$\mu^{(\mathrm{I})}(\bar{n}_{\mathrm{I}}) = 2\bar{g}\bar{n}_{\mathrm{I}} - \frac{k_0^2\Omega^2}{8\left(k_0^2 + \bar{g}\bar{n}_{\mathrm{I}}\right)^2}, \tag{2.24a}$$

$$\mu^{(\mathrm{II})}(\bar{n}_{\mathrm{II}}) = 2\left(1+\gamma\right)\bar{g}\bar{n}_{\mathrm{II}} - \frac{k_0^2\Omega^2}{8\left(k_0^2 - 2\gamma\bar{g}\bar{n}_{\mathrm{II}}\right)^2}, \tag{2.24b}$$

$$\mu^{(\mathrm{III})}(\bar{n}_{\mathrm{III}}) = 2\bar{g}\bar{n}_{\mathrm{III}} + \frac{k_0^2 - \Omega}{2}. \tag{2.24c}$$

where we have introduced $\bar{g} = \left(g + g_{\uparrow\downarrow}\right)/4$ and $\gamma = G_2/G_1 = \left(g - g_{\uparrow\downarrow}\right)/\left(g + g_{\uparrow\downarrow}\right)$. Analogously, the pressure $P(\bar{n}) = \bar{n}^2\partial\varepsilon/\partial\bar{n}$ in the three phases is given by

$$P^{(\mathrm{I})}(\bar{n}_{\mathrm{I}}) = \bar{g}\bar{n}_{\mathrm{I}}^2\left[1 + \frac{\Omega^2}{8\left(k_0^2 + \bar{g}\bar{n}_{\mathrm{I}}\right)^2}\right], \tag{2.25a}$$

$$P^{(\mathrm{II})}(\bar{n}_{\mathrm{II}}) = \bar{g}\bar{n}_{\mathrm{II}}^2\left[1 + \gamma - \frac{\gamma\Omega^2}{4\left(k_0^2 - 2\gamma\bar{g}\bar{n}_{\mathrm{II}}\right)^2}\right], \tag{2.25b}$$

$$P^{(\mathrm{III})}(\bar{n}_{\mathrm{III}}) = \bar{g}\bar{n}_{\mathrm{III}}^2. \tag{2.25c}$$

The critical values of the Rabi frequency Ω characterizing the phase transitions can be identified by imposing that the chemical potential (2.24) and the pressure (2.25) be equal

in the two phases at equilibrium. The transition between the stripe and the plane-wave phases has a first-order nature and is characterized by different values of the densities of the two phases. The density differences are, however, extremely small and are not visible in Fig. 2.3. However, in the low density (or weak coupling) limit, i.e. $g_{\sigma\sigma'}\bar{n} \ll k_0^2$, the critical value of the Raman coupling $\Omega^{(\mathrm{I-II})}$ characterizing the transition between phases I and II becomes density-independent and is given by the expression [64, 58]

$$\Omega^{(\mathrm{I-II})} = 2k_0^2\sqrt{\frac{2\gamma}{1+2\gamma}}\,. \tag{2.26}$$

The (I-II) phase transition is accompanied by a jump in both the parameters k_1 and $|\langle\sigma_z\rangle|$.

The transition between the plane-wave and the single-minimum phases has instead a second-order nature and is characterized by a jump in the compressibility $(\partial P/\partial\bar{n})^{-1}$ if $G_2 \neq 0$ and by a divergent behavior of the magnetic polarizability (see Sect. 2.3). It takes place at a value of the Raman coupling higher than $\Omega^{(\mathrm{I-II})}$, namely [58]

$$\Omega^{(\mathrm{II-III})} = 2\left(k_0^2 - 2G_2\right), \tag{2.27}$$

provided that the condition $\bar{n} < \bar{n}^{(c)}$ is satisfied, where $\bar{n}^{(c)}$ is a critical density whose meaning will be explained in a while. For densities higher than $\bar{n}^{(c)}$ one has instead a first-order transition directly between phases I and III, characterized by a jump in the momentum k_1.

If we plotted the phase diagram in the P-Ω plane, we would find that the three phases connect each other at a tricritical point identified by a well-defined value of the pressure P and of the Raman coupling Ω. The tricriticality cannot, in principle, show up in the $\bar{n}$-Ω plane of Fig. 2.3, due to the discontinuities in the density at the first-order phase transitions. However, the differences in the densities of the two phases at the (I-II) and the (I-III) phase transitions are always found to be very small for reasonable values of the spin-orbit and the interaction parameters. Neglecting such differences, one finds that also in the $\bar{n}$-Ω all the transition lines intersect at a single point. The corresponding value of the density $\bar{n}^{(c)}$ can be calculated by imposing the energies per particle ε in the three phases to be all equal. This procedure yields the result $\bar{n}^{(c)} = k_0^2/(2\gamma g)$.

2.2.2. Effects of non-zero detuning and spin-asymmetric interactions

The results discussed in the previous paragraph can be easily generalized to account for the presence of a non-vanishing magnetic detuning δ and of spin-asymmetric interactions $g_{\uparrow\uparrow} \neq g_{\downarrow\downarrow}$. In general one can introduce three interaction parameters: $G_1 = \bar{n}(g_{\uparrow\uparrow} + g_{\downarrow\downarrow} + 2g_{\uparrow\downarrow})/8$, $G_2 = \bar{n}(g_{\uparrow\uparrow} + g_{\downarrow\downarrow} - 2g_{\uparrow\downarrow})/8$ and $G_3 = \bar{n}(g_{\uparrow\uparrow} - g_{\downarrow\downarrow})/4$. In the case of the states $|\uparrow\rangle = |F=1, m_F=0\rangle$ and $|\downarrow\rangle = |F=1, m_F=-1\rangle$ of ^{87}Rb employed in [29] the values of the scattering lengths are $a_{\uparrow\uparrow} = 101.41\,a_B$ and $a_{\downarrow\downarrow} = a_{\uparrow\downarrow} = 100.94\,a_B$, where a_B is the Bohr radius. This corresponds to $0 < G_2 = G_3/2 \ll G_1$. However, since the differences among the scattering lengths are very small, by properly choosing the detuning δ, this

effect can be well compensated. For example, using first order perturbation theory, one finds that the correction to the energy per particle (2.15) is given, in the low density (weak coupling) limit, by [58]

$$\varepsilon^{(1)} = \left(\frac{\delta}{2} + G_3\right) \frac{k_1}{k_0} (|C_+|^2 - |C_-|^2) \,. \tag{2.28}$$

By choosing $\delta = -2G_3$ the correction (2.28) vanishes, thus ensuring that the properties of the ground state of the system and the transition frequencies are not affected by the inclusion of the new terms in the Hamiltonian.

In the most general case of arbitrarily large δ and G_3, the ground state wave function can be still worked out by resorting to an ansatz similar to (2.9), namely [59, 61, 60]

$$\Psi(\boldsymbol{r}) = \sqrt{\bar{n}} \left[C_+ \begin{pmatrix} \cos\theta_+ \\ -\sin\theta_+ \end{pmatrix} \mathrm{e}^{\mathrm{i}k_+ x} + C_- \begin{pmatrix} \sin\theta_- \\ -\cos\theta_- \end{pmatrix} \mathrm{e}^{-\mathrm{i}k_- x} \right] , \tag{2.29}$$

where now the two momentum components have different wave vectors k_+ and k_-. The relation between $\theta_\pm$ and $k_\pm$, being fixed by the single-particle Hamiltonian (2.2), is again given by Eq. (2.10), namely $2\theta_\pm = \arccos(k_\pm/k_0)$. The energy per particle takes a more involved form,

$$\begin{aligned}
\varepsilon = {} & \frac{k_0^2}{2} - \left(\frac{1+S}{2} \frac{k_+^2}{2} + \frac{1-S}{2} \frac{k_-^2}{2} \right) \\
& - \frac{\Omega}{2k_0} \left(\frac{1+S}{2} \sqrt{k_0^2 - k_+^2} + \frac{1-S}{2} \sqrt{k_0^2 - k_-^2} \right) + \frac{\delta}{2} \left(\frac{1+S}{2} \frac{k_+}{k_0} - \frac{1-S}{2} \frac{k_-}{k_0} \right) \\
& + G_1 \left\{ 1 + \frac{1-S^2}{4k_0^2} \left[\left(k_0^2 - k_+ k_-\right) + \sqrt{\left(k_0^2 - k_+^2\right)\left(k_0^2 - k_-^2\right)} \right] \right\} \\
& + G_2 \left\{ \left(\frac{1+S}{2} \frac{k_+}{k_0} - \frac{1-S}{2} \frac{k_-}{k_0} \right)^2 + \frac{1-S^2}{4k_0^2} \left[\left(k_0^2 - k_+ k_-\right) - \sqrt{\left(k_0^2 - k_+^2\right)\left(k_0^2 - k_-^2\right)} \right] \right\} \\
& + G_3 \left[\left(\frac{1+S}{2} \frac{k_+}{k_0} - \frac{1-S}{2} \frac{k_-}{k_0} \right) + \frac{1-S^2}{2k_0} \left(k_+ - k_-\right) \right] ,
\end{aligned} \tag{2.30}$$

where we have introduced the variable $S = |C_+|^2 - |C_-|^2 \in [-1, 1]$. By minimizing numerically the previous expression one can determine the values of the variational parameters S, k_+ and k_-. The ground state is found to be compatible with a stripe phase and three different kinds of plane-wave states, as shown in Fig. 2.4.

The stripe phase is energetically favorable provided the miscibility condition $g_{\uparrow\uparrow} g_{\downarrow\downarrow} > g_{\uparrow\downarrow}^2$ is satisfied. It is characterized by the presence of both momentum components of Eq. (2.29), although with different weights $|C_+|$ and $|C_-|$, giving rise to fringes with wavelength $2\pi/(k_+ + k_-)$. The presence of spin-asymmetric coupling constants can result in different values for the contrasts (2.21) of fringes in the density profile of each spin component. According to Eq. (2.28), for small values of G_3 this effect can be compensated with a proper choice of the magnetic detuning δ; however, for larger values

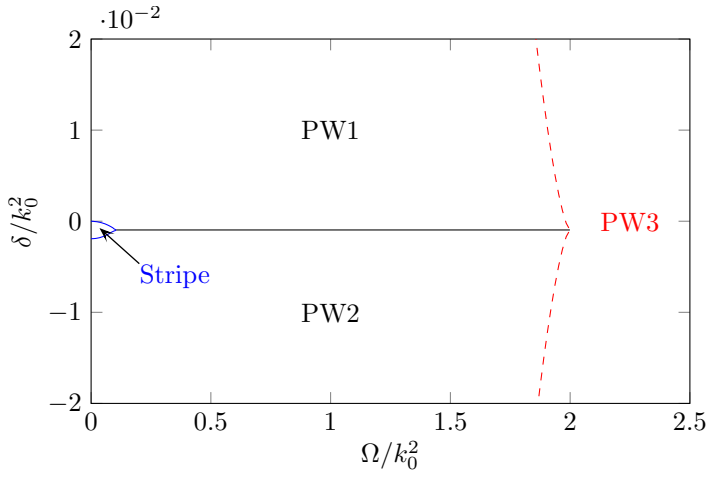

Figure 2.4. Detuning versus Rabi coupling phase diagram in the experimental conditions of [29]. The blue solid lines identify the transition from the stripe to the PW1 and PW2 phases, while the transition from PW1 to PW2 is indicated by the black solid line. The dashed red lines denote instead the transition from PW1 and PW2 to PW3. The parameters are $k_0^2 = 2\pi \times 3.54\,\mathrm{kHz}$, density in the center of the trap $n_0 = 1.9 \times 10^{14}\,\mathrm{cm}^{-3}$ and the scattering lengths given in the main text.

of G_3, higher-order corrections to the energy per particle have to be taken into account, and an exact compensation is no longer possible.

The plane-wave phases appearing in Fig. 2.4 correspond to the case where only one of the two momentum components of the wave function (2.9) is present. For definiteness, let us assume $C_+ = 1$ and $C_- = 0$; the energy per particle corresponding to this configuration takes the form

$$\varepsilon_{\mathrm{PW}} = \frac{k_0^2}{2} - \frac{\Omega}{2k_0}\sqrt{k_0^2 - k_+^2} - \left(k_0^2 - 2G_2\right)\frac{k_+^2}{2k_0^2} + G_1 + \left(\frac{\delta}{2} + G_3\right)\frac{k_+}{k_0}\,, \tag{2.31}$$

with the canonical momentum k_+ being the sole variational parameter to be determined. Minimization of (2.31) with respect to k_+ is straightforward, and yields three different plane-wave regimes, differing by the value of the momentum and, hence, of the magnetization [61]. The difference can be better understood in terms of the properties of the single-particle dispersion (2.3). For low values of Ω and δ the lower branch of (2.3) as a function of p_x has two minima, which are nondegenerate if $\delta \neq 0$; if $\delta > 0$ the global minimum occurs at negative values of the momentum (PW1 regime), while if $\delta < 0$ it takes place at positive momenta (PW2 regime). At higher values of Ω or δ the dispersion (2.3) has instead a single minimum, and one enters the PW3 regime. The critical values of the parameters Ω and δ at which the transitions between the various regimes take place are actually modified by the presence of the spin-dependent terms G_2 and G_3 in the interaction Hamiltonian; for instance, the transition between the PW1 and the PW2 states occurs at $\delta = -2G_3$ (another example of this effect is provided by the interaction-dependent shift of the critical Raman coupling $\Omega^{(\mathrm{II-III})}$ with respect to the single-particle result $2k_0^2$, see Eq. (2.27)).

One should also notice that the expression (2.31) actually corresponds to the energy per particle (2.15) for the symmetric case, with an additional term equal to the correction (2.28), which accounts for the presence of the magnetic detuning δ and of spin-asymmetric coupling constants. However, different from the calculation yielding Eq. (2.28), the validity of Eq. (2.31) is not limited to the perturbative regime. As a consequence, in the plane-wave and the single-minimum phases exact compensation of spin-asymmetric interactions through the choice $\delta = -2G_3$ is possible also for arbitrarily large values of G_3 [60].

A major feature of the phase diagram of Fig. 2.4 is that the stripe phase occupies a very small region in the Ω–δ plane. This is typical in systems where the values of the coupling constants $g_{\sigma\sigma'}$ are very close to each other, such as in the case of the states of ^{87}Rb considered above. Indeed, both the critical Raman coupling and the critical magnetic detuning needed for the transition to the plane-wave phase depend crucially on the difference between the intraspecies and the interspecies coupling constants. For example, using the above values of the scattering lengths, and taking $\delta = -2G_3$ to compensate for the small asymmetry in the intraspecies couplings, the value of the critical Raman coupling is given by Eq. (2.26) and corresponds to $\Omega^{(\mathrm{I-II})} = 0.095\, k_0^2$. This value is further reduced if δ is not equal to the compensation value.

For later purposes it is also useful to calculate, for a fixed value of Ω, the values of the magnetic detuning at which the transitions from the stripe to the PW1 and PW2 phases occur. These quantities are essentially proportional to the difference $\Delta\mu$ between the chemical potentials in the two phases. An analytic estimate can be obtained in the $\Omega \to 0$ limit, where the variational procedure based on the ansatz (2.29) is able to provide the exact condensate wave function in all the phases. In particular, in this limit one has $k_\pm \to k_0$, and the energy per particle (2.30) reduces to

$$\varepsilon_{\Omega\to 0} = G_1 + \left(\frac{\delta}{2} + G_3\right) S + G_2 S^2 \,. \tag{2.32}$$

The previous expression must be minimized with respect to S taking the constraint $|S| \leq 1$ into account. After a straightforward calculation one finds the result

$$S_{\min} = \begin{cases} -1 & \text{for} \quad \delta + 2G_3 > 4G_2 \\ -\dfrac{\delta + 2G_3}{4G_2} & \text{for} \quad |\delta + 2G_3| \leq 4G_2 \\ 1 & \text{for} \quad \delta + 2G_3 < -4G_2 \end{cases} \tag{2.33}$$

for the value of S minimizing (2.32). The first and the third value of $S_{\min}$ given in Eq. (2.33) correspond to a fully polarized PW1 and PW2 state, respectively, while the middle one yields a spin-mixed configuration. The latter turns into the stripe phase when one considers finite values of the Raman coupling Ω. The critical values of the magnetic detuning δ at which the system leaves the spin-mixed phase are identified by the condition

$$|\delta_{\mathrm{cr}} + 2G_3| = 4G_2 \,. \tag{2.34}$$

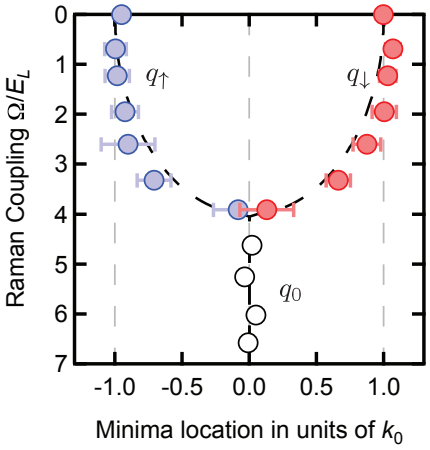

Figure 2.5. Measured values of the canonical momentum versus Ω at $\delta = 0$. The data points correspond to the minima of the dispersion $\varepsilon_-(\boldsymbol{q})$ given in Eq. (2.3). The Raman coupling is expressed in units of the recoil energy $E_L = k_0^2/2$. Reprinted by permission from Macmillan Publishers Ltd: Lin *et al.*, Nature **471**, 83-86, © 2011.

A procedure analogous to the one described above allows to determine numerically the critical magnetic detunings also at finite values of the Raman coupling Ω. In general, one finds that the range of values of δ compatible with the stripe phase is reduced with respect to the $\Omega \to 0$ case. The blue curves in Fig. 2.4 show the results of this calculation in the experimental conditions of [29]. In this case, the stripe phase is energetically favored only in a very narrow range of values of δ around the compensation value $\delta = -2G_3$, the width of the range being of the order of $10^{-3}\, k_0^2$ at $\Omega \to 0$, and even smaller for larger Ω. As a consequence, a tiny magnetic field (arising, for instance, from external fluctuations) can easily bring the system from the stripe phase into one of the plane-wave phases. The stability of the stripe phase can be strongly enhanced if one increases significantly the value of G_2, as we will discuss in Sect. 5.2.

2.2.3. Experimental results for the ground state

The emergence of a double minimum in the single-particle spectrum and the Ω dependence of the value of k_1 was experimentally observed by Lin *et al.* by measuring the velocity of the expanding cloud after the release of the trap [29] (see Fig. 2.5). The double-minimum structure vanishes at the predicted value (2.27) of the Raman coupling giving the transition between the plane-wave and the single-minimum phases. In the same experiment, at a lower value of Ω, they identified another transition between a mixed phase, characterized by two different canonical momentum components overlapping in space, and a de-mixed phase, where the two components coexist but are spatially separated. The critical Raman coupling at which the latter transition has been observed is in good agreement with the prediction $\Omega^{(\mathrm{I-II})} = 0.19\, E_r = 0.095\, k_0^2$ for the transition frequency between the stripe and the plane-wave phases, obtained from Eq. (2.26) with the ^{87}Rb value $\gamma = 0.0012$. However, it has not been possible to observe directly

the density modulations because of the smallness of their contrast and periodicity (see Chap. 5).

Finally, we mention that the critical density $\bar{n}^{(c)}$ is very large in the experimental conditions of [29], thus preventing the access to the regime where the first-order transition between the stripe and the single-minimum phases takes place. A strong reduction of the value of $\bar{n}^{(c)}$ could be achieved, for example, by considering configurations where the interspecies coupling strength $g_{\uparrow\downarrow}$ is significantly smaller than the intraspecies ones $g_{\uparrow\uparrow}$, $g_{\downarrow\downarrow}$, as discussed in Sect. 5.2.

2.3. Magnetic polarizability and compressibility

2.3.1. Calculation and properties of the magnetic polarizability

As we already pointed out in Par. 2.2.1, the transition between the plane-wave and the single-minimum phases is characterized by a divergent behavior of the magnetic polarizability χ_M. This quantity is defined as the linear response

$$\chi_M = \lim_{h\to 0} \frac{\langle\sigma_z\rangle_h - \langle\sigma_z\rangle_{h=0}}{h} \tag{2.35}$$

to a static perturbation of the form $-h\sigma_z$, where $\langle\sigma_z\rangle_h$ and $\langle\sigma_z\rangle_{h=0}$ denote the ground state expectation value of σ_z in the presence and in the absence of the perturbation, respectively. The calculation of χ_M can be carried out by resorting to the generalized ansatz (2.29), which, as we saw in Par. 2.2.2, is able to account for the effects of a Zeeman field on the ground state wave function. The energy per particle is given again by Eq. (2.30) with $G_3 = 0$ and the replacement $\delta/2 \to -h$; it is convenient to separate the contribution of the perturbation from the other terms and write $\varepsilon = \varepsilon_0 - h\langle\sigma_z\rangle_h$, with

$$\langle\sigma_z\rangle_h = \frac{1+S}{2}\frac{k_+}{k_0} - \frac{1-S}{2}\frac{k_-}{k_0}\,. \tag{2.36}$$

Let $\mathbf{x}_h = (S_h,\, k_{+,h},\, k_{-,h})$ be the vector of the values of the variational parameters minimizing ε for a fixed value of h, which satisfies the set of conditions

$$\frac{\partial}{\partial \mathrm{x}_i}\left(\varepsilon_0 - h\langle\sigma_z\rangle_h\right)\Big|_{\mathbf{x}_h} = 0\,, \qquad i = 1,2,3\,.$$

By taking the total derivative of the previous expression with respect to h, and evaluating it at $h = 0$, one finds the relation

$$\sum_{j=1}^{3} \frac{\partial^2\varepsilon_0}{\partial \mathrm{x}_i \partial \mathrm{x}_j}\Big|_{\mathbf{x}_0} \frac{\mathrm{d}\mathrm{x}_j}{\mathrm{d}h}\Big|_{h=0} = \frac{\partial\langle\sigma_z\rangle_h}{\partial \mathrm{x}_i}\Big|_{\mathbf{x}_0}\,, \qquad i = 1,2,3\,, \tag{2.37}$$

where $\mathbf{x}_0 = (S_0, k_1, k_1)$ is the $h = 0$ value of $\mathbf{x}_h$. The magnetic polarizability can then be calculated through the formula

$$\chi_M = \frac{\mathrm{d}\langle\sigma_z\rangle_h}{\mathrm{d}h}\Big|_{h=0} = \sum_{i=1}^{3} \frac{\partial\langle\sigma_z\rangle_h}{\partial \mathrm{x}_i}\Big|_{\mathbf{x}_0} \frac{\mathrm{d}\mathrm{x}_i}{\mathrm{d}h}\Big|_{h=0} = \sum_{i,j=1}^{3} \frac{\partial\langle\sigma_z\rangle_h}{\partial \mathrm{x}_i}\Big|_{\mathbf{x}_0} \left(\mathcal{H}^{-1}\right)_{ij} \frac{\partial\langle\sigma_z\rangle_h}{\partial \mathrm{x}_j}\Big|_{\mathbf{x}_0}\,, \tag{2.38}$$

where $\mathcal{H}_{ij} = \partial^2\varepsilon_0/\left(\partial \mathrm{x}_i \partial \mathrm{x}_j\right)\big|_{\mathbf{x}_0}$ denotes the elements of the Hessian matrix of ε_0 calculated at $\mathbf{x}_0$, and we made use of result (2.37). Equation (2.38) allows to express the magnetic polarizability in terms of the derivatives of ε_0 and $\langle\sigma_z\rangle_h$ with respect to the variational parameters, evaluated in their $h = 0$ value. After some algebra, the value of χ_M can be determined in each phase in a straightforward way.

In the stripe phase one has $S_0 = 0$ and k_1 given by Eq. (2.20). From Eq. (2.38) one finds a rather involved expression for the magnetic polarizability as a function of the Raman coupling Ω,

$$\chi_M^{(\mathrm{I})}(\Omega) = \frac{k_0^2\Omega^4 - 4\left(k_0^2 + G_1\right)^2\left(2k_0^2 + G_1 + G_2\right)\Omega^2 + 16\left(k_0^2 + G_1\right)^4\left(k_0^2 + G_2\right)}{a_4\Omega^4 - a_2\Omega^2 + a_0}\,, \quad (2.39)$$

with the coefficients a_0, a_2 and a_4 in the denominator given by

$$\begin{aligned} a_0 &= 32G_2\left(k_0^2 + G_1\right)^4\left(k_0^2 + G_2\right)\,, \\ a_2 &= 4\left(k_0^2 + G_1\right)^2\left[\left(G_1 + 2G_2\right)\left(G_1 + G_2\right) + k_0^2\left(G_1 + 4G_2\right)\right]\,, \\ a_4 &= k_0^2\left(G_1 + 2G_2\right)\,. \end{aligned}$$

In the weak coupling limit G_1, $G_2 \ll k_0^2$ Eq. (2.39) reduces to the simplified form

$$\chi_M^{(\mathrm{I})}(\Omega) \approx \frac{\Omega^2 - 4k_0^4}{\left(G_1 + 2G_2\right)\Omega^2 - 8G_2k_0^4}\,, \quad (2.40)$$

which diverges at the critical frequency (2.26) providing the transition to the plane-wave phase. However, this divergence only appears due to the weak coupling assumption; using the full expression (2.39), which includes higher-order terms in the coupling constants, one finds that the value of $\chi_M^{(\mathrm{I})}$ remains finite at the transition.

In the plane-wave and the single-minimum phases, the magnetic polarizability takes the simple form [59]

$$\chi_M^{(\mathrm{II})}(\Omega) = \frac{\Omega^2}{\left(k_0^2 - 2G_2\right)\left[4\left(k_0^2 - 2G_2\right)^2 - \Omega^2\right]}\,, \quad (2.41a)$$

$$\chi_M^{(\mathrm{III})}(\Omega) = \frac{2}{\Omega - 2\left(k_0^2 - 2G_2\right)}\,, \quad (2.41b)$$

and exhibits a divergent behavior at the transition between the two phases. Indeed, when approaching the transition (2.27) from above or below, the values of χ_M differ by a factor 2, revealing the second-order nature of the phase transition [65, §144]. It is worth pointing out that, if $G_2 = 0$, the calculation of χ_M reduces to the ideal gas value, which is found to be related to the effective mass (2.4) by the simple relation

$$\frac{m^*}{m} = 1 + k_0^2\,\chi_M\,. \quad (2.42)$$

The divergent behavior of the magnetic polarizability near the second-order phase transition was experimentally confirmed by Zhang *et al.* through the study of the center-of-mass oscillation [66] (see also the discussion in Chap. 4).

2.3.2. Thermodynamic compressibility

The thermodynamic compressibility $\kappa_T = (\partial P/\partial \bar{n})^{-1}$ in all the phases can be calculated from the expressions (2.25) of the pressure,

$$1/\kappa_T^{(\mathrm{I})} = 2G_1 + \frac{G_1 k_0^2 \Omega^2}{4\left(k_0^2 + G_1\right)^3}\,, \tag{2.43a}$$

$$1/\kappa_T^{(\mathrm{II})} = 2\left(G_1 + G_2\right) - \frac{G_2 k_0^2 \Omega^2}{2\left(k_0^2 - 2G_2\right)^3}\,, \tag{2.43b}$$

$$1/\kappa_T^{(\mathrm{III})} = 2G_1\,. \tag{2.43c}$$

For an interacting Bose gas, the compressibility (2.43) has always a finite value. It is discontinuous at the first-order transition between the stripe and the plane-wave phases; furthermore, if $G_2 \neq 0$, it exhibits a jump also at the second-order transition between the plane-wave and the single-minimum phases. However, as we will show in Sect. 3.3, the sound velocity is continuous across the latter transition.

3. Dynamic properties of the uniform phases

In the previous chapter we have seen that the ground-state properties of a Bose-Einstein condensate are significantly affected by the presence of spin-orbit coupling. It is reasonable to expect that also the dynamic behavior of these systems is deeply modified. In this chapter, following [67], we calculate the dynamic density response function in the plane-wave and in the single-minimum phases, characterized by a uniform ground-state density (Section 3.1). The poles of the response function yield the excitation spectrum, which is found to exhibit exotic features, such as the emergence of a rotonic structure when one approaches the transition from the plane-wave to the stripe phase. The knowledge of the density response function also allows to study other quantities of interest, like the contribution of each excited state to the static response and the static structure factor (Section 3.2). We also point out novel features occurring in the phonon regime, including the presence of two different sound velocities in the plane-wave phase, and the suppression of the sound velocity near the transition between the plane-wave and the single-minimum phases (Section 3.3).

3.1. Dynamic density response and excitation spectrum

3.1.1. Calculation of the dynamic density response function

The calculation of the dynamic density response function of a spin-orbit-coupled BEC can be carried out by a proper extension of the method presented in Par. 1.3.3. Let us add the time-dependent perturbation $V_\lambda = -\lambda \mathrm{e}^{\mathrm{i}(\boldsymbol{q}\cdot\boldsymbol{r}-\omega t)}\mathrm{e}^{\eta t} + \mathrm{H.c.}$ to the single-particle Hamiltonian (2.2). The condensate wave function Ψ_λ describing the system in the presence of this external field is found by solving the time-dependent Gross-Pitaevskii equation

$$\mathrm{i}\frac{\partial \Psi_\lambda}{\partial t} = \left[h_0^{\mathrm{SO}} + V_\lambda + \frac{1}{2}\left(g + g_{\uparrow\downarrow}\right)\left(\Psi_\lambda^\dagger \Psi_\lambda\right) + \frac{1}{2}\left(g - g_{\uparrow\downarrow}\right)\left(\Psi_\lambda^\dagger \sigma_z \Psi_\lambda\right)\sigma_z\right]\Psi_\lambda\,, \tag{3.1}$$

where h_0^{SO} is the single-particle Hamiltonian (2.2) with $\delta = 0$. In the small-λ limit the solution of Eq. 3.1 can be written as[1]

$$\Psi_\lambda(\boldsymbol{r}, t) = \mathrm{e}^{-\mathrm{i}\mu t}\left[\Psi_0(\boldsymbol{r}) + \begin{pmatrix} u_{\lambda,\uparrow}(\boldsymbol{r}) \\ u_{\lambda,\downarrow}(\boldsymbol{r}) \end{pmatrix}\mathrm{e}^{-\mathrm{i}\omega t} + \begin{pmatrix} v^*_{\lambda,\uparrow}(\boldsymbol{r}) \\ v^*_{\lambda,\downarrow}(\boldsymbol{r}) \end{pmatrix}\mathrm{e}^{\mathrm{i}\omega t}\right]. \tag{3.2}$$

[1] As in Par. 1.3.3, hereafter we do not include explicitly the contributions of the $\mathrm{e}^{\eta t}$ factors until the end of the calculation.

The first term in the right-hand side of Eq. (3.2) represents the ground-state wave function $\Psi_0 = (\psi_{0\uparrow}\ \psi_{0\downarrow})^T$ of the system, with μ the corresponding chemical potential, which have different expressions in each phase. The terms proportional to the amplitudes $u_{\lambda,\sigma}(\boldsymbol{r})$ and $v_{\lambda,\sigma}(\boldsymbol{r})$, with $\sigma =\uparrow,\downarrow$, correspond to the small oscillations of the order parameter with respect to the ground state configuration, caused by the external perturbation.

The procedure to evaluate the small amplitudes is analogous to the one we used in Par. 1.3.3 in the case of the standard Bose gas. We insert the ansatz (3.2) into the Gross-Pitaevskii equation (3.1), keeping only the linear terms in λ, $u_{\lambda,\sigma}(\boldsymbol{r})$ and $v_{\lambda,\sigma}(\boldsymbol{r})$, and we collect the terms with the same oscillatory behavior $\mathrm{e}^{-\mathrm{i}\omega t}$ and $\mathrm{e}^{\mathrm{i}\omega t}$ in time. This yields the following four coupled differential equations:

$$\begin{aligned}\Big[\tilde{h}_{0\uparrow} - \mu + 2g\,|\psi_{0\uparrow}(\boldsymbol{r})|^2 + g_{\uparrow\downarrow}\,|\psi_{0\downarrow}(\boldsymbol{r})|^2 - \omega\Big]\, u_{\lambda,\uparrow}(\boldsymbol{r}) + g[\psi_{0\uparrow}(\boldsymbol{r})]^2 v_{\lambda,\uparrow}(\boldsymbol{r}) \\ + \left[\frac{\Omega}{2} + g_{\uparrow\downarrow}\psi^*_{0\downarrow}(\boldsymbol{r})\,\psi_{0\uparrow}(\boldsymbol{r})\right] u_{\lambda,\downarrow}(\boldsymbol{r}) + g_{\uparrow\downarrow}\psi_{0\uparrow}(\boldsymbol{r})\psi_{0\downarrow}(\boldsymbol{r})\,v_{\lambda,\downarrow}(\boldsymbol{r}) = \lambda\psi_{0\uparrow}(\boldsymbol{r})\mathrm{e}^{\mathrm{i}\boldsymbol{q}\cdot\boldsymbol{r}}\,,\end{aligned} \tag{3.3a}$$

$$\begin{aligned}\Big[\tilde{h}_{0\downarrow} - \mu + 2g\,|\psi_{0\downarrow}(\boldsymbol{r})|^2 + g_{\uparrow\downarrow}\,|\psi_{0\uparrow}(\boldsymbol{r})|^2 - \omega\Big]\, u_{\lambda,\downarrow}(\boldsymbol{r}) + g[\psi_{0\downarrow}(\boldsymbol{r})]^2 v_{\lambda,\downarrow}(\boldsymbol{r}) \\ + \left[\frac{\Omega}{2} + g_{\uparrow\downarrow}\psi^*_{0\uparrow}(\boldsymbol{r})\,\psi_{0\downarrow}(\boldsymbol{r})\right] u_{\lambda,\uparrow}(\boldsymbol{r}) + g_{\uparrow\downarrow}\psi_{0\uparrow}(\boldsymbol{r})\psi_{0\downarrow}(\boldsymbol{r})\,v_{\lambda,\uparrow}(\boldsymbol{r}) = \lambda\psi_{0\downarrow}(\boldsymbol{r})\mathrm{e}^{\mathrm{i}\boldsymbol{q}\cdot\boldsymbol{r}}\,,\end{aligned} \tag{3.3b}$$

$$\begin{aligned}\Big[\tilde{h}_{0\uparrow} - \mu + 2g\,|\psi_{0\uparrow}(\boldsymbol{r})|^2 + g_{\uparrow\downarrow}\,|\psi_{0\downarrow}(\boldsymbol{r})|^2 + \omega\Big]\, v^*_{\lambda,\uparrow}(\boldsymbol{r}) + g[\psi_{0\uparrow}(\boldsymbol{r})]^2 u^*_{\lambda,\uparrow}(\boldsymbol{r}) \\ + \left[\frac{\Omega}{2} + g_{\uparrow\downarrow}\psi^*_{0\downarrow}(\boldsymbol{r})\,\psi_{0\uparrow}(\boldsymbol{r})\right] v^*_{\lambda,\downarrow}(\boldsymbol{r}) + g_{\uparrow\downarrow}\psi_{0\uparrow}(\boldsymbol{r})\psi_{0\downarrow}(\boldsymbol{r})\,u^*_{\lambda,\downarrow}(\boldsymbol{r}) = \lambda^*\psi_{0\uparrow}(\boldsymbol{r})\mathrm{e}^{-\mathrm{i}\boldsymbol{q}\cdot\boldsymbol{r}}\,,\end{aligned} \tag{3.3c}$$

$$\begin{aligned}\Big[\tilde{h}_{0\downarrow} - \mu + 2g\,|\psi_{0\downarrow}(\boldsymbol{r})|^2 + g_{\uparrow\downarrow}\,|\psi_{0\uparrow}(\boldsymbol{r})|^2 + \omega\Big]\, v^*_{\lambda,\downarrow}(\boldsymbol{r}) + g[\psi_{0\downarrow}(\boldsymbol{r})]^2 u^*_{\lambda,\downarrow}(\boldsymbol{r}) \\ + \left[\frac{\Omega}{2} + g_{\uparrow\downarrow}\psi^*_{0\uparrow}(\boldsymbol{r})\,\psi_{0\downarrow}(\boldsymbol{r})\right] v^*_{\lambda,\uparrow}(\boldsymbol{r}) + g_{\uparrow\downarrow}\psi_{0\uparrow}(\boldsymbol{r})\psi_{0\downarrow}(\boldsymbol{r})\,u^*_{\lambda,\uparrow}(\boldsymbol{r}) = \lambda^*\psi_{0\downarrow}(\boldsymbol{r})\mathrm{e}^{-\mathrm{i}\boldsymbol{q}\cdot\boldsymbol{r}}\,,\end{aligned} \tag{3.3d}$$

where we have defined the operators $\tilde{h}_{0\uparrow,\downarrow} = \left[(-\mathrm{i}\nabla_x \mp k_0)^2 - \nabla_\perp^2\right]/2$. After solving Eqs. (3.3), the density response function can be deduced in a straightforward way through Eq. (1.94), which for a system with two spin states becomes

$$\chi(\boldsymbol{q},\omega) = \lambda^{-1}\sum_{\sigma=\uparrow,\downarrow}\int \mathrm{d}\boldsymbol{r}\,\mathrm{e}^{-\mathrm{i}\boldsymbol{q}\cdot\boldsymbol{r}}\left[\psi^*_{0\sigma}(\boldsymbol{r})u_{\lambda,\sigma}(\boldsymbol{r}) + \psi_{0\sigma}(\boldsymbol{r})v_{\lambda,\sigma}(\boldsymbol{r})\right]. \tag{3.4}$$

Before going on with the evaluation of $\chi(\boldsymbol{q},\omega)$, we mention that the procedure we have just shown is well suited to investigate also the spin-density response function; for this it suffices to use $\sigma_z V_\lambda$ instead of V_λ as the external perturbation to be added to the single-particle Hamiltonian (2.2).

3.1.2. Dynamic density response in the uniform phases

The derivation of Eqs. (3.3) in the previous paragraph was carried out without the need to assume any specific form for the ground-state wave functions $\psi_{0\uparrow,\downarrow}$ of the spin-orbit-coupled BEC. However, the solutions of Eqs. (3.3) depend on the phase in which they are evaluated. In this chapter we will focus on the plane-wave and the single-minimum phases, characterized by a uniform ground-state density; the investigation of the dynamic properties of the stripe phase will be postponed to Chap. 5.

As we have seen in Chap. 2, the ground-state wave function in the plane-wave and the single-minimum phases can be generally written as

$$\Psi_0(\boldsymbol{r}) = \sqrt{\bar{n}} \begin{pmatrix} \cos\theta \\ -\sin\theta \end{pmatrix} \mathrm{e}^{\mathrm{i}k_1 x} , \tag{3.5}$$

where the momentum k_1 is given by Eq. (2.23) in the plane-wave phase (we choose to work in the plane-wave state having positive momentum) and by $k_1 = 0$ in the single-minimum phase, and θ is related to k_1 through Eq. (2.10). The corresponding chemical potential μ is given by Eq. (2.24b) in phase II and by Eq. (2.24c) in phase III.

The solutions of Eqs. (3.3), with $\psi_{0\uparrow,\downarrow}$ given by the two spin components of Eq. (3.5), are of the form $u_{\lambda,\sigma}(\boldsymbol{r}) = u_{\lambda,\sigma}\mathrm{e}^{\mathrm{i}k_1 x}\mathrm{e}^{\mathrm{i}\boldsymbol{q}\cdot\boldsymbol{r}}$ and $v_{\lambda,\sigma}(\boldsymbol{r}) = v_{\lambda,\sigma}\mathrm{e}^{-\mathrm{i}k_1 x}\mathrm{e}^{\mathrm{i}\boldsymbol{q}\cdot\boldsymbol{r}}$ ($\sigma = \uparrow, \downarrow$). The coefficients $u_{\lambda,\sigma}$ and $v_{\lambda,\sigma}$ are found by solving the following system of inhomogeneous equations:

$$(\mathcal{L} - \mathcal{J}\omega) \begin{pmatrix} u_{\lambda,\uparrow} \\ v_{\lambda,\uparrow} \\ u_{\lambda,\downarrow} \\ v_{\lambda,\downarrow} \end{pmatrix} = \lambda\sqrt{\bar{n}} \begin{pmatrix} \cos\theta \\ \cos\theta \\ -\sin\theta \\ -\sin\theta \end{pmatrix} , \tag{3.6}$$

where we have introduced the matrices $\mathcal{J} = \mathrm{diag}(1, -1, 1, -1)$ and

$$\mathcal{L} = \frac{1}{2} \begin{pmatrix} 2\varepsilon_{\uparrow u} & g\bar{n}(1+\cos 2\theta) & \Omega - g_{\uparrow\downarrow}\bar{n}\sin 2\theta & -g_{\uparrow\downarrow}\bar{n}\sin 2\theta \\ g\bar{n}(1+\cos 2\theta) & 2\varepsilon_{\uparrow v} & -g_{\uparrow\downarrow}\bar{n}\sin 2\theta & \Omega - g_{\uparrow\downarrow}\bar{n}\sin 2\theta \\ \Omega - g_{\uparrow\downarrow}\bar{n}\sin 2\theta & -g_{\uparrow\downarrow}\bar{n}\sin 2\theta & 2\varepsilon_{\downarrow u} & g\bar{n}(1-\cos 2\theta) \\ -g_{\uparrow\downarrow}\bar{n}\sin 2\theta & \Omega - g_{\uparrow\downarrow}\bar{n}\sin 2\theta & g\bar{n}(1-\cos 2\theta) & 2\varepsilon_{\downarrow v} \end{pmatrix} . \tag{3.7}$$

The diagonal entries of the matrix $\mathcal{L}$ are given by

$$2\varepsilon_{\uparrow u} = (q_x + k_1 - k_0)^2 + q_\perp^2 + 2g\bar{n}(1+\cos 2\theta) + g_{\uparrow\downarrow}\bar{n}(1-\cos 2\theta) - \mu , \tag{3.8a}$$
$$2\varepsilon_{\uparrow v} = (q_x - k_1 + k_0)^2 + q_\perp^2 + 2g\bar{n}(1+\cos 2\theta) + g_{\uparrow\downarrow}\bar{n}(1-\cos 2\theta) - \mu , \tag{3.8b}$$
$$2\varepsilon_{\downarrow u} = (q_x + k_1 + k_0)^2 + q_\perp^2 + 2g\bar{n}(1-\cos 2\theta) + g_{\uparrow\downarrow}\bar{n}(1+\cos 2\theta) - \mu , \tag{3.8c}$$
$$2\varepsilon_{\downarrow v} = (q_x - k_1 - k_0)^2 + q_\perp^2 + 2g\bar{n}(1-\cos 2\theta) + g_{\uparrow\downarrow}\bar{n}(1+\cos 2\theta) - \mu . \tag{3.8d}$$

The expressions for $u_{\lambda,\sigma}$ and $v_{\lambda,\sigma}$ can be obtained straightforwardly from Eq. (3.6) after some algebra. By inserting them in Eq. (3.4) one finally finds the following result

for the dynamic density response (recall that near the poles one should replace ω with $\omega + \mathrm{i}\eta$, with $\eta \to 0^+$):

$$\chi(\boldsymbol{q},\omega) = \frac{-Nq^2\left[\omega^2 - 4k_1 q\cos\alpha\,\omega + a(q,\alpha)\right]}{\omega^4 - 4k_1 q\cos\alpha\,\omega^3 + b_2(q,\alpha)\,\omega^2 + k_1 q\cos\alpha\,b_1(q,\alpha)\,\omega + b_0(q,\alpha)}\,. \tag{3.9}$$

Here $q \equiv |\boldsymbol{q}|$ denotes the modulus of the wave vector $\boldsymbol{q}$, while $\alpha \in [0,\,\pi]$ is the polar angle characterizing its direction with respect to the x axis. The coefficients a and b_i in (3.9) are even functions of q and $\cos\alpha$, implying that $b_i(q,\alpha) = b_i(q,\pi \pm \alpha)$ (the same for a), and their actual values depend on whether one is in phase II or III (see App. A). In the plane-wave phase, the odd terms in ω entering the response function reflect the lack of parity and time-reversal symmetry of the ground state wave function; in the single-minimum phase, however, one has $k_1 = 0$ and thus the symmetry is restored. It is also worth pointing out that, since V_λ commutes with the unitary transformation yielding the Hamiltonian in the spin-rotated frame (see Sect. 2.1), the expression for $\chi(\boldsymbol{q},\omega)$ is the same as in the original laboratory frame, and thus all the results based on the calculation in the spin-rotated frame are relevant for actual experiments.

The response function (3.9) reduces to a simplified form in two limiting cases. A first case is when $G_2 = 0$ and $\Omega = 0$. In this limit the denominator can be rewritten in a factorized form, and χ reduces to the usual Bogoliubov form $\chi(\boldsymbol{q},\omega) = -Nq^2/[\omega^2 - q^2(2G_1 + q^2/4)]$, characterizing the response of a BEC gas in the absence of spin-orbit coupling (see Eq. (1.97)). A second case is the ideal Bose gas ($G_1 = G_2 = 0$), where the Hamiltonian of the system reduces to the single-particle term (2.2), and the excitation frequencies, given by the poles of the response function, take the simple form

$$\omega_\pm(\boldsymbol{q}) = \varepsilon_\pm(\boldsymbol{p}_1 + \boldsymbol{q}) - \varepsilon_-(\boldsymbol{p}_1)\,, \tag{3.10}$$

where $\boldsymbol{p}_1 = k_1\hat{\boldsymbol{e}}_x$ is the momentum where Bose-Einstein condensation takes place, and $\varepsilon_\pm$ are the two branches of the single-particle spectrum (2.3) with $\delta = 0$.

3.1.3. Excitation spectrum in the uniform phases

The frequencies of the elementary excitations in the plane-wave and the single-minimum phases are given by the poles of the response function (3.9), i.e., by the zeros of

$$\omega^4 - 4k_1 q\cos\alpha\,\omega^3 + b_2\,\omega^2 + k_1 q\cos\alpha\,b_1\,\omega + b_0 = 0\,. \tag{3.11}$$

The solutions of this equation provide two separated branches, as shown in Fig. 3.1(a) and (b) for phase II and phase III, respectively. The lower branch is gapless and exhibits a phonon dispersion at small q, whose properties will be discussed in detail in Sect. 3.3. The upper branch is instead gapped as a consequence of the presence of the Raman coupling. For example, in phase III the gap between the two branches is given, at $\boldsymbol{q} = 0$, by $\Delta = \sqrt{\Omega(\Omega + 4G_2)}$. Differently from the single-minimum phase, the excitation spectrum in the plane-wave phase is not symmetric under inversion of q_x into $-q_x$, as a consequence of the symmetry-breaking terms appearing in (3.9). For negative values of

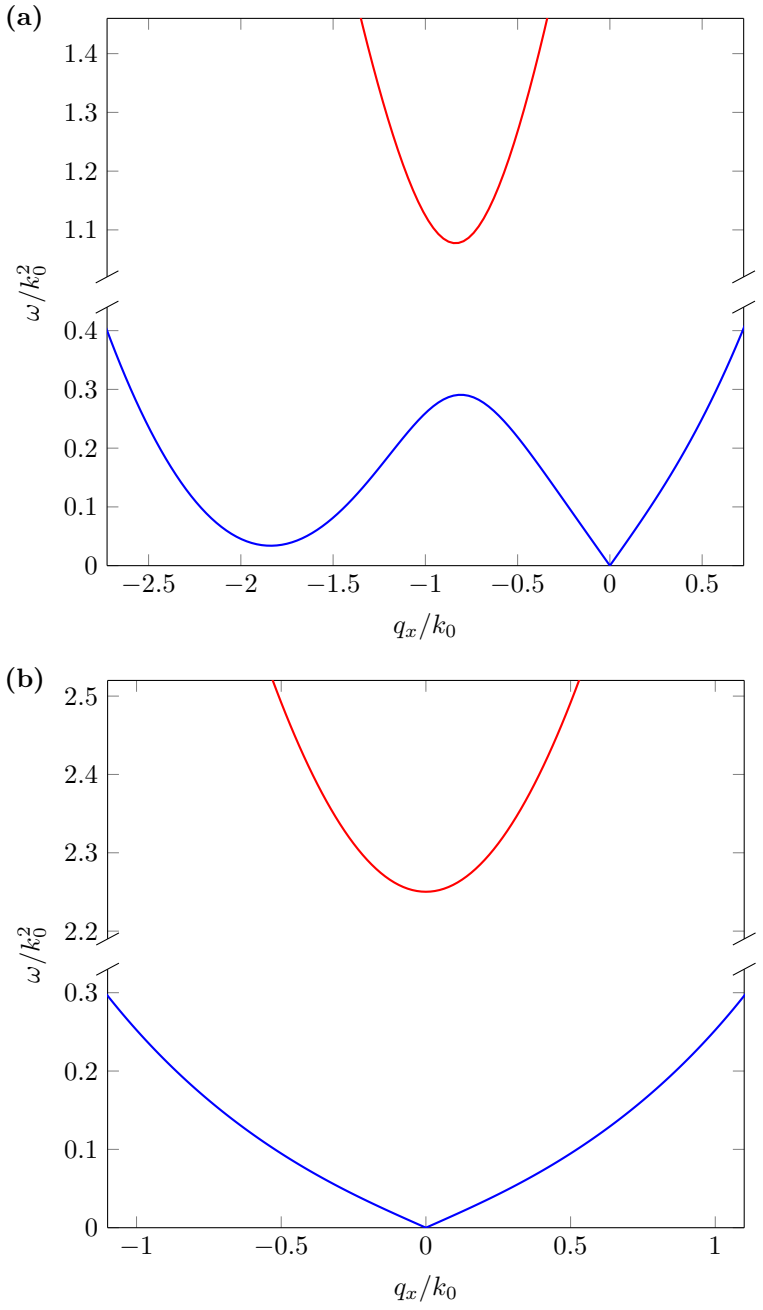

Figure 3.1. Excitation spectrum **(a)** in phase II ($\Omega/k_0^2 = 0.85$) and **(b)** in phase III ($\Omega/k_0^2 = 2.25$) as a function of q_x ($q_y = q_z = 0$), calculated in the experimental condition of [66]. The blue and red lines represent the lower and upper branches, respectively. In phase II the spectrum is not symmetric and exhibits a roton minimum for negative q_x, whose energy becomes smaller and smaller as one approaches the transition to the stripe phase at $\Omega/k_0^2 = 0.095$. The other parameters: $G_1/k_0^2 = 0.12$, $\gamma = G_2/G_1 = 10^{-3}$.

q_x, the lower branch in phase II exhibits a very peculiar feature, resulting in the emergence of a roton minimum, which becomes more and more pronounced as one approaches the transition to the stripe phase [68, 67]. The occurrence of the rotonic structure in spin-orbit-coupled BECs shares interesting analogies with the case of dipolar gases in quasi-2D configurations [69] and of condensates with soft-core, finite-range interactions [70, 71]. The physical origin of the roton minimum is quite clear: in phase II the ground state is twofold degenerate, and it is very favorable for atoms to be transferred from the BEC state with momentum $\boldsymbol{p} = k_1 \hat{\boldsymbol{e}}_x$ to the empty state at $\boldsymbol{p} = -k_1 \hat{\boldsymbol{e}}_x$. The excitation spectrum has been recently measured using Bragg spectroscopy techniques, confirming the occurrence of a characteristic rotonic structure [72, 73] (see also [74] for the case of shaken optical lattices)[2].

3.1.4. Quantum depletion

Before going on with the study of the dynamic properties in the uniform phases, it is worth taking one step backward and investigating the effects of spin-orbit coupling on the quantum depletion of the condensate. One can expect that, especially close to the second-order phase transition, the spin-orbit terms in the single-particle Hamiltonian (2.2) emphasize the role of quantum fluctuations. This effect must be small in order to be able to apply the mean-field approach for the description of the quantum phases of the system. As we saw in Par. 1.2.1, the quantum depletion of a Bose gas can be evaluated starting from the Bogoliubov amplitudes. The steps of the calculation of such amplitudes in our spin-orbit-coupled system actually resemble those reported in the previous paragraphs for the density response function. We express the condensate wave function as in Eq. (3.2) and we solve the linearized GP equations (3.3) dropping the terms proportional to the perturbation strength λ. In the plane-wave and the single-minimum phases the amplitudes can be written as $u_{\uparrow,\downarrow}(\boldsymbol{r}) = u_{\boldsymbol{q}\uparrow,\downarrow} \mathrm{e}^{\mathrm{i}k_1 x} \mathrm{e}^{\mathrm{i}\boldsymbol{q}\cdot\boldsymbol{r}}$ and $v_{\uparrow,\downarrow}(\boldsymbol{r}) = v_{\boldsymbol{q}\uparrow,\downarrow} \mathrm{e}^{-\mathrm{i}k_1 x} \mathrm{e}^{\mathrm{i}\boldsymbol{q}\cdot\boldsymbol{r}}$, where $u_{\boldsymbol{q}\uparrow,\downarrow}$ and $v_{\boldsymbol{q}\uparrow,\downarrow}$ can be found by solving the equation

$$(\mathcal{L} - \mathcal{J}\omega) \begin{pmatrix} u_{\boldsymbol{q}\uparrow} \\ v_{\boldsymbol{q}\uparrow} \\ u_{\boldsymbol{q}\downarrow} \\ v_{\boldsymbol{q}\downarrow} \end{pmatrix} = 0 \,, \tag{3.12}$$

with $\mathcal{L}$ and $\mathcal{J}$ given as in Par. 3.1.2. The eigenfrequencies ω can be found by imposing the condition $\det(\mathcal{L} - \mathcal{J}\omega) = 0$, which yields again Eq. (3.11). For each one of the two branches of the excitation spectrum there is a different set of amplitudes, which we label with a superscript $\ell = 1, 2$; the normalization condition reads

$$\sum_{\sigma=\uparrow,\downarrow} \left(\left| u^{\ell}_{\boldsymbol{q}\sigma} \right|^2 - \left| v^{\ell}_{\boldsymbol{q}\sigma} \right|^2 \right) = 1 \,. \tag{3.13}$$

[2] In the experiments of Refs. [74, 72, 73] the excitation spectrum has been measured on top of the BEC state with momentum $\boldsymbol{p} = -k_1 \hat{\boldsymbol{e}}_x$, for which the roton minimum, differently from the case discussed above, appears at positive values of q_x.

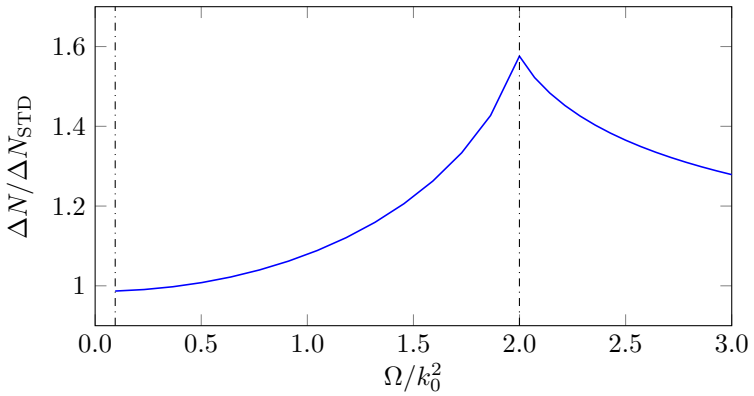

Figure 3.2. Enhancement of the quantum depletion of a Bose-Einstein condensate due to spin-orbit coupling as a function of the Raman coupling Ω, evaluated in the plane-wave and the single-minimum phases. The vertical dash-dotted lines indicate the critical values of Ω at which the I-II and II-III phase transitions take place. The parameters are $G_1/k_0^2 = 0.12$ and $\gamma = G_2/G_1 = 10^{-3}$.

Once the values of the amplitudes are available, one can calculate the number of atoms $\Delta N = N - N_0$ out of the condensate through the relation

$$\Delta N = \frac{V}{(2\pi)^3} \sum_{\ell=1,2} \sum_{\sigma=\uparrow,\downarrow} \int \mathrm{d}\boldsymbol{q} \left| v^{\ell}_{\boldsymbol{q}\sigma} \right|^2 , \tag{3.14}$$

which generalizes Eq. (1.34) to the case of a spin-1/2 Bose gas. This integral has a simple analytic expression in the $\Omega \to 0$ limit, i.e. for a standard two-component BEC without spin-orbit coupling:

$$\Delta N_{\rm STD} = \frac{V}{3\pi^2} \left[(2G_1)^{3/2} + (2G_2)^{3/2} \right] . \tag{3.15}$$

At finite Ω the quantum depletion ΔN can be conveniently computed numerically. In Fig. 3.2 we report the results in the experimental conditions of [29]. One can notice that, although quantum fluctuations are enhanced by spin-orbit coupling, the effect is small for the current values of the spin-orbit parameters, even close to the second-order phase transition between the plane-wave and the single-minimum phases. This justifies our mean-field description of spin-orbit-coupled Bose gases.

3.2. Static response function and static structure factor

The static response function $\chi(\boldsymbol{q}) \equiv \chi(\boldsymbol{q}, \omega = 0)/N$ can be derived directly from (3.9). Its $q = 0$ value $\mathcal{K} \equiv \chi(q = 0)$ is given by

$$\mathcal{K}_{\rm II}^{-1} = 2G_1 + \frac{2G_2 k_1^2 \left(k_1^2 \cos^2\alpha + k_0^2 \sin^2\alpha - 2G_2 \right)}{k_1^2 \left(k_0^2 \cos^2\alpha - 2G_2 \right) + k_0^4 \sin^2\alpha} , \tag{3.16}$$

$$\mathcal{K}_{\rm III}^{-1} = 2G_1 \tag{3.17}$$

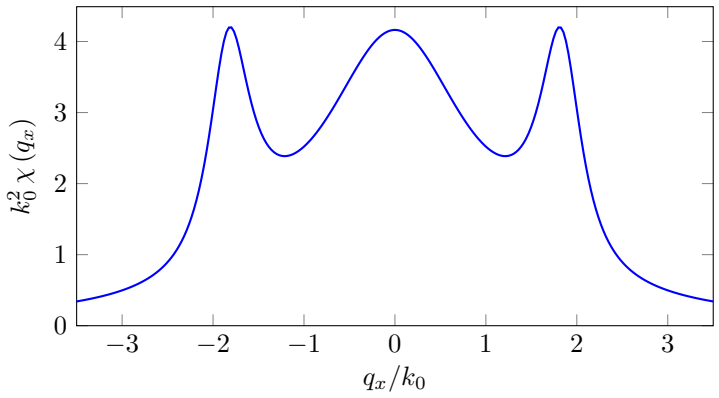

Figure 3.3. Static response in phase II as a function of q_x ($q_y = q_z = 0$). The curve is symmetric and exhibits a typical peak near the roton momentum. The parameters are $\Omega/k_0^2 = 0.85$, $G_1/k_0^2 = 0.12$ and $\gamma = G_2/G_1 = 10^{-3}$.

in the plane-wave and the single-minimum phases, respectively. The anisotropy of $\mathcal{K}$ in phase II caused by the spin interaction term G_2 is revealed by the last term of Eq. (3.16) which depends on the polar angle α. It is also worth pointing out that $\mathcal{K}_{\rm II}$ coincides with the thermodynamic compressibility $\kappa_T^{(\rm II)}$ (2.43b) only along the x direction, i.e. when $\sin\alpha = 0$. In this case, $\mathcal{K}$ also exhibits a jump at the transition between phases II and III. This marks a difference with respect to the behavior of the frequencies of the elementary excitation, fixed by Eq. (3.11), which are always continuous functions of Ω at the transition for all values of $\boldsymbol{q}$.

Far from the phonon regime, the occurrence of the roton minimum is reflected in an enhancement in the static response function $\chi(q_x)$ close to the roton momentum, as shown in Fig. 3.3, representing a typical tendency of the system towards crystallization. When the roton frequency vanishes, $\chi(q_x)$ exhibits a divergent behavior. A simple analytic expression for the corresponding value of the Raman coupling Ω is obtained in the weak coupling limit $G_1, G_2 \ll k_0^2$, where we find that the critical value exactly coincides with the value (2.26) characterizing the transition between the plane-wave and the stripe phases. For larger values of the coupling constants G_1 and G_2, the critical value takes place for values of the Raman coupling smaller than the value at the transition, exhibiting the typical spinoidal behavior of first-order liquid-crystal phase transitions.

In Sect. 1.3 we saw that the dynamic structure factor at $T = 0$ can be calculated from the response function (3.9) through the relation $S(\boldsymbol{q},\omega) = \pi^{-1}\mathrm{Im}\,\chi(\boldsymbol{q},\omega)$ for $\omega \geq 0$, and $S(\boldsymbol{q},\omega) = 0$ for negative ω. In the plane-wave phase, the condition $\mathrm{Im}\,\chi(\boldsymbol{q},\omega) = -\mathrm{Im}\,\chi(-\boldsymbol{q},-\omega)$, characterizing the imaginary part of the response function, is still satisfied, but the symmetry relation $\mathrm{Im}\,\chi(\boldsymbol{q},\omega) = \mathrm{Im}\,\chi(-\boldsymbol{q},\omega)$ is not ensured, and consequently one finds $S(\boldsymbol{q},\omega) \neq S(-\boldsymbol{q},\omega)$. This means that several equalities involving sum rules, which we derived in Sect. 1.3 assuming the invariance of the ground state under either parity or time reversal symmetry (see Eq. (1.71) and the discussion below), do no longer hold in that form in the plane-wave phase. However, they can be reformulated to be valid in more general situations starting from the relations (1.56)–

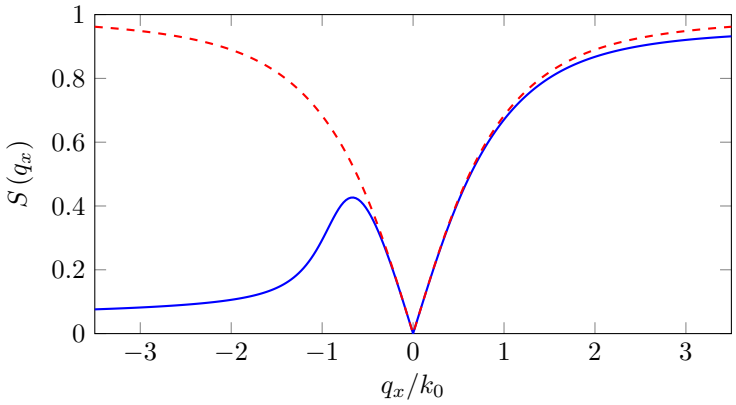

Figure 3.4. Contribution of the lower branch to the static structure factor in phase II as a function of q_x (blue solid line), compared with the total $S(q_x)$ (red dashed line). The parameters are $\Omega/k_0^2 = 0.85$, $G_1/k_0^2 = 0.12$ and $\gamma = G_2/G_1 = 10^{-3}$.

(1.59) and (1.61). An example is the f-sum rule $\int \mathrm{d}\omega\, \omega[S(\boldsymbol{q},\omega) + S(-\boldsymbol{q},\omega)] = Nq^2$, which is exactly satisfied, as one can deduce from the correct large-ω behavior of the density response function: $\chi(\boldsymbol{q},\omega)_{\omega\to\infty} = -Nq^2/\omega^2$ (see Eq. (1.81)). On the other hand, one should recall that the inversion invariance of the static structure factor $S(\boldsymbol{q})$ is an intrinsic feature, which is always ensured regardless the symmetry properties of the underlying configuration (see the discussion above Eq. (1.74)).

It is worth pointing out that, despite the strong enhancement exhibited by the static response function $\chi(q_x)$, the static structure factor $S(q_x)$ does not exhibit any peaked structure near the roton point. This is different from what happens, for example, in superfluid helium[3]. In Fig. 3.4 we show the static structure factor $S(q_x)$ together with the contribution to the integral $S(q_x) = \int \mathrm{d}\omega\, S(q_x,\omega)/N$ arising from the lower branch of the elementary excitations. The figure shows that the lower-branch contribution is not symmetric for exchange of q_x into $-q_x$, even if the total $S(q_x)$ is symmetric, as we have shown previously. Remarkably, the strength carried by the lower branch is significantly peaked for intermediate values of q_x between the phonon and the roton regimes, in the so-called maxon region, where the lower branch of the excitation spectrum exhibits a maximum.

3.3. Velocity and density vs spin nature of the sound mode

The low frequency excitations at small q, i.e. the sound waves, can be easily obtained by setting $\omega = cq$, where c is the sound velocity, and keeping the leading terms proportional

[3] At finite temperature T one instead expects the static structure factor to be significantly peaked near the roton minimum, provided the roton energy is small compared to T, as a consequence of the thermal excitations of rotons, similarly to what is predicted for quasi-2D dipolar gases [75].

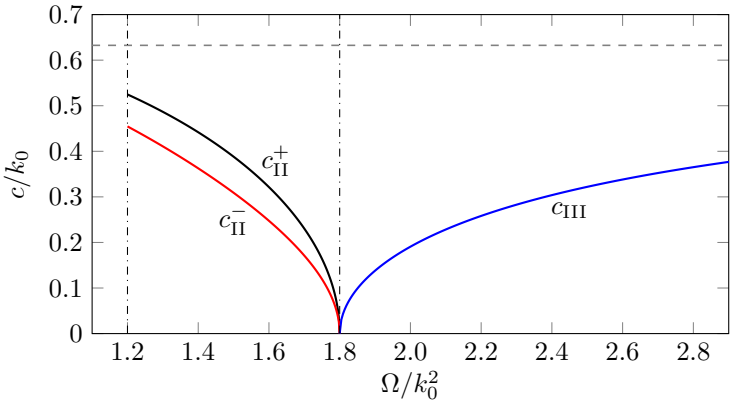

Figure 3.5. Sound velocity as a function of the Raman coupling for the following choice of parameters: $G_1/k_0^2 = 0.2$, $G_2/k_0^2 = 0.05$. The two sound velocities in phase II correspond to phonons propagating in the direction parallel (c_{II}^{+}) and antiparallel (c_{II}^{-}) to k_1. The horizontal dashed line corresponds to the value $\sqrt{2G_1} = 0.63\,k_0$ of the sound velocity in the absence of spin-orbit and Raman coupling. The vertical dash-dotted lines indicate the critical values of Ω at which the I-II and II-III phase transitions take place.

to q^2 in Eq. (3.11). This allows us to obtain the sound velocity in the plane-wave and the single-minimum phases,

$$c_{\mathrm{II}} = \frac{1}{k_0^4 - 2G_2k_1^2}\Bigg\{ G_2k_1\left(k_0^2 - k_1^2\right)\cos\alpha + \sqrt{2\left[G_1k_0^4 + G_2k_1^2\left(k_0^2 - 2G_1 - 2G_2\right)\right]\left[k_0^4 - 2G_2k_1^2 - k_0^2\left(k_0^2 - k_1^2\right)\cos^2\alpha\right]}\Bigg\}, \tag{3.18}$$

$$c_{\mathrm{III}} = \sqrt{2G_1\left(1 - \frac{2k_0^2\cos^2\alpha}{\Omega + 4G_2}\right)}. \tag{3.19}$$

Approaching the transition between the two phases, both sound velocities exhibit a strong reduction along the x direction ($\cos\alpha = \pm 1$), caused by the spin-orbit coupling. This suppression can be understood in terms of the increase of the effective mass (2.4) associated with the single-particle dispersion (2.3). At the transition, where the velocity of sound modes propagating along the x direction vanishes, the elementary excitations exhibit a different q^2 dependence. On the other hand, the sound velocities along the other directions ($\alpha \neq 0$, $\alpha \neq \pi$) remain finite at the transition. The sound velocity in phase II shows a further interesting feature, caused by the lack of parity symmetry. The asymmetry effect in c_{II} is due to the presence of the first term in the numerator of (3.18), therefore the symmetry will be recovered if $G_2 = 0$ or $\alpha = \pi/2$ (corresponding to phonons propagating along the directions orthogonal to the x axis).

The role played by the spin degree of freedom in the propagation of the sound can be better understood by relating the sound velocity to the magnetic polarizability χ_M

(2.41a)–(2.41b) and the $q = 0$ static response $\mathcal{K}$ (3.16)–(3.17). One finds the result

$$c(\alpha)c(\alpha+\pi) = \frac{1 + k_0^2\,\chi_M \sin^2\alpha}{\mathcal{K}\,(1 + k_0^2\,\chi_M)}\,, \tag{3.20}$$

holding in both phases II and III. The above equation generalizes the relation $c^2 = 1/\kappa_T = \partial P/\partial\bar{n}$ between the sound velocity and the compressibility holding in usual superfluids (see Eqs. (1.22)–(1.23)). It explicitly shows that, along the x direction, where $\sin\alpha = 0$, the sound velocity c vanishes at the transition because of the divergent behavior of the magnetic polarizability. The sound velocity along the x axis as a function of Ω is shown in Fig. 3.5 for a configuration with relatively large G_2, emphasizing the difference between $c_{\rm II}^{+} = c_{\rm II}(\alpha = 0)$ and $c_{\rm II}^{-} = c_{\rm II}(\alpha = \pi)$, i.e., between the velocities of sound waves propagating in opposite directions along the x axis. Notice that the sound velocity, in the absence of spin-orbit and Raman coupling, would correspond to the value $c = \sqrt{2G_1}$ (horizontal) dashed line. This value is asymptotically reached only for very large values of Ω. The suppression effect exhibited by the sound velocity near the II-III phase transition is particularly remarkable in the single-minimum phase III, where Bose-Einstein condensation takes place in the $\boldsymbol{p} = 0$ state and the compressibility of the gas is unaffected by spin-orbit coupling. It explicitly reveals the mixed density and spin nature of the sound waves, with the spin nature becoming more and more important as one approaches the phase transition where χ_M diverges.

The combined density and spin nature of sound waves is also nicely revealed by the relative amplitudes of the density $\delta n = \delta n_\uparrow + \delta n_\downarrow$ and spin density $\delta s_z = \delta n_\uparrow - \delta n_\downarrow$ oscillations in the $q \to 0$ limit, characterizing the propagation of sound. This quantities can be easily evaluated within the hydrodynamic approach, which will be discussed in Sect. 4.2. Here we anticipate that, in terms of the magnetic polarizability χ_M, one finds

$$\left(\frac{\delta s_z}{\delta n}\right)_{\rm II} = \frac{\sqrt{1 + (k_0^2 - 2G_2)\,\chi_M}}{1 + k_0^2\,\chi_M} + \frac{k_0\,\chi_M\cos\alpha}{1 + k_0^2\,\chi_M}\sqrt{\frac{2\,[G_2 + G_1\,(1 + k_0^2\,\chi_M)]}{1 + k_0^2\,\chi_M\sin^2\alpha}}\,, \tag{3.21}$$

$$\left(\frac{\delta s_z}{\delta n}\right)_{\rm III} = \frac{2k_0\,\chi_M\cos\alpha\,\sqrt{G_1}}{\sqrt{2\,(1 + k_0^2\,\chi_M)\,\big(1 + k_0^2\,\chi_M\sin^2\alpha\big)}} \tag{3.22}$$

in the plane-wave and the single-minimum phases, respectively. The above equations show that, near the transition between phases II and III, the amplitude of the spin-density fluctuations δs_z of the sound waves propagating along the x direction ($\sin\alpha = 0$) is strongly enhanced with respect to the density fluctuations δn, as a consequence of the divergent behavior of the magnetic polarizability. In particular, very close to the phase transition the relative amplitude is given by

$$\frac{\delta s_z}{\delta n} \sim \sqrt{2G_1\chi_M} \tag{3.23}$$

in both phases II and III. This suggests that an effective way to excite these phonon modes near the transition is through a coupling with the spin degree of freedom, as

recently achieved in two-photon Bragg experiments on Fermi gases [76]. For sound waves propagating in the direction orthogonal to x the situation is instead different. In particular in phase III sound waves are purely density oscillations ($\delta s_z = 0$).

It is finally interesting to understand the role played by the sound waves in terms of sum rules. The phonon mode exhausts the compressibility sum rule $\int \mathrm{d}\omega\, [S(\boldsymbol{q},\omega) + S(-\boldsymbol{q},\omega)]/\omega$ at small q, as one can easily prove from (3.9). However, different from ordinary superfluid, it gives only a small contribution to the f-sum rule $\int \mathrm{d}\omega\, \omega[S(\boldsymbol{q},\omega) + S(-\boldsymbol{q},\omega)] = Nq^2$ as one approaches the second-order transition. This contribution becomes vanishingly small at the transition for wave vectors $\boldsymbol{q}$ oriented along the x direction. Also, the static structure factor $S(\boldsymbol{q})$ is strongly quenched compared to usual BECs. This results in an enhancement of the quantum fluctuations of the order parameter, as predicted by the uncertainty principle inequality [77, 78]. However, as we have already seen in Par. 3.1.4, this effect is small because the sound velocity vanishes only along the x direction [58].

4. Collective modes in harmonic traps

In this chapter we discuss the collective excitations for a harmonically trapped BEC with spin-orbit coupling. First one should notice that, in typical experimental conditions, the spin-orbit coupling strength, usually quantified by the recoil energy $E_r = k_0^2/2$, is much larger than the trapping frequencies. As a consequence, one expects that the three phases occurring in uniform matter due to the spin-orbit coupling survive also in the presence of harmonic trapping. This can be verified by solving numerically the Gross-Pitaevskii equation

$$\mathrm{i}\frac{\partial \Psi}{\partial t} = \left[h_0^{\mathrm{SO}} + V_{\mathrm{ext}}(\boldsymbol{r}) + \frac{1}{2}\left(g + g_{\uparrow\downarrow}\right)\left(\Psi^\dagger \Psi\right) + \frac{1}{2}\left(g - g_{\uparrow\downarrow}\right)\left(\Psi^\dagger \sigma_z \Psi\right)\sigma_z\right]\Psi \tag{4.1}$$

for the condensate wave function, with $V_{\mathrm{ext}}(\boldsymbol{r}) = (\omega_x^2 x^2 + \omega_y^2 y^2 + \omega_z^2 z^2)/2$ representing the external trapping potential. Fig. 4.1 gives an example of the momentum distribution and the spin polarization of a trapped spin-orbit-coupled BEC as a function of the Raman coupling. For simplicity, we have considered harmonic trapping only along the x direction. One can see that the three phases discussed in the bulk case show up also here. It is worth mentioning that in the low density limit, where the interaction energy is much smaller than the recoil energy, the value of Ω/k_0^2 at the transitions (2.26) and (2.27) is almost density-independent, therefore even in the presence of a trap they can be well identified using the results obtained in the bulk.

The first part of this chapter, following [59], is devoted to the study of the dipole mode. By resorting to a sum-rule approach, we derive an expression for the frequency of the center-of-mass oscillation (Section 4.1), which turns out to be deeply affected by the coupling with the spin degree of freedom, and can deviate significantly from the harmonic oscillator value. A crucial role in this coupling is played by the magnetic polarizability. Further information on the nature of the lowest dipole mode can be obtained by calculating the oscillation amplitudes of the most relevant physical quantities. In the second part of the chapter, which is based on part of [67], the frequencies of the collective modes of a spin-orbit-coupled Bose gas are investigated through the hydrodynamic formalism (Section 4.2). In particular, we show that simple analytic estimations for these frequencies can be obtained in the special case of spin-independent coupling constants.

4.1. Dipole mode: a sum-rule approach

Among the various excitations exhibited by a trapped spin-orbit-coupled gas, the dipole mode deserves a special attention. It corresponds to the oscillation of the center-of-mass

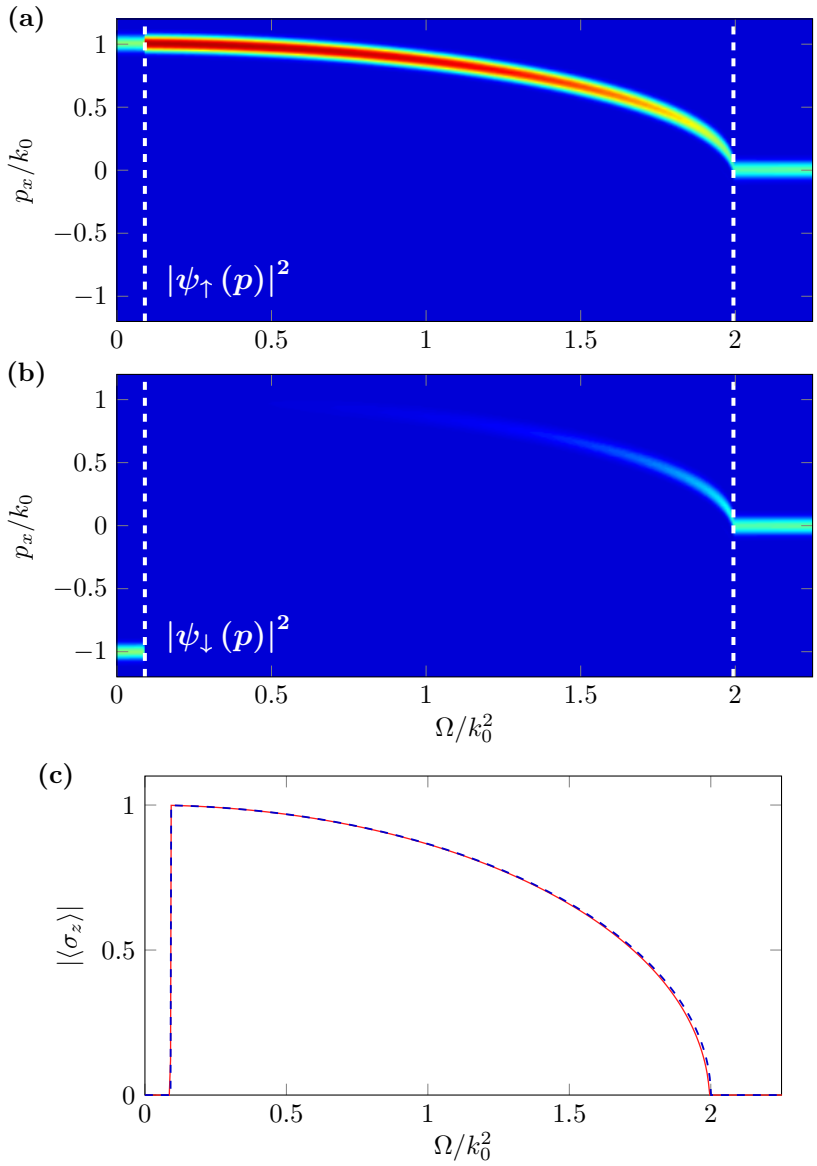

Figure 4.1. (a)–(b). Momentum distribution for the two spin components as a function of Ω. The white dashed lines indicate the transition frequencies calculated using (2.26) and (2.27). **(c).** Spin polarization $|\langle\sigma_z\rangle| = |N_\uparrow - N_\downarrow|/N$ as a function of Ω in the trapped case (red solid line) and in the uniform case using the density in the center of the trap (blue dashed line). The parameters are chosen as follows: $\omega_x = 2\pi \times 40\,\mathrm{Hz}$, $\omega_x/k_0^2 = 0.01$, $\delta = 0$, $g_{\uparrow\uparrow} = g_{\downarrow\downarrow} = 4\pi \times 101.20\,a_B$, $g_{\uparrow\downarrow} = 4\pi \times 100.94\,a_B$, where a_B is the Bohr radius. The density in the center of the trap corresponds to $n \simeq 1.9 \times 10^{13}\,\mathrm{cm}^{-3}$.

of the system, and can be easily excited experimentally [79]. For a conventional trapped gas without spin-orbit coupling, the oscillation along a certain direction, for example the x axis, is excited by the dipole operator $X = \sum_j x_j$, and its frequency is equal to the frequency ω_x of the harmonic trap (Kohn's theorem). In the presence of spin-orbit-coupling, the behavior of the dipole oscillation can be studied using the formalism of sum rules [59], which has already been presented in Sect. 1.3.

4.1.1. Sum rules and excitation frequency of the dipole operator

The starting point of our analysis is represented by the k-th moment of the dynamic structure factor for the dipole operator X which, according to the general definition (1.55), is given at zero temperature by

$$m_k(X) = \sum_n (E_n - E_0)^k \, |\langle n|X|0\rangle|^2 \, . \tag{4.2}$$

Here $|0\rangle$ and $|n\rangle$ are, respectively, the ground state and the n-th excited state of the many-body Hamiltonian (2.5), now including the external trapping potential in the single-particle contributions

$$h_0^{\mathrm{SO}}(j) = \frac{1}{2}\left[(p_{x,j} - k_0\sigma_{z,j})^2 + p_{\perp,j}^2\right] + \frac{\Omega}{2}\sigma_{x,j} + \frac{\delta}{2}\sigma_{z,j} + V_{\mathrm{ext}}(\boldsymbol{r}_j) \, . \tag{4.3}$$

The energies corresponding to $|0\rangle$ and $|n\rangle$ are denoted by E_0 and E_n, respectively.

We already learned from Eqs. (1.56)–(1.59) that some moments can be easily calculated by employing the completeness relation and the commutation rules involving the Hamiltonian of the system. In the case of the dipole operator one finds, for example, that the energy-weighted moment takes the model-independent value

$$m_1(X) = \frac{1}{2}\,\langle 0|[X,[H,X]]|0\rangle = \frac{N}{2} \, , \tag{4.4}$$

with N the total number of atoms. Equation (4.4) is usually referred to as the f-sum rule for the dipole operator. Notice that this sum rule is not affected by the spin terms in the Hamiltonian, despite the fact that the commutator of H with X explicitly depends on the spin-orbit coupling:

$$[H,X] = -\mathrm{i}\,(P_x - k_0\Sigma_z) \, , \tag{4.5}$$

where $P_x = \sum_j p_{x,j}$ is the total momentum of the gas along the x direction, and $\Sigma_z = \sum_j \sigma_{z,j}$ is the total spin operator along z. Equation (4.5) actually reflects the fact that the equation of continuity (and hence, in our case, the dynamic behavior of the center-of-mass coordinate) is deeply influenced by the coupling with the spin variable.

Another important sum rule is the inverse energy-weighted sum rule (also called dipole polarizability). In the presence of harmonic trapping, this sum rule can be calculated in a straightforward way using the commutation relation

$$[H,P_x] = \mathrm{i}\omega_x^2 X \tag{4.6}$$

and the completeness relation. One finds

$$m_{-1}(X) = \frac{m_1(P_x)}{\omega_x^4} = \frac{N}{2\omega_x^2}\,. \tag{4.7}$$

Both sum rules (4.4) and (4.7) are insensitive to the presence of the spin terms in the single-particle Hamiltonian (4.3), as well as to the two-body interaction. This does not mean, however, that the dipole dynamics is not affected by the spin-orbit coupling. This effect is accounted for by another sum rule, particularly sensitive to the low energy region of the excitation spectrum: the inverse cubic energy-weighted sum rule, for which we find the exact result

$$m_{-3}(X) = \frac{m_{-1}(P_x)}{\omega_x^4} = \frac{N}{2\omega_x^2}\left(1 + k_0^2\,\chi_M\right)\,. \tag{4.8}$$

In order to derive the previous equation we made use of both the commutation relations (4.6) and (4.5). The quantity χ_M corresponds to the magnetic polarizability already defined in Sect. 2.3, and given in terms of sum rules by $\chi_M = 2m_{-1}(\Sigma_z)/N$. It is worth mentioning that the above results for the sum rules $m_1(X)$, $m_{-1}(X)$ and $m_{-3}(X)$ hold exactly for the Hamiltonian (2.5), including the interaction terms. Their validity is not restricted to the mean-field approximation and is ensured for both Bose and Fermi statistics, at zero as well as at finite temperature. In particular the sum rule $m_{-3}(X)$, being sensitive to the magnetic polarizability, is expected to exhibit a nontrivial temperature dependence across the BEC transition.

Equation (4.8) exploits the crucial role played by the spin-orbit coupling proportional to k_0. The effect is particularly important when the magnetic polarizability takes a large value. A large increase of χ_M is associated with the occurrence of a dipole soft mode, as can be inferred by taking the ratio between the inverse and cubic inverse energy-weighted sum rules $m_{-1}(X)$ and $m_{-3}(X)$, yielding the rigorous upper bound

$$\omega_D^2 = \frac{m_{-1}(X)}{m_{-3}(X)} = \frac{\omega_x^2}{1 + k_0^2\,\chi_M} \tag{4.9}$$

to the lowest dipole excitation energy (see Eq. (1.63) with $p = -2$). The calculation of the magnetic polarizability χ_M for a trapped gas can be carried out in the same way as in uniform matter (see Sect. 2.3), with the difference that the condensate wave function is now provided by the solution of (4.1) rather than by the ansatz (2.9).

4.1.2. Optimized excitation operator approach

The estimate (4.9) for the frequency of the dipole oscillation can be improved by assuming that the operator exciting this mode is given by a combination of the kind $F = P_x + \eta k_0 \Sigma_z$. Here η is a real variational parameter, to be determined by minimizing the collective frequency fixed by the ratio $m_1(F)/m_{-1}(F)$, corresponding to the estimate provided by Eq. (1.63) with $p = 0$. The energy-weighted and inverse energy-weighted

moments of the operator F can be calculated in a straightforward way, and are given by

$$m_1(F) = \frac{1}{2}\langle 0|[F,[H,F]]|0\rangle = \frac{N}{2}(-2\eta^2 k_0^2 \Omega\langle\sigma_x\rangle + \omega_x^2) \tag{4.10}$$

and

$$m_{-1}(F) = \frac{N}{2}[1+(1+\eta)^2 k_0^2 \chi_M]\,, \tag{4.11}$$

respectively. In deriving the Eq. (4.10) we have explicitly used the sum-rule result for the energy-weighted moment relative to the spin operator Σ_z,

$$m_1(\Sigma_z) = \frac{1}{2}\langle 0|[\Sigma_z,[H,\Sigma_z]]|0\rangle = -N\Omega\langle\sigma_x\rangle\,. \tag{4.12}$$

In the previous expressions $\langle\sigma_x\rangle = N^{-1}\int \mathrm{d}\boldsymbol{r}\, s_x(\boldsymbol{r})$ represents the spin polarization along x, which can be evaluated directly from Eq. (2.13). Using the results of Chap. 2 one easily finds $\langle\sigma_x\rangle = -(\Omega/2)/(k_0^2+G_1)$ and $\langle\sigma_x\rangle = -(\Omega/2)/(k_0^2-2G_2)$ in the stripe and the plane-wave phase, respectively, while in the single-minimum phase one has $\langle\sigma_x\rangle = -1$.

As we mentioned before, an upper bound to the frequency of the lowest mode excited by the operator F is provided by the expression

$$\omega_D^2 = \frac{m_1(F)}{m_{-1}(F)} = \frac{-2\eta^2 k_0^2\Omega\langle\sigma_x\rangle + \omega_x^2}{1+(1+\eta)^2 k_0^2\chi_M}\,. \tag{4.13}$$

Notice that the choice $\eta = 0$ in Eq. (4.13) reproduces the previous estimate (4.9). In the opposite $\eta \gg 1$ limit Eq. (4.13) yields instead

$$\omega_D^2 = \frac{m_1(\Sigma_z)}{m_{-1}(\Sigma_z)} = -2\Omega\langle\sigma_x\rangle/\chi_M\,. \tag{4.14}$$

We are now in a position to estimate the dipole frequency by minimizing Eq. (4.13) with respect to the parameter η. The variational procedure actually provides two solutions. However, the upper solution is physically meaningful only for very small values of Ω, where it approaches the frequency ω_x of the center-of-mass sloshing mode. For higher Ω the upper solution takes large values and the coupling with other modes, not accounted for by our ansatz for the excitation operator F, becomes important.

In Fig. 4.2 we report the results for the lowest dipole solution, together with those for the magnetic polarizability. In particular, Fig. 4.2(a) shows the behavior of the magnetic polarizability as a function of the Raman coupling Ω, calculated by solving numerically (4.1) in the presence of harmonic trapping along the x direction (red dashed lines), and by the relations (2.41a) and (2.41b) in uniform matter using the density in the center of the trap (blue solid lines). Figure 4.2(b) shows the frequency of the dipole oscillation predicted from Eq. (4.9) using the same values of χ_M presented in (a). This frequency reveals important deviations from the oscillation frequency ω_x caused by the spin-orbit and Raman couplings for all values of Ω. In the same figure we also show the prediction (4.9) for the dipole frequency, obtained by setting $\eta = 0$ in (4.13). This turns out to be an excellent estimate except for very small values of the Raman coupling. Actually,

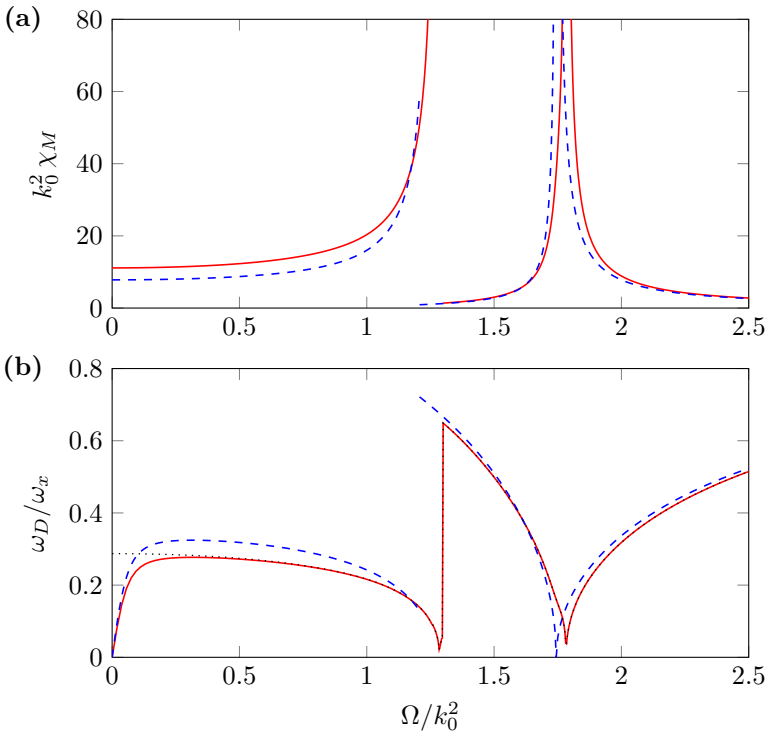

Figure 4.2. (a). Magnetic polarizability χ_M as a function of Ω calculated in a trap (red solid lines) and in uniform matter using the density in the center of trap (blue dashed lines). **(b)**. The corresponding lowest mode frequency ω_D with $\langle\sigma_x\rangle$ and χ_M calculated in the harmonic trap (red solid lines) and in uniform matter (blue dashed lines). The black dotted line corresponds to the prediction (4.9). The parameters are $k_0^2 = 2\pi \times 320\,\mathrm{Hz}$, $\omega_x = 2\pi \times 20\,\mathrm{Hz}$, the density in the center of the trap $n \simeq 2.6 \times 10^{13}\,\mathrm{cm}^{-3}$, the atomic mass of ^{87}Rb, and the scattering lengths $a_{\uparrow\uparrow} = a_{\downarrow\downarrow} = 100\,a_B$, $a_{\uparrow\downarrow} = 60\,a_B$, where a_B is the Bohr radius, corresponding to $G_1/k_0^2 \simeq 0.257$ and $G_2/k_0^2 \simeq 0.064$.

in the $\Omega \ll \omega_x$ limit the value of η minimizing Eq. (4.13) is no longer small, and the mode turns out to be a pure spin oscillation, its frequency vanishing linearly with Ω (see Eq. (4.14)). In this limit the mode does not exhibit any significant coupling with the center-of-mass oscillation. At the transition between the phases I and II the lowest dipole frequency exhibits a sudden jump and then starts decreasing for larger values of Ω. In the thermodynamic limit, it vanishes at the transition between the phases II and III as a consequence of the divergent behavior of χ and, above the transition, it increases to reach asymptotically the oscillator value ω_x at large Ω.

In Fig. 4.3 we show the magnetic polarizability and the frequency of the lowest dipole mode in the plane-wave and the single-minimum phases in the experimental conditions of [66]. The theoretical curves for the dipole frequency correspond to the estimate (4.9) which, as we mentioned above, is very accurate in the wide range of Raman coupling $\Omega \gg \omega_x$. The black squares in (a) and the circles in (b) are the experimental results of [66]. In this experiment, the magnetic polarizability has been extracted from the

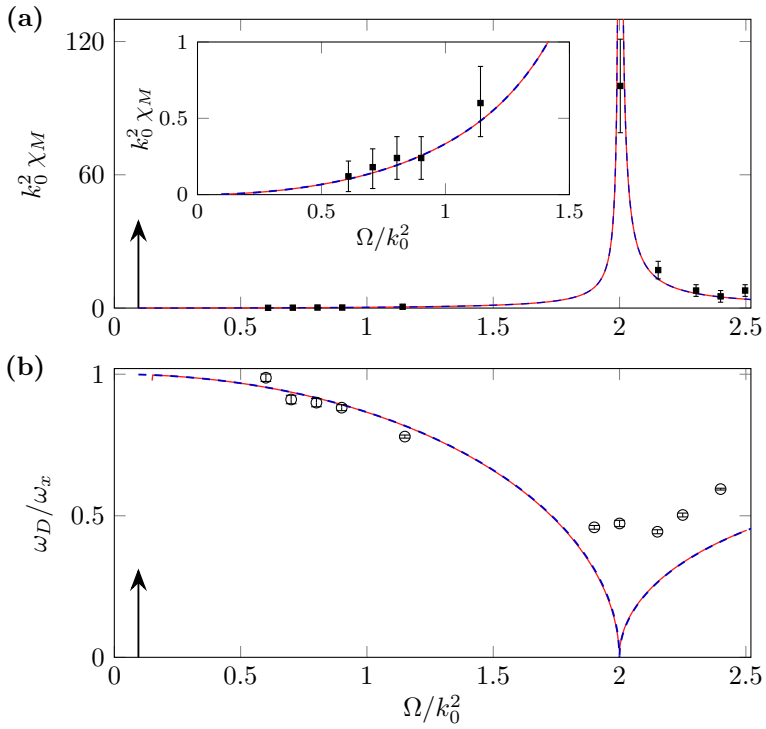

Figure 4.3. (a). Magnetic polarizability χ_M as a function of Ω calculated in a trap (red solid lines) and in uniform matter using the density in the center of trap (blue dashed lines). **(b)**. Dipole frequency predicted by (4.9), using the values of χ_M shown above, represented by the red solid lines and the blue dashed lines respectively. The parameters are $k_0^2 = 2\pi \times 4.42\,\mathrm{kHz}$, $\omega_x = 2\pi \times 45\,\mathrm{Hz}$, the scattering lengths $a_{\uparrow\uparrow} = a_{\downarrow\downarrow} = 101.20\,a_B$, $a_{\uparrow\downarrow} = 100.94\,a_B$, where a_B is the Bohr radius, and the atomic mass of ^{87}Rb. The density in the center of the trap is $n \simeq 1.37 \times 10^{14}\,\mathrm{cm}^{-3}$. The black squares and circles in the figures are the experimental data of [66]. The black arrows indicates the transition between phases I and II.

measurement of the oscillation amplitudes of some relevant quantities (see the discussion in Par. 4.1.3). Due to the very small value of G_2, one can combine Eqs. (4.9) and (2.4), the latter holding for $G_2 = 0$, to relate the dipole frequency to the effective mass in phases II and III:

$$\omega_D = \sqrt{\frac{m}{m^*}}\,\omega_x\,. \tag{4.15}$$

Figure 4.3(a) shows in a clear way the divergent behavior of the magnetic polarizability at the transition between phases II and III, which is responsible for the strong reduction of the dipole frequency. The GP simulations are practically indistinguishable from the calculations of χ_M (and hence of ω_D) based on uniform matter ingredients. In Fig. 4.3(b) one can see that, far from the transition point at $\Omega \simeq 2k_0^2$, the theoretical curves for the dipole frequency agree very well with the experimental data, while near the transition nonlinear effects play a major role, as discussed in [66] (see also the discussion in the next paragraph). The lack of data points in the region below the transition is due to the

occurrence of a dynamic instability, which makes the observation of the dipole oscillation very difficult [80].

It is worth mentioning that, despite its strong spin nature, the lowest frequency mode exhausts almost completely the dipole polarizability sum rule $m_{-1}(X)$, except in the $\Omega \ll \omega_x$ region. As a consequence, it can be easily excited by displacing the trapping potential.

4.1.3. Dipole mode and oscillation amplitudes

The combined spin-orbit nature of the lowest dipole mode is also nicely revealed by the relative amplitudes of the oscillating values of the center-of-mass position (A_X), the momentum(A_{P_x}) and the spin polarization (A_{Σ_z}). These amplitudes can be calculated in the present approach by writing the many-body oscillating wave function as

$$|\Psi(t)\rangle = \mathrm{e}^{\mathrm{i}\alpha(t)\delta F}\mathrm{e}^{\beta(t)G}\,|0\rangle\ , \tag{4.16}$$

where $\delta F = F - \langle F\rangle_0$ plays the role of the excitation operator (in this paragraph we use $\langle\,\rangle_0$ and $\langle\,\rangle_t$ to denote the expectation values on the states $|0\rangle$ and $|\Psi(t)\rangle$, respectively), while G represents the restoring force defined by the commutation relation $[H,\,G] = \delta F$, and α, β are time-dependent parameters. The equations governing the time evolution of these parameters can be obtained through a variational Lagrange procedure, which consists in imposing the condition of stationarity to the action functional:

$$\delta\left[\int \mathrm{d}t\left(\langle\Psi(t)|H|\Psi(t)\rangle - \mathrm{i}\,\langle\Psi(t)|\,\frac{\partial}{\partial t}\,|\Psi(t)\rangle\right)\right] = 0\,. \tag{4.17}$$

Since we are interested in small amplitude oscillations, we can expand the quantities appearing in the previous equation up to second order in α and β, which after a bit of algebra yields

$$\delta\left\{\int \mathrm{d}t\left[2m_1(G)\dot{\alpha}\beta + m_1(F)\alpha^2 + m_1(G)\beta^2\right]\right\} = 0\,. \tag{4.18}$$

The Euler-Lagrange equation for α and β then read

$$\dot{\alpha}(t) = -\beta(t)\,, \tag{4.19a}$$

$$\dot{\beta}(t) = \omega_D^2\alpha(t)\,, \tag{4.19b}$$

where ω_D is given by Eq. (4.13), and we have used the relation $m_1(G) = m_{-1}(F)$. By solving Eqs. (4.19) one finds that α and β oscillate with frequency ω_D, and their oscillation amplitudes are related through $A_\beta = \omega_D A_\alpha$.

The time dependence of the relevant quantities $\langle X\rangle_t$, $\langle P_x\rangle$ and $\langle\Sigma_z\rangle$ can be expressed at linear order in α and β as

$$\langle X\rangle_t = -N\alpha\,, \tag{4.20a}$$

$$\langle P_x\rangle_t = \langle P_x\rangle_0 + N\left[1 + (1+\eta)k_0^2\chi_M\right]\beta\,, \tag{4.20b}$$

$$k_0\langle\Sigma_z\rangle_t = k_0\langle\Sigma_z\rangle_0 + N(1+\eta)k_0^2\chi_M\beta\,, \tag{4.20c}$$

from which one finds the following relationships between the spin, the center-of-mass and the momentum oscillation amplitudes:

$$A_{\Sigma_z} = A_X \omega_D (1+\eta) k_0 \chi_M \,, \tag{4.21a}$$

$$\frac{A_{P_x}}{k_0} = A_{\Sigma_z} \frac{1+(1+\eta)k_0^2\chi_M}{(1+\eta)k_0^2\chi_M} \,. \tag{4.21b}$$

For $\Omega \ll \omega_x$, as discussed above, the lowest frequency mode is mainly a spin oscillation (large η), and one finds that the center-of-mass position is basically at rest ($A_X \sim 0$), while $A_{P_x}/k_0 \sim A_{\Sigma_z}$. For larger values of Ω the lowest frequency is instead well approximated by the choice $\eta = 0$, and the relations (4.21) take the useful form

$$A_{\Sigma_z} = A_X \frac{\omega_x \, k_0 \, \chi_M}{\sqrt{1+k_0^2 \, \chi_M}} \,, \tag{4.22a}$$

$$\frac{A_{P_x}}{k_0} = A_{\Sigma_z} \frac{1+k_0^2 \, \chi_M}{k_0^2 \, \chi_M} \,. \tag{4.22b}$$

The connection between the momentum and spin amplitudes has been already pointed out in [66] (see Fig. 4 therein). It provides a practical way to determine experimentally the magnetic polarizability χ_M. Near the transition point between the plane-wave and the single-minimum phase the ratio A_{Σ_z}/A_X between the spin and the center-of-mass amplitudes diverges like $\sqrt{\chi_M}$, in analogy with the behavior exhibited by the ratio between the spin and the density amplitudes in the propagation of sound (see Eq. (3.23)). These divergent behavior emphasizes the role of nonlinear effects, which is likely at the origin of the finite values of the dipole frequencies observed at the transition (see Fig. 4.3 and the discussion in [66]).

4.2. Hydrodynamic formalism for spin-orbit-coupled Bose gases

4.2.1. Hydrodynamic equations and current operator

In Par. 1.2.2 we have seen that hydrodynamic theory provides a useful approach to describe the phonon regime in the excitation spectrum of a superfluid. To implement this formalism for a spinor BEC one has to write both the spin-up and the spin-down components of the order parameter in terms of their modulus and phase, i.e. $\psi_\uparrow = \sqrt{n_\uparrow} \mathrm{e}^{\mathrm{i}\phi_\uparrow}$ and $\psi_\downarrow = -\sqrt{n_\downarrow} \mathrm{e}^{\mathrm{i}\phi_\downarrow}$ (the minus sign in the latter expression is for later convenience) [68, 67]. In the following we will choose to work with a different set of variables, namely the total density $n = n_\uparrow + n_\downarrow$, the spin density $s_z = n_\uparrow - n_\downarrow$, the global phase $\phi = (\phi_\uparrow + \phi_\downarrow)/2$ and the relative phase $\xi = (\phi_\uparrow - \phi_\downarrow)/2$. The hydrodynamic energy functional can be obtained by rewriting Eq. (2.7) in terms of these variables and neglecting the quantum pressure terms (we also include an external potential V_{ext} to study trapped configurations). After

a bit of algebra one finds

$$E_{\mathrm{hd}}\left[n, s_z, \phi, \xi\right] = \int \mathrm{d}\boldsymbol{r} \left\{ \frac{n}{2}\left(|\nabla\phi|^2 + |\nabla\xi|^2\right) + s_z\left(\nabla\phi\right)\cdot\left(\nabla\xi\right) - k_0\left(n\nabla_x\xi + s_z\nabla_x\phi\right) + \frac{k_0^2}{2}n - \frac{\Omega}{2}\sqrt{n^2 - s_z^2}\cos 2\xi + V_{\mathrm{ext}}n + g_1 n^2 + g_2 s_z^2 \right\}, \tag{4.23}$$

with $g_1 = (g + g_{\uparrow\downarrow})/4$ and $g_2 = (g - g_{\uparrow\downarrow})/4$. The four hydrodynamic equations describing our system can be obtained by imposing the condition of stationarity to the hydrodynamic action,

$$\delta\left[\int \mathrm{d}t\,\mathrm{d}\boldsymbol{r}\left(n\frac{\partial\phi}{\partial t} + s_z\frac{\partial\xi}{\partial t}\right) + \int \mathrm{d}t\, E_{\mathrm{hd}}\right] = 0\,, \tag{4.24}$$

which yields

$$\frac{\partial\phi}{\partial t} + \frac{1}{2}\left(|\nabla\phi|^2 + |\nabla\xi|^2\right) - k_0\nabla_x\xi - \frac{\Omega}{2}\frac{n}{\sqrt{n^2 - s_z^2}}\cos 2\xi + \frac{k_0^2}{2} + V_{\mathrm{ext}} + 2g_1 n = 0\,, \tag{4.25a}$$

$$\frac{\partial\xi}{\partial t} + \left(\nabla\phi\right)\cdot\left(\nabla\xi\right) - k_0\nabla_x\phi + \frac{\Omega}{2}\frac{s_z}{\sqrt{n^2 - s_z^2}}\cos 2\xi + 2g_2 s_z = 0\,, \tag{4.25b}$$

$$\frac{\partial n}{\partial t} + \nabla\cdot\left(n\nabla\phi + s_z\nabla\xi\right) - k_0\nabla_x s_z = 0\,, \tag{4.25c}$$

$$\frac{\partial s_z}{\partial t} + \nabla\cdot\left(n\nabla\xi + s_z\nabla\phi\right) - k_0\nabla_x n - \Omega\sqrt{n^2 - s_z^2}\sin 2\xi = 0\,. \tag{4.25d}$$

Remarkably, the equation of continuity (4.25c) is crucially affected by spin-orbit coupling (cfr. Eq. (1.45a)). This follows from the fact that the current is not simply given by the canonical momentum operator, as happens in usual superfluids, but contains an additional spin contribution. In Par. 1.3.2 we saw that the current density operator satisfies the continuity equation $[H, \hat{n}(\boldsymbol{r})] = \mathrm{i}\nabla\cdot\hat{\boldsymbol{j}}$, where $\hat{n}(\boldsymbol{r}) = \sum_j \delta(\boldsymbol{r} - \boldsymbol{r}_j)$ is the total density operator. By explicitly carrying out the commutator one identifies the current as

$$\hat{\boldsymbol{j}}(\boldsymbol{r}) = \hat{\boldsymbol{p}}(\boldsymbol{r}) - k_0\hat{\sigma}_z(\boldsymbol{r})\hat{\boldsymbol{e}}_x\,, \tag{4.26}$$

where $\hat{\boldsymbol{p}}(\boldsymbol{r}) = \sum_j[\boldsymbol{p}_j\delta(\boldsymbol{r} - \boldsymbol{r}_j) + \mathrm{H.c.}]/2$ and $\hat{\sigma}_z(\boldsymbol{r}) = \sum_j \sigma_{z,j}\,\delta(\boldsymbol{r} - \boldsymbol{r}_j)$ are the momentum and spin density operators, respectively. The expression (4.26) for the current explicitly reveals the presence of a gauge field associated to the vector potential $\boldsymbol{A} = k_0\sigma_z\hat{\boldsymbol{e}}_x$. The spin term appearing in the current also reflects the violation of Galilean invariance in the spin-orbit Hamiltonian [80].

4.2.2. Equilibrium configuration and collective modes

The hydrodynamic equations (4.25) can be used to study both the equilibrium configuration and the collective modes of a spin-orbit-coupled BEC. In this paragraph we will limit the discussion to the plane-wave and the single-minimum phases (the investigation

of the stripe phase requires more sophisticated calculations, see Chap. 5), and we will focus on the study of the phonon regime of the excitation spectrum, characterized by long wavelengths and low frequencies. In such conditions Eqs. (4.25) take a strongly simplified form. Indeed, from Eq. (4.25d) one can see that, for oscillations whose frequency ω is much smaller than the Raman coupling Ω, the relative phase is locked[1], $2\xi = \phi_\uparrow - \phi_\downarrow = 0$. As a consequence, the relevant hydrodynamic equations reduce to the first three (4.25) with $\xi = 0$.

In order to study the frequencies of the collective modes, we first need to find the equilibrium values of the relevant physical quantities predicted by Eqs. (4.25a)–(4.25c). We recall that the equilibrium configuration of the system is characterized by a time-independent density $n = n_0(\boldsymbol{r})$ and spin density $s = s_{z0}(\boldsymbol{r})$, and by a phase $\phi = -\mu t + \phi_0(\boldsymbol{r})$, with μ the chemical potential. Inserting these expression into Eqs. (4.25a)–(4.25c), in uniform matter ($V_{\text{ext}} = 0$) one finds the solutions $n_0 = \bar{n}$, $s_{z0} = \bar{n}k_1/k_0$ and $\phi_0 = k_1 x$, with k_1 given by Eq. (2.23) in the plane-wave phase and $k_1 = 0$ in the single-minimum phase (see Chap. 2); the corresponding chemical potentials μ coincide with (2.24b) and (2.24c), respectively. For trapped configurations, the equilibrium values of the phase and of the densities can be easily determined in the case $g_2 = 0$, corresponding to $g_1 = g/2$. From Eqs. (4.25b) and (4.25c) one finds that the gradient of the phase ϕ_0, which is related to the spin polarization s_{z0}/n_0 through

$$\nabla\phi_0 = k_0 \frac{s_{z0}}{n_0} \hat{\boldsymbol{e}}_x \,, \tag{4.27}$$

is independent of density in both phases II and III, its expression coinciding with that of the wave vector $k_1\hat{\boldsymbol{e}}_x$ mentioned above. Then, Eq. (4.25a) yields the characteristic Thomas-Fermi form for the density profile,

$$n_0(\boldsymbol{r}) = \frac{1}{g}\left[\mu - \kappa_0 - V_{\text{ext}}(\boldsymbol{r})\right] \,, \tag{4.28}$$

where the constant quantity κ_0 is given by $-\Omega^2/8k_0^2$ in phase II and by $(k_0^2 - \Omega)/2$ in phase III. As usual, the chemical potential μ is fixed by the normalization condition.

Similarly to what we did in Par. 1.2.2, we now look for solutions of the hydrodynamic equations representing small oscillations of the variables with respect their equilibrium values, and thus we write $n = n_0 + \delta n$, $s_z = s_{z0} + \delta s_z$ and $\phi = -\mu t + \phi_0 + \delta\phi$. Linearization of Eq. (4.25b) yields the important relation

$$k_0 \nabla_x \delta\phi - k_0^2 Z \left(-\frac{s_{z0}}{n_0}\frac{\delta n}{n_0} + \frac{\delta s_z}{n_0} \right) - 2g_2 \delta s_z = 0 \tag{4.29}$$

between the phase gradient, the density, and the spin fluctuations, where we have defined the dimensionless quantity

$$Z = \frac{\Omega}{2k_0^2(1 - s_{z0}^2/n_0^2)^{3/2}} \,. \tag{4.30}$$

[1]The oscillation of the relative phase plays a crucial role in the excitation of the upper branch, whose frequency is of the order of Ω.

Analogously, from (4.25a) and (4.25c) one can derive the equations for the phase and the density oscillations,

$$\frac{\partial}{\partial t}\delta\phi + (\nabla\phi_0)\cdot(\nabla\delta\phi) - k_0^2 Z\frac{s_{z0}}{n_0}\left(-\frac{s_{z0}}{n_0}\frac{\delta n}{n_0}+\frac{\delta s_z}{n_0}\right)+2g_1\delta n = 0 \tag{4.31}$$

and

$$\frac{\partial}{\partial t}\delta n + \nabla\cdot(n_0\nabla\delta\phi) - k_0\nabla_x\left[n_0\left(-\frac{s_{z0}}{n_0}\frac{\delta n}{n_0}+\frac{\delta s_z}{n_0}\right)\right] = 0\,. \tag{4.32}$$

The solutions of the hydrodynamic equations (4.29), (4.31) and (4.32) in uniform matter ($V_{\rm ext}=0$) are able to reproduce the results (3.18) and (3.19) for the sound velocity in phase II and phase III, respectively. This can be verified by looking for solutions of the form

$$\begin{pmatrix}\delta n(\boldsymbol{r})\\ \delta s_z(\boldsymbol{r})\\ \delta\phi(\boldsymbol{r})\end{pmatrix} = \mathrm{e}^{\mathrm{i}(\boldsymbol{q}\cdot\boldsymbol{r}-\omega t)}\begin{pmatrix}\delta n_{\boldsymbol{q}}\\ \delta s_{z\boldsymbol{q}}\\ \delta\phi_{\boldsymbol{q}}\end{pmatrix} \tag{4.33}$$

in the $q\to 0$ limit, where the eigenfrequencies exhibit the usual phonon dispersion $\omega = cq$. Within the same procedure one can also derive the expressions for the ratio $\delta s_{z\boldsymbol{q}}/\delta n_{\boldsymbol{q}}$, which in the $q\to 0$ limit reduce to the results (3.21) and (3.22) that we anticipated in Sect. 3.3.

Let us now consider again the case $g_2=0$, where the ratio $s_{0z}/n_0 = k_1/k_0$ is independent of density and the quantity Z defined in (4.30) is related to the effective mass (2.4) by $1-Z^{-1}=m/m^*$. By using the equalities (4.27) and (4.29) one can reformulate Eqs. (4.31) and (4.32) in terms of the fluctuations of the total density and of the global phase only. These equations are then reduced to the simple form

$$\frac{\partial}{\partial t}\delta n + \nabla_\perp\cdot(n_0\,\nabla_\perp\delta\phi) + \frac{m}{m^*}\nabla_x\,(n_0\nabla_x\delta\phi) = 0\,, \tag{4.34a}$$

$$\frac{\partial}{\partial t}\delta\phi + g\,\delta n = 0\,, \tag{4.34b}$$

which bear a strong resemblance with the corresponding equalities (1.45) holding for usual BECs. Combining (4.34a) and (4.34b) one finds the following equation for the density:

$$\frac{\partial^2}{\partial t^2}\delta n = g\left[\nabla_\perp\cdot(n_0\nabla_\perp\delta n) + \frac{m}{m^*}\nabla_x\,(n_0\nabla_x\delta n)\right]\,. \tag{4.35}$$

In uniform matter, where the equilibrium density $n_0=\bar{n}$ is constant, Eq. (4.35) yields the relation $c^2 = g\bar{n}/m^*$ for the sound velocity along the x direction, consistent with the results (3.18) and (3.19) for $g_{\uparrow\downarrow}=g$. In the presence of a harmonic trapping potential $V_{\rm ext}(\boldsymbol{r}) = (\omega_x x^2+\omega_y y^2+\omega_z z^2)/2$, where the equilibrium density profile (4.28) corresponds to an inverted parabola, the solutions of the hydrodynamic equations (4.35) coincide with those one finds for usual BECs, with the simple replacement of the trap frequency ω_x with $\omega_x\sqrt{m/m^*}$. This gives the result $\omega_D = \omega_x\sqrt{m/m^*}$ for the dipole frequency, which reproduces the estimate (4.15) obtained with a sum-rule approach and holding if $G_2=0$. Equation (4.35) also shows that, for any other hydrodynamic mode involving a motion

of the gas along the x axis, a similar effect of strong reduction of the frequency close to the second-order transition should be expected. This is the case, for example, of the scissors mode for deformed traps in the x-y or x-z plane, where the collective frequency takes the form $\sqrt{(m/m^*)\omega_x^2+\omega_y^2}$ and $\sqrt{(m/m^*)\omega_x^2+\omega_z^2}$ respectively.

5. The stripe phase

The stripe phase is doubtlessly the most intriguing configuration appearing in the phase diagram of Chapter 2. It has been the object of several recent theoretical investigations [81, 64, 82, 83, 84, 85, 86, 87, 88, 89, 90]. As we already pointed out, the stripe phase is characterized by the spontaneous breaking of two continuous symmetries. The breaking of gauge symmetry yields superfluidity, while the breaking of translational invariance is responsible for the occurrence of a crystalline structure. The simultaneous presence of these two broken symmetries is typical of supersolids [63, 91, 92, 93]. As we shall see, it is at the origin of the appearance of two gapless excitations as well as of a band structure in the excitation spectrum [85].

This chapter is divided into two parts. The first part (Section 5.1) is devoted to a discussion of some important properties of the ground state and of the dynamics of the stripe phase in uniform matter, which have been reported in [85]. Many relevant quantities that we will consider, such as the contrast of the density modulations (2.21), will turn out to depend crucially on the value of the Raman coupling Ω. Therefore, in order to enhance the effects of the presence of the stripes one needs to use relatively large values of Ω. On the other hand, the stripe phase is favored only in a range of low values of the Raman coupling lying below the transition frequency $\Omega^{(\mathrm{I-II})}$. In the following we will consider configurations with relatively large values of the parameter G_2 which, as can be seen from Equation (2.26), allows to obtain a significant increase of the critical value of Ω. This is not, however, the situation in current experiments with ^{87}Rb atoms [29, 66], where G_2 is instead extremely small. In the second part of the chapter (Section 5.2) we will illustrate a procedure to increase the value of G_2 with available experimental techniques, which has been proposed by us in [94].

5.1. Static and dynamic properties of the stripe phase

5.1.1. Ground state and excitation spectrum

In Sect. 2.2 the ground state in the stripe phase has been described by means of an approximated wave function, based on the ansatz (2.9), which takes into account only first-order harmonic terms. The exact wave function also includes higher-order harmonics, whose appearance is a consequence of the nonlinearity of the Gross-Pitaevskii theory, and can be written as

$$\Psi_0(\boldsymbol{r}) = \sqrt{\bar{n}} \sum_{\bar{K}} \begin{pmatrix} a_{-k_1+\bar{K}} \\ -b_{-k_1+\bar{K}} \end{pmatrix} \mathrm{e}^{\mathrm{i}(\bar{K}-k_1)x} \,. \tag{5.1}$$

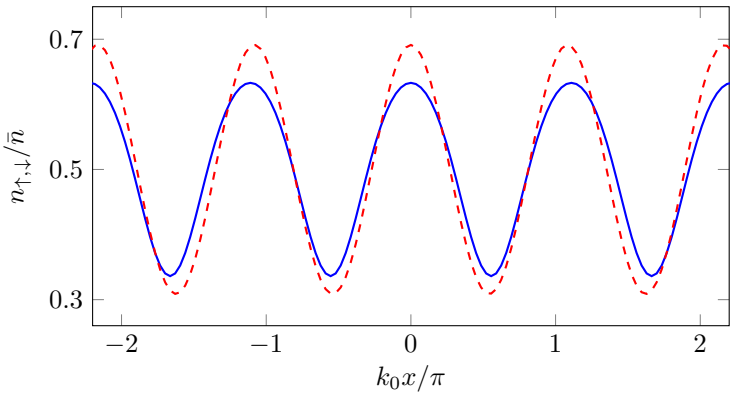

Figure 5.1. Density profile in the stripe phase along the x direction, calculated within the first-order harmonic approximation (2.9) (red dashed line) and from (5.1) including the higher-order harmonics (blue solid line). The parameters are $\Omega/k_0^2 = 1.0$, $G_1/k_0^2 = 0.3$, and $G_2/k_0^2 = 0.08$, yielding the transition frequency $\Omega^{(\mathrm{I}-\mathrm{II})}/k_0^2 \simeq 1.3$.

This expression has the characteristic form of the wave function of a system exhibiting a periodic lattice structure along the x direction only [95]. The wave vector $k_1 = \pi/d$ is related to the period d of the stripes, while $\bar{K} = 2nk_1$, with $n = 0, \pm 1, \ldots$, correspond to the reciprocal lattice vectors. The expansion coefficients $a_{-k_1+\bar{K}}$ and $b_{-k_1+\bar{K}}$ can be determined, together with the value of k_1, by a procedure of minimization of the mean-field energy functional (2.7). The energy minimization gives rise to the presence of terms with opposite phase ($\mathrm{e}^{\pm \mathrm{i}k_1 x}$, $\mathrm{e}^{\pm 3\mathrm{i}k_1 x}$, $\ldots$), responsible for the density modulations and characterized by the symmetry condition $a_{-k_1+\bar{K}} = b^*_{k_1-\bar{K}}$, causing the vanishing of the spin polarization $\langle \sigma_z \rangle$. Figure 5.1 shows an example of density profile in the stripe phase, calculated for a configuration with relatively large values of G_2 and Ω/k_0^2 in order to emphasize the contrast in the density modulations.

To evaluate the elementary excitations in the stripe phase we resort to the standard Bogoliubov approach described in Par. 1.2.1. Thus, we write the deviations of the order parameter with respect to equilibrium as

$$\Psi(\boldsymbol{r}, t) = \mathrm{e}^{-\mathrm{i}\mu t} \left[\Psi_0(\boldsymbol{r}) + \begin{pmatrix} u_\uparrow(\boldsymbol{r}) \\ u_\downarrow(\boldsymbol{r}) \end{pmatrix} \mathrm{e}^{-\mathrm{i}\omega t} + \begin{pmatrix} v^*_\uparrow(\boldsymbol{r}) \\ v^*_\downarrow(\boldsymbol{r}) \end{pmatrix} \mathrm{e}^{\mathrm{i}\omega t} \right] \tag{5.2}$$

and we solve the corresponding linearized time-dependent Gross-Pitaevskii equations. We recall that these equations are formally the same as Eqs. (3.3) with $\lambda = 0$. They can be conveniently solved by expanding $u_{\uparrow,\downarrow}(\boldsymbol{r})$ and $v_{\uparrow,\downarrow}(\boldsymbol{r})$ in the Bloch form in terms of the reciprocal lattice vectors:

$$u_{\boldsymbol{q}\uparrow,\downarrow}(\boldsymbol{r}) = \mathrm{e}^{-\mathrm{i}k_1 x} \sum_{\bar{K}} U_{\boldsymbol{q}\uparrow,\downarrow\bar{K}} \, \mathrm{e}^{\mathrm{i}\boldsymbol{q}\cdot\boldsymbol{r} + \mathrm{i}\bar{K}x} \,, \tag{5.3}$$

$$v_{\boldsymbol{q}\uparrow,\downarrow}(\boldsymbol{r}) = \mathrm{e}^{\mathrm{i}k_1 x} \sum_{\bar{K}} V_{\boldsymbol{q}\uparrow,\downarrow\bar{K}} \, \mathrm{e}^{\mathrm{i}\boldsymbol{q}\cdot\boldsymbol{r} - \mathrm{i}\bar{K}x} \,, \tag{5.4}$$

where $\boldsymbol{q}$ is the wave vector of the excitation. This ansatz is also well suited to calculate the density and spin-density dynamic response function, similarly to what we did in

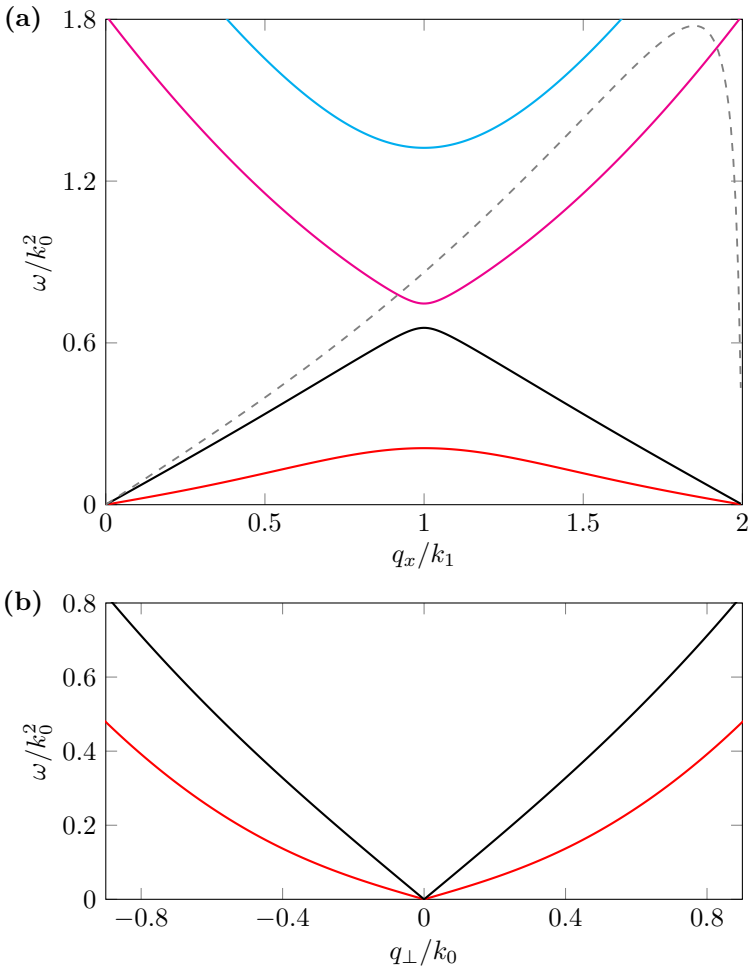

Figure 5.2. **(a)**: Lowest four excitation bands (solid lines) along the x direction ($q_\perp = 0$). The dashed line corresponds to the Feynman relation $\omega = q_x^2/2S(q_x)$. **(b)**: Lowest two excitation bands in the transverse direction ($q_x = 0$). The parameters are the same as in Fig. 5.1.

Sect. 3.1, by adding to the Hamiltonian a perturbation proportional to $e^{i(\boldsymbol{q}\cdot\boldsymbol{r}-\omega t)+\eta t}$ and $\sigma_z e^{i(\boldsymbol{q}\cdot\boldsymbol{r}-\omega t)+\eta t}$ with $\eta \to 0^+$, respectively.

The spectrum of the elementary excitations in the stripe phase is reported in Fig. 5.2 for the same parameters used in Fig. 5.1. We have considered both excitations propagating in the x direction orthogonal to the stripes (labelled with the wave vector q_x) and in the transverse directions parallel to the stripes (identified by the wave vector $q_\perp$). A peculiar feature, distinguishing the stripe phase from the other uniform phases, is the occurrence of two gapless bands. The excitation energies along the x direction vanish at the Brillouin wave vector $q_B = 2k_1$, which is a usual situation in crystals. A similar double gapless band structure has been predicted recently in condensates with soft-core, finite-range interactions [71, 70, 96].

In Fig. 5.3 we compare the sound velocities of the two gapless branches in the longitudinal (c_x) and transverse ($c_\perp$) directions. We find that c_x is always smaller than $c_\perp$,

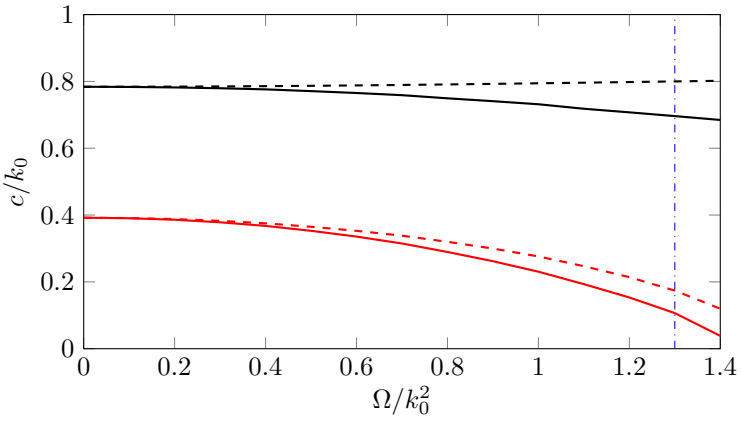

Figure 5.3. Sound velocities in the first (red) and second (black) bands along the x (c_x, solid lines) and transverse ($c_\perp$, dashed lines) directions as a function of Ω. The blue dash-dotted line represents the transition from the stripe phase to the plane-wave phase. The values of the parameters G_1/k_0^2 and G_2/k_0^2 are the same as in Fig. 5.1.

reflecting the inertia of the flow caused by the presence of the stripes. The value of $c_\perp$ in the second band (second sound) is well reproduced by the Bogoliubov expression $\sqrt{2G_1}$ (equal to $0.78\,k_0$ in our case) for the sound velocity. Notice that the sound velocity in the first band (first sound) becomes lower and lower as the Rabi frequency increases, approaching the transition to the plane-wave phase. The Bogoliubov solutions in the stripe phase exist also for values of Ω larger than the critical value $\Omega^{(\mathrm{I}-\mathrm{II})} = 1.3\,k_0^2$, due to the first-order nature of the transition (effect of metastability).

The quantum depletion of the condensate in the stripe phase can be evaluated with a procedure analogous to the one illustrated in Par. 3.1.4 for the uniform phases. We have checked that the increase due to spin-orbit coupling is always small, thereby confirming the validity of the mean-field approach also for the description of the stripe phase.

5.1.2. Static structure factor and static response function

The nature of the excitation bands can be understood by calculating the static structure factors for the density and the spin density operators, which can be written as

$$S(\boldsymbol{q}) = N^{-1} \sum_{\ell} |\langle 0|\hat{\rho}_{\boldsymbol{q}}|\ell\rangle|^2 \tag{5.5}$$

and

$$S_\sigma(\boldsymbol{q}) = N^{-1} \sum_{\ell} |\langle 0|\hat{\sigma}_{z,\boldsymbol{q}}|\ell\rangle|^2 \tag{5.6}$$

respectively. In these equations $\hat{\rho}_{\boldsymbol{q}} = \sum_j \mathrm{e}^{\mathrm{i}\boldsymbol{q}\cdot\boldsymbol{r}_j}$ and $\hat{\sigma}_{z,\boldsymbol{q}} = \sum_j \sigma_{z,j}\mathrm{e}^{\mathrm{i}\boldsymbol{q}\cdot\boldsymbol{r}_j}$ are the $\boldsymbol{q}$-components of the above-mentioned operators, while ℓ is the band index. A possible strategy to calculate these quantities consists in evaluating the dynamic response

functions for the density and the spin-density operators with the procedure we mentioned in the previous paragraph. By considering the imaginary parts of these functions one gets the corresponding dynamic structure factors (see Eq. (1.54)), $S(\boldsymbol{q},\omega) = \sum_\ell |\langle 0|\hat{\rho}_{\boldsymbol{q}}|\ell\rangle|^2 \delta(\omega-\omega_{\ell 0})$ and $S_\sigma(\boldsymbol{q},\omega) = \sum_\ell |\langle 0|\hat{\sigma}_{z,\boldsymbol{q}}|\ell\rangle|^2 \delta(\omega-\omega_{\ell 0})$, where $\omega_{\ell 0}$ is the excitation frequency of the ℓ-th state. Integrating the latter quantities with respect to ω ranging from 0 to $+\infty$ one finally obtains the static structure factors; the contribution of the single ℓ-th mode can be found by restricting the integration over a sufficiently narrow range of frequencies around $\omega_{\ell 0}$.

In Fig. 5.4 we show the static structure factors for wave vectors along the x axis, as well as the contributions to the total sum coming from the two gapless branches ($\ell = 1, 2$). The figure clearly shows that, at small q_x, the lower branch is basically a spin excitation, while the upper branch is a density mode. The density nature of the upper branch, at small q_x, is further confirmed by the comparison with the Feynman relation $\omega = q_x^2/2S(q_x)$ (see Fig. 5.2a). A two-photon Bragg scattering experiment with laser frequencies far from resonance, being sensitive to the density response, will consequently excite only the upper branch at small q_x. We recall that Bragg scattering experiments actually measure the imaginary part of the response function of the system at a certain finite temperature; if this temperature is low enough, the imaginary part of the response function can be identified with the $T = 0$ value of the dynamic structure factor $S(q_x,\omega)$ [38, Chap. 7]. Notice that, differently from $S(q_x)$, the spin structure factor $S_\sigma(q_x)$ does not vanish as $q_x \to 0$, being affected by the higher energy bands as a consequence of the Raman term in Hamiltonian (2.2). As q_x increases, the lower branch actually reveals a hybrid character and, when approaching the Brillouin wave vector $q_B = 2k_1$, it is responsible for the divergent behavior of the density static structure factor (see Fig. 5.4a), which is again a typical feature exhibited by crystals.

It is worth pointing out that the occurrence of two gapless excitations is not by itself a signature of supersolidity and is exhibited also by uniform mixtures of BECs without spin-orbit and Raman couplings [9], as well as by the plane-wave phase of the Rashba Hamiltonian with $SU(2)$ invariant interactions ($G_2 = 0$) [97, 98, 99]. Only the occurrence of a band structure, characterized by the vanishing of the excitation energy and by the divergent behavior of the structure factor at the Brillouin wave vector, can be considered an unambiguous evidence of the density modulations characterizing the stripe phase. The divergent behavior near the Brillouin zone is even more pronounced (see Fig. 5.5) if one investigates the static response function

$$\chi(q_x) = 2N^{-1} \sum_\ell \frac{|\langle 0|\hat{\rho}_{q_x}|\ell\rangle|^2}{\omega_{\ell 0}}\,, \tag{5.7}$$

proportional to the inverse energy-weighted moment of the dynamic structure factor.

The divergent behaviors of $S(q_x)$ and $\chi(q_x)$ can be rigorously proven using the Bogoliubov [100] and the uncertainty principle [77, 78] inequalities applied to systems with spontaneously broken continuous symmetries. These inequalities are based, respectively, on the relations

$$\tilde{m}_{-1}(F)\,\tilde{m}_1(G) \geq |\langle [F,G]\rangle|^2 \tag{5.8}$$

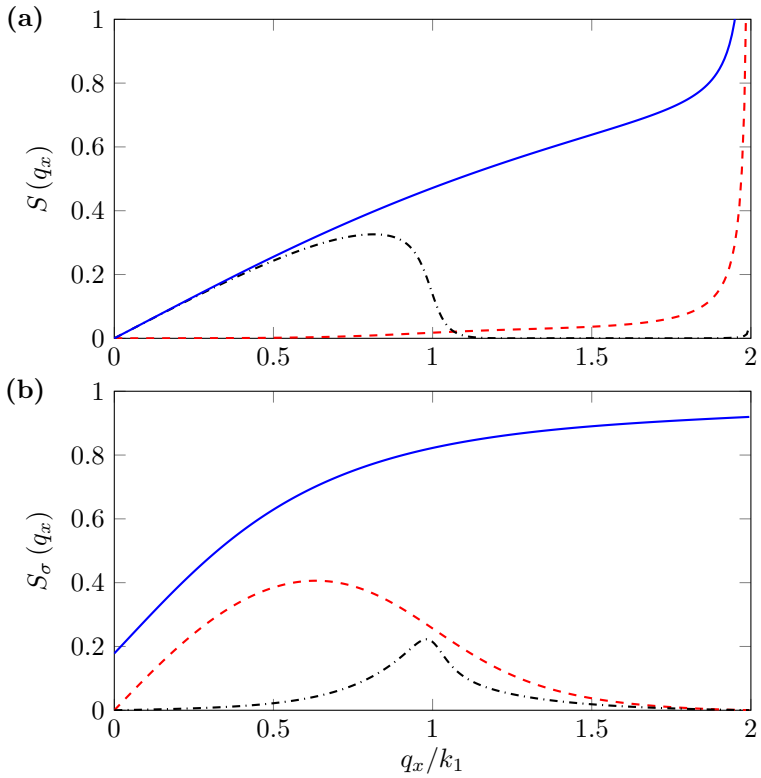

Figure 5.4. Density **(a)** and spin density **(b)** static structure factor as a function of q_x (blue solid line). The contributions of the first (red dashed line) and second (black dash-dotted line) bands are also shown. The parameters are the same as in Fig. 5.1.

and

$$\tilde{m}_0(F)\,\tilde{m}_0(G) \geq |\langle [F,G]\rangle|^2\,, \tag{5.9}$$

where, for a general operator $\mathcal{O}$, the quantities $\tilde{m}_k(\mathcal{O})$ are defined in terms of its k-th moments $m_k(\mathcal{O})$ as

$$\tilde{m}_k(\mathcal{O}) = m_k(\mathcal{O}) + m_k(\mathcal{O}^\dagger) = \sum_\ell \left(|\langle 0|\mathcal{O}|\ell\rangle|^2 + |\langle 0|\mathcal{O}^\dagger|\ell\rangle|^2\right)\omega_{\ell 0}^k\,. \tag{5.10}$$

By making the following choice for the operators entering Eqs. (5.8) and (5.9):

$$F = \hat{\rho}_{q_x} = \sum_j \mathrm{e}^{\mathrm{i}q_x x_j}\,, \quad G = \frac{1}{2}\sum_j \left[p_{x,j}\,\mathrm{e}^{-\mathrm{i}(q_x - q_B)x_j} + \mathrm{H.\,c.}\right]\,, \tag{5.11}$$

with $q_B = 2k_1$ the Brillouin wave vector defined above, one finds that the commutator $\langle [F,G]\rangle = q_x N \langle \mathrm{e}^{\mathrm{i}q_B x}\rangle$, appearing on the right-hand side of the inequalities, coincides with the relevant crystalline order parameter and is proportional to the contrast of the density modulations. The "symmetrized" moments $\tilde{m}_{-1}(F)$ and $\tilde{m}_0(F)$ are instead proportional to the static response $\chi(q_x)$ and to the static structure factor $S(q_x)$, respectively (see

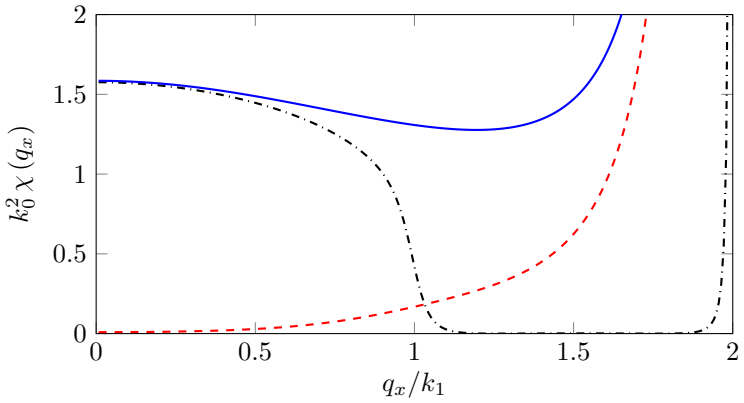

Figure 5.5. Static response as a function of q_x (blue solid line). The contributions of the first (red dashed line) and second (black dash-dotted line) bands are also shown. The parameters are the same as in Fig. 5.1.

Eqs. (1.83) and (1.72)). It is not difficult to show that $\tilde{m}_1(G)$ and $\tilde{m}_0(G)$ are proportional, respectively, to $(q_x - q_B)^2$ and to $|q_x - q_B|$ as $q_x \to q_B$ due to the translational invariance of the Hamiltonian. This causes the divergent behaviors $S(q_x) \propto 1/|q_x - q_B|$ and $\chi(q_x) \propto 1/(q_x - q_B)^2$, with a weight factor proportional to the square of the order parameter. The value of the crystalline order parameter $\langle e^{iq_B x}\rangle$ is larger for larger values of Ω. For this reason it is useful to work with large values of the spin interaction parameter G_2, allowing for large values of the Raman coupling[1]. The experimental achievement of configurations with relatively large G_2 will be the subject of the next section.

5.2. Experimental perspectives for the stripe phase

In the discussion of Par. 2.2.3, where we dealt with the experimental exploration of the phase diagram of spin-orbit-coupled BECs, we mentioned that the relevant range of parameters for the investigation of the stripe phase is already within experimental reach. In particular, in the experiments of [29] and [72], a phase transition has been detected close to the theoretical prediction $\Omega^{(\mathrm{I-II})} = 0.19\,E_r$ (see Eq. (2.26)) for the critical Raman coupling below which the occurrence of the stripe phase is expected. However, there is still no direct experimental evidence of the periodic modulations in the density profile characterizing the stripe phase. The main reason is that, in the conditions of current experiments with spin-orbit-coupled ^{87}Rb BECs [29, 66, 73], the contrast and the wavelength of the fringes are too small to be revealed. Another issue is represented by the fragility of the stripe phase against fluctuations of external magnetic fields, which has already been discussed in Par. 2.2.2.

In Ref. [94] we have proposed a procedure to make the experimental detection of

[1]For ^{87}Rb the value of G_2 is small and the divergency effect in $S(q_x)$ is weak. In this case, the sound velocity of the lowest band is small, and the dispersion practically exhibits a q^2-like behavior at small q.

the fringes a realistic perspective, improving their contrast and their wavelength, and increasing the stability of the stripe phase against magnetic fluctuations.

In order to achieve a larger value of the contrast (2.21), one needs to enlarge the range of values of Ω compatible with the existence of the stripe phase. As can be seen from Eq. (2.26), an efficient way to increase the critical Raman coupling $\Omega^{(\mathrm{I-II})}$ is to reduce the value of the interspecies coupling constant $g_{\uparrow\downarrow}$. A possibility is to look for hyperfine states characterized by a small (or tunable) interspecies scattering length. Here we discuss a different strategy, based on the idea of reducing the effective interspecies coupling by means of suitable trapping conditions. In particular, one can trap the atomic gas in a 2D configuration, with tight confinement of the spin-up and spin-down components around two different positions, displaced by a distance d along the z direction. This configuration can be realized with a spin-dependent trapping potential of the form

$$V_{\mathrm{ext}}(z) = \frac{\omega_z^2}{2}\left(z - \frac{d}{2}\sigma_z\right)^2 , \tag{5.12}$$

produced either through magnetic gradient techniques or via spin-dependent optical potentials. In the absence of Raman coupling one can assume a Gaussian profile $\psi_{\uparrow,\downarrow} \propto (1/\sqrt[4]{\pi a_z^2})\, \mathrm{e}^{-(z\mp d/2)^2/2a_z^2}$ for the z dependence of the spin-up and spin-down wave functions, with $a_z = 1/\sqrt{\omega_z}$ the oscillator length along z. The integration over z of the interaction terms in the energy functional (2.7) gives rise to effective 2D coupling constants $\tilde{g}_{\alpha\beta}$ given by[2]

$$\tilde{g}_{\uparrow\uparrow,\downarrow\downarrow} = \frac{1}{\sqrt{2\pi}a_z} g_{\uparrow\uparrow,\downarrow\downarrow} , \qquad \tilde{g}_{\uparrow\downarrow} = \frac{1}{\sqrt{2\pi}a_z} g_{\uparrow\downarrow} \mathrm{e}^{-d^2/2a_z^2} . \tag{5.13}$$

Equation (5.13) explicitly shows that the effect of the relative displacement of the two densities causes a quenching of the interspecies coupling constant with respect to the intraspecies ones, and hence an enhancement of the ratio

$$\gamma = \frac{\tilde{G}_2}{\tilde{G}_1} = \frac{g_{\uparrow\uparrow} + g_{\downarrow\downarrow} - 2g_{\uparrow\downarrow}\mathrm{e}^{-d^2/2a_z^2}}{g_{\uparrow\uparrow} + g_{\downarrow\downarrow} + 2g_{\uparrow\downarrow}\mathrm{e}^{-d^2/2a_z^2}} . \tag{5.14}$$

In an analogous way one finds that also the effective Raman coupling, to be used in 2D, is lowered with respect to the physical coupling Ω according to the law $\tilde{\Omega} = \mathrm{e}^{-d^2/4a_z^2}\Omega$, reflecting the reduction of the overlap between the two wave functions.

In conclusion, in the presence of a spin-dependent displacement caused by a tight axial trapping potential, the new configuration can be described formulating the Hamiltonian in 2D, with the effective Raman coupling given by $\tilde{\Omega}$, and the interaction term obtained from the last row of the functional (2.7), with the replacement of the 3D densities with their 2D counterparts $\int \mathrm{d}z\, n$ and of the coupling constants with the renormalized values (5.13). The main difference with respect to the original 3D problem is the increase of the ratio (5.14) fixed by the value of d, with the consequent increase of the critical

[2] In the present section we consider realistic spin-asymmetric coupling constants $g_{\uparrow\uparrow} \neq g_{\downarrow\downarrow}$, and we assume that their difference is small enough to be compensated by choosing $\delta = -2G_3$ (see Par. 2.2.2).

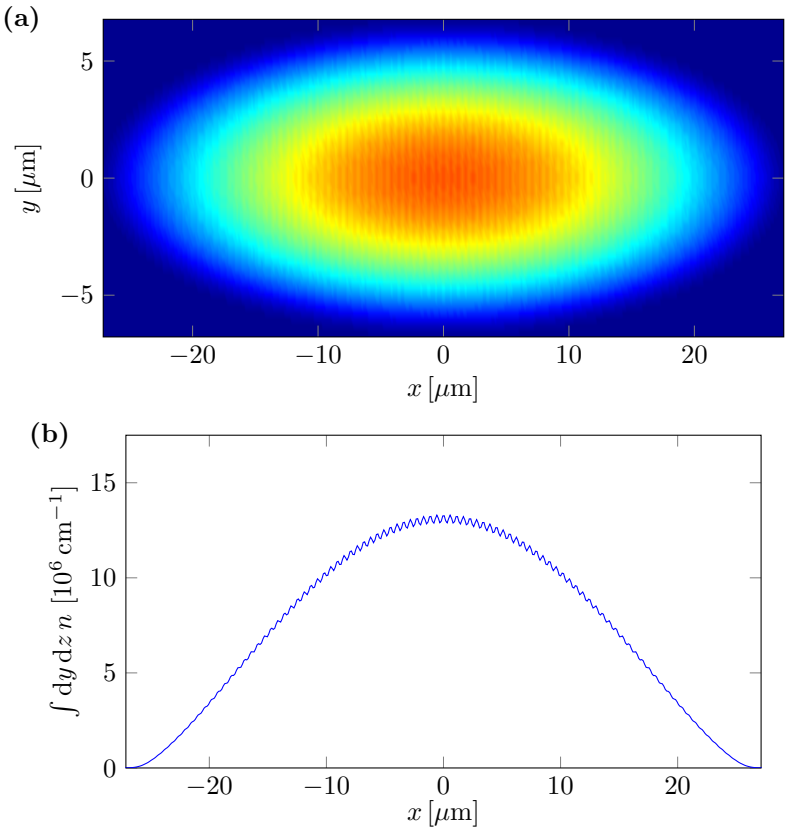

Figure 5.6. Integrated density profiles $\int \mathrm{d}z\, n$ **(a)** and $\int \mathrm{d}y\, \mathrm{d}z\, n$ **(b)** in the stripe phase, evaluated in the conditions described in the text, and without separation of the traps for the two spin components ($d = 0$).

value of the Raman coupling and of the reachable contrast of fringes in the stripe phase. For example, choosing the value $d = a_z$ and the ^{87}Rb hyperfine states mentioned in Par. 2.2.2, one finds the value $\gamma = 0.25$ for the ratio (5.14), to be compared with the value $\gamma = 0.0012$ for the $d = 0$ case. This yields much larger values for the maximum reachable contrast. Another important consequence of the new spin bilayer configuration concerns the value of the critical density $n^{(c)} = 2E_r/[\gamma(\tilde{g}_{\uparrow\uparrow} + \tilde{g}_{\downarrow\downarrow})]$, needed to reach the tricritical point where the striped, the plane-wave, and the single-minimum phases meet. The value of $n^{(c)}$ is actually significantly reduced with respect to the one in the $d = 0$ case, due to the much larger value of γ.

In order to check the validity of the 2D picture described above, and to provide quantitative predictions in real configurations, we have solved numerically the 3D Gross-Pitaevskii equation for a gas of $N = 4 \times 10^4$ ^{87}Rb atoms trapped by a 3D harmonic potential. The parameters $k_0 = 5.54\,\mu\mathrm{m}^{-1}$ and $E_r = 2\pi \times 1.77\,\mathrm{kHz}$ are chosen consistently with Ref. [29]. The results are shown in Figs. 5.6 and 5.7 for the trapping frequencies $(\omega_x, \omega_y, \omega_z) = 2\pi \times (25, 100, 2500)$ Hz. Figure 5.6 corresponds to $d = 0$, while Fig. 5.7 corresponds to $d = a_z = 0.22\,\mu\mathrm{m}$. In both Figs. 5.6 and Fig. 5.7 we have chosen values of the Raman coupling equal to one-half the critical value needed to enter the

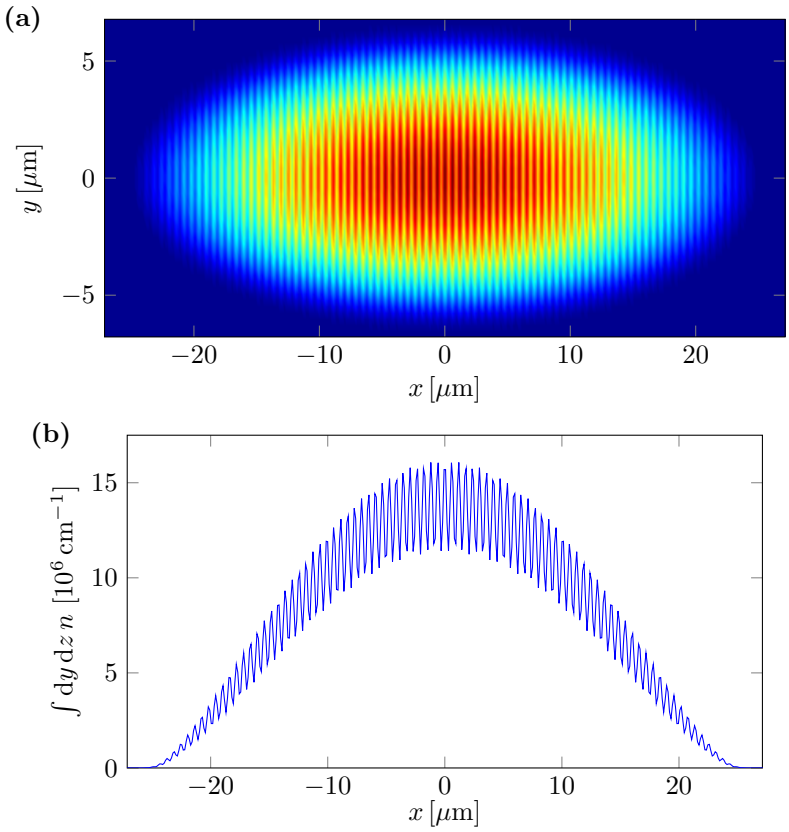

Figure 5.7. Integrated density profiles $\int \mathrm{d}z\, n$ **(a)** and $\int \mathrm{d}y\, \mathrm{d}z\, n$ **(b)** in the stripe phase, evaluated in the conditions described in the text, and with traps separated along z by a distance $d = a_z$, which helps increasing the visibility of the fringes with respect to Fig. 5.6.

plane-wave phase, in order to ensure a larger stability to the stripe phase. In Fig. 5.6 this corresponds to $\Omega = (1/2)\Omega^{(\mathrm{I-II})}(\gamma) = 0.095\, E_r$ ($\gamma = 0.0012$), while in Fig. 5.7 to $\Omega = (1/2)\mathrm{e}^{d^2/4a_z^2}\Omega^{(\mathrm{I-II})}(\gamma) = 1.47\, E_r$ ($\gamma = 0.25$). The density plotted in the top panels corresponds to the 2D density, obtained by integrating the full 3D density along the z direction; in the bottom panels we show the double integrated density $\int \mathrm{d}y\, \mathrm{d}z\, n$ as a function of the most relevant x variable. The figures clearly show that in the conditions of almost equal coupling constants (Fig. 5.6) the density modulations are very small, while their effect is strongly amplified in Fig. 5.7, where the interspecies coupling is reduced with respect to the intraspecies values by the factor ~ 0.61. We have also verified that, with the above choice of the parameters, the solution of the 2D Gross-Pitaevskii equations, with the same radial trapping conditions and the renormalized values $\tilde{g}_{\uparrow\downarrow}$ and $\tilde{\Omega}$, is not only in qualitative, but also quantitative agreement with the results of the full 3D Gross-Pitaevskii calculation reported in Fig. 5.7.

It is also worth noticing that, since the suggested procedure reduces significantly the value of the interspecies coupling constant and at the same time increases the value of the local 3D density, it also has the positive effect of significantly increasing the energy difference between the stripe and the plane-wave phase, thereby making the former much

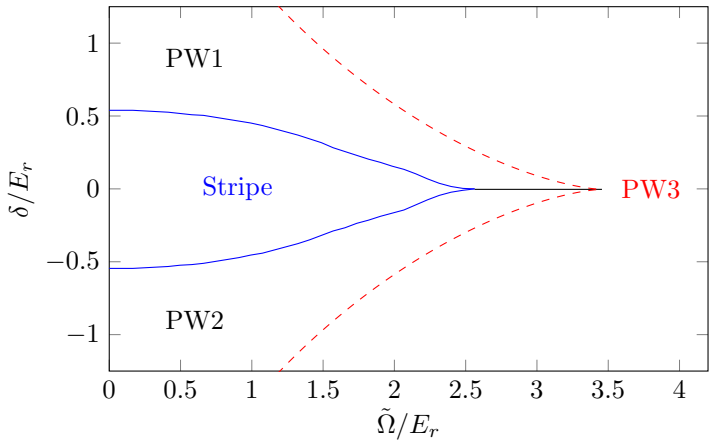

Figure 5.8. Detuning versus effective Rabi coupling phase diagram in the conditions of Fig. 5.7. The definitions of the various phases and of the transition lines is the same as in Fig. 2.4 (notice that here we are expressing the quantities in units of the recoil energy E_r instead of k_0^2).

more robust against magnetic perturbations. For example, in the case considered in the above 3D Gross-Pitaevskii simulation with $d = a_z$ (Fig. 5.7), a magnetic detuning of the order of $0.37\,E_r$ is needed to bring the system into the spin-polarized phase, while in the absence of displacement (Fig. 5.6) the critical value is much smaller ($\sim 0.001\,E_r$). This effect is clearly visible by comparing the detuning versus effective Rabi coupling phase diagram for the $d = a_z$ case, shown Fig. 5.8, with the one of Fig. 2.4 corresponding to the conditions of current experiments.

We have also checked that the quality of stripes is not significantly affected using a relatively softer confinement along z. For example, reducing the frequency by a factor 4, i.e. using $\omega_z = 2\pi \times 625\,\mathrm{Hz}$, while keeping $d = a_z$ and the same value of Ω, we find that the contrast is still significant (0.14 instead of 0.16). The critical magnetic detuning needed to destabilize the stripe phase is reduced because of the smaller value of the local 3D density ($0.23\,E_r$ instead of $0.37\,E_r$).

Let us finally address the problem of the small spatial separation of the fringes, given by π/k_1, which turns out to be of the order of a fraction of a micron in standard conditions. One possibility to increase the wavelength of the stripes is to lower the value of k_0 by using lasers with a smaller relative incident angle. In the following we discuss a more drastic procedure which consists of producing, after the realization of the stripe phase, a $\pi/2$ Bragg pulse with a short time duration (smaller than the time $1/E_r$ fixed by the recoil energy), followed by the sudden release of the trap. This pulse can transfer to the condensate a momentum k_B or $-k_B$ along the x direction, where k_B is chosen equal to $2k_1 - \epsilon$ with ϵ small compared to k_1. The $\pi/2$ pulse has the effect of splitting the condensate into various pieces, with different momenta. The situation is schematically shown in Fig. 5.9 for the spin-down component, where the initial condensate wave function, which in the stripe phase is a linear combination with canonical momenta $\pm k_1$, corresponding to momenta $k_0 - k_1$ and $k_0 + k_1$ in the laboratory frame, after the Bragg pulse will be decomposed into six pieces. Two of them, those

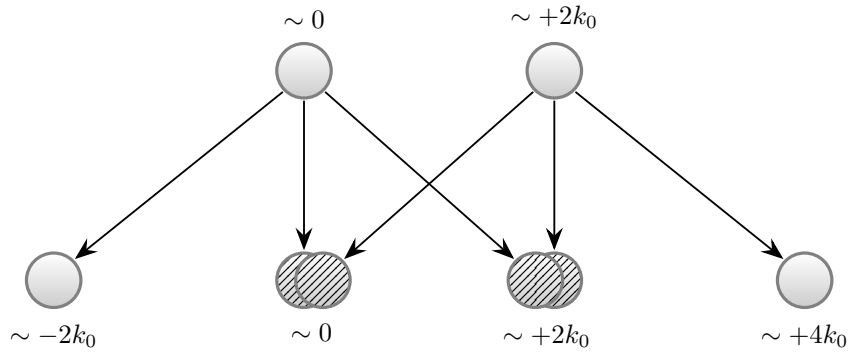

Figure 5.9. Schematical description of the splitting of the spin-down component of the stripe wave function into different momentum component caused by a $\pi/2$ Bragg pulse transferring momentum $2k_1 - \epsilon$.

labeled in the lower part of the figure with momentum ~ 0, will be practically at rest after the pulse and are able to interfere with fringes of wavelength $2\pi/\epsilon$, which can easily become large and visible *in situ*. It is worth noticing that these two latter pieces originate from the two different momentum components of the order parameter (2.9) in the stripe phase and involve 1/3 of the total number of atoms. The corresponding interference effect would be consequently absent in the plane-wave phase, where only one momentum component characterizes the order parameter. The other pieces produced by the Bragg pulse carry much higher momenta and will fly away rapidly after the release of the trap and of the laser fields. In Fig. 5.10 we show a typical behavior of the density profile obtained by modifying the condensate wave function in momentum space according to the prescription discussed above.

The coherent nature characterizing the two momentum components of the order parameter (2.9) could be revealed by the application of a fast $\pi/2$ rf pulse described by the unitary transformation $\hat{U} = \mathrm{e}^{\mathrm{i}\theta_{\mathrm{rf}}\sigma_x/2}$, with $\theta_{\mathrm{rf}} = \pi/2$. The rf pulse mixes the two spin components of the order parameter and gives rise to interference fringes of wavelength $\pi/(k_0 - k_1)$ in the spin density distribution $n_\uparrow - n_\downarrow$, as a consequence of the transformation law $\hat{U}^{-1}\sigma_z\hat{U} = \cos\theta_{\mathrm{rf}}\,\sigma_z - \sin\theta_{\mathrm{rf}}\,\sigma_y$ and of the resulting interference effect associated with the spin average of the transverse operator σ_y in the striped phase. The spin density, after the $\pi/2$ rf pulse, takes the form

$$\frac{n_\uparrow - n_\downarrow}{\bar{n}} = \frac{k_0 + k_1}{2k_0}\sin[2(k_0 - k_1)x] \tag{5.15}$$

apart from an unimportant phase factor, plus additional rapidly oscillating terms associated with higher momentum components. The total density is instead unaffected by the rf pulse. In Fig. 5.11 we show the results of our 3D Gross-Pitaevskii simulation, where n_0 is the 1D total density calculated in the center of the trap in the absence of spin-orbit coupling. In the figure we have included only the long wavelength modulations in the calculation of the spin density $n_\uparrow - n_\downarrow$.

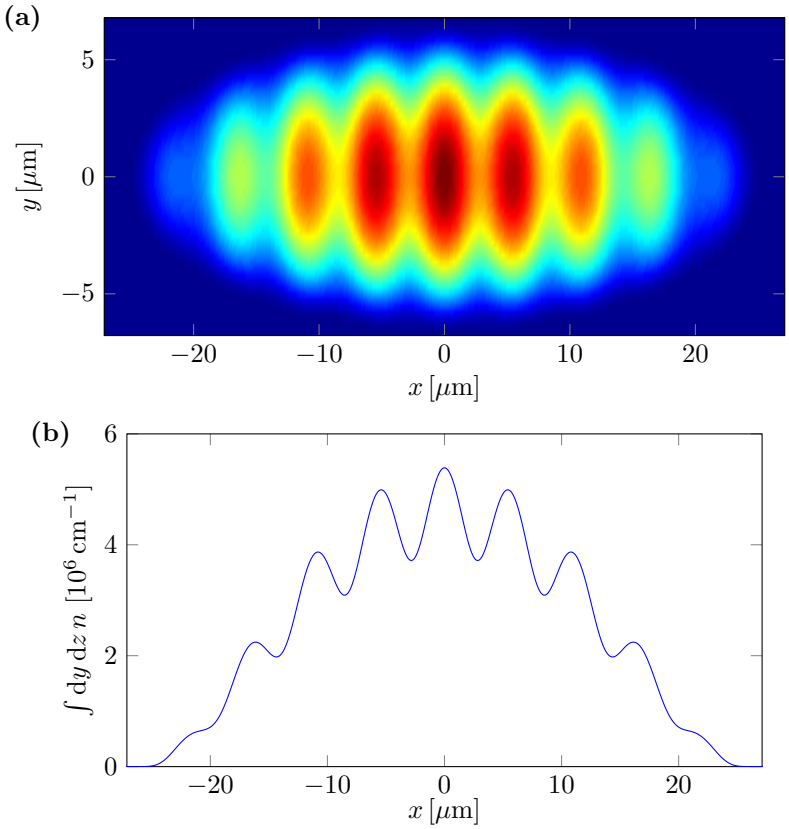

Figure 5.10. Integrated density profiles $\int \mathrm{d}z\, n$ **(a)** and $\int \mathrm{d}y\, \mathrm{d}z\, n$ **(b)** in the stripe phase, in the same conditions as Fig. 5.7, after the application of a $\pi/2$ Bragg pulse with transferred momentum $k_B = 1.8\, k_1$.

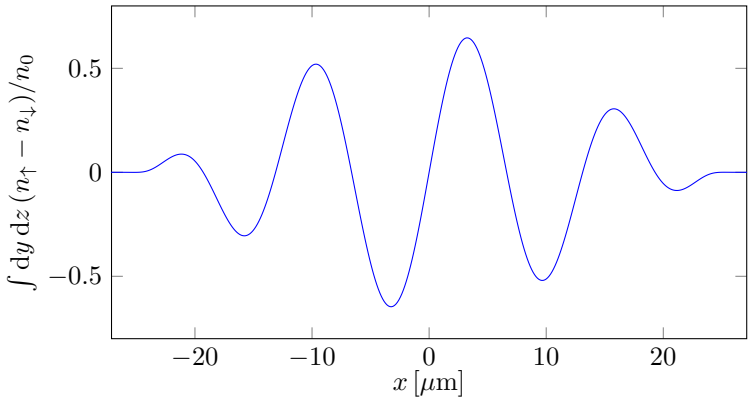

Figure 5.11. Results of 3D Gross-Pitaevskii simulation for the integrated spin-density profile $\int \mathrm{d}y\, \mathrm{d}z\, (n_\uparrow - n_\downarrow)$ in the stripe phase, in the same conditions as Fig. 5.7, after the application of a fast $\pi/2$ rf pulse.

Conclusions and outlook

In this thesis we have studied theoretically some relevant properties of spin-orbit-coupled Bose-Einstein condensates in the simplest realization of a spin-1/2 configuration, characterized by equal Rashba and Dresselhaus coupling strengths. We have pointed out the occurrence of novel features both in the ground state and in the dynamic behavior of these systems, some of which have been confirmed in recent experiments.

The energy spectrum of the single-particle Hamiltonian of a spin-orbit-coupled Bose-Einstein condensate exhibits, for enough low values of the Raman coupling and of the magnetic detuning, a typical double-minimum structure. This structure gives rise to new exotic configurations at the many-body level. The phase diagram of the system is characterized by the existence of three phases: the stripe, the plane-wave and the single-minimum phase. These phases merge in a characteristic tricritical point. The phase transition between the stripe and the plane-wave phase has a first-order nature, while the transition between the plane-wave and the single-minimum phase is of second order and is characterized by a divergent behavior of the magnetic polarizability.

The quantum phases of the system also exhibit interesting dynamical features. The calculation of the excitation spectrum in the two phases with a uniform ground-state density shows, at small momenta, a strong reduction of the sound velocity close to the second-order phase transition, as well as an asymmetry effect in the sound velocity in the plane-wave phase. At finite momenta, the appearance of a roton minimum in the plane-wave phase, whose gap becomes smaller and smaller as one approaches the transition to the stripe phase, reveals the tendency of the system towards crystallization.

Important changes in the dynamical behavior of the system due to spin-orbit coupling can also be observed in harmonically trapped configurations. In particular, the dipole oscillation frequency is strongly suppressed close to the second-order transition between the plane-wave and the single-minimum phase, in analogy with the case of the sound velocity mentioned above. By resorting to the hydrodynamic formalism one can prove that, due to the divergent behavior of the effective mass, a similar effect of strong reduction of the frequency close to the second-order transition takes place for any hydrodynamic mode involving a motion of the gas along the direction of spin-orbit coupling.

Among the three phases exhibited by the ground state of a spin-orbit-coupled Bose gas, the stripe phase deserves a special attention. This phase exhibits typical density modulations, which are the consequence of a mechanism of spontaneous breaking of translational invariance. This is at the origin of a double gapless band structure in its excitation spectrum. Due to the simultaneous presence of both superfluid and crystalline order, the stripe phase shares important analogies with supersolids.

The detection of the density modulations characterizing the stripe phase is difficult because the contrast and the wavelength of the fringes are too small in current experi-

mental conditions. Moreover, fluctuations of external magnetic field can easily drive the system into a different phase. In the final part of this thesis we have discussed a procedure, based on the space separation of the two spin components into a two-dimensional bilayer configuration and on the application of a $\pi/2$ Bragg pulse, which allows to realize striped configurations characterized by high-contrast and long-wavelength fringes. The same procedure also yields an increase of the stability of the stripe phase against magnetic fluctuations. The results of our numerical simulations show that the experimental detection of this intriguing configuration in atomic gases is a realistic perspective.

Outlook. A very relevant prospect related to the present work is represented by the possibility of investigating experimentally the fascinating physics of the stripe phase, which would open new perspectives for the identification of supersolid phenomena in ultracold atomic gases. Apart from the procedure discussed in the last part of the thesis, one can consider other schemes that can be used to reduce the effective interspecies coupling constants and, hence, to increase the contrast of the fringes and their stability. One possibility is represented by the application of a one-dimensional spin-dependent optical lattice along a direction perpendicular to the one where spin-orbit coupling occurs. Another interesting option consists in simulating spin-orbit coupling with a single-component condensate in a double-well potential; for this, one can use laser-assisted tunneling techniques to couple the two lowest-energy states localized around the two minima of the potential. A better theoretical understanding of the above schemes could provide alternative experimentally feasible strategies to realize visible and stable striped configurations.

Another possible theoretical extension of this work concerns the 2D geometry proposed to detect the stripes. This configuration would allow to study how the presence of the stripes affects the physics of the Berezinskii-Kosterlitz-Thouless phase transition in a Bose superfluid.

Finally, considering the case of a gas at finite temperature in the plane-wave phase, it would be interesting to study the effects of the thermal excitations of rotons, which result in a significant peak in the static structure factor when one approaches the transition to the stripe phase.

A. Coefficients in the density response function

The coefficients in the response function (3.9) can be expressed as follows. In phase II:

$$
\begin{aligned}
a = & -\frac{q^4}{4} + \left[\left(k_0^2+3k_1^2\right)\cos^2\alpha - 2\left(k_0^2-G_2\right) + \frac{2G_2k_1^2}{k_0^2}\right] q^2 \\
& + 4\left(k_0^2-2G_2\right)\left[\left(k_0^2-k_1^2\right)\cos^2\alpha - k_0^2 + \frac{2G_2k_1^2}{k_0^2}\right] , \\
b_0 = & \frac{q^8}{16} - \left[\left(k_0^2+k_1^2\right)\cos^2\alpha - k_0^2 - G_1 + G_2\right]\frac{q^6}{2} \\
& + \left\{\left(k_0^2-k_1^2\right)^2\cos^4\alpha - 2\left[k_0^2\left(k_0^2-k_1^2\right) + G_1\left(k_0^2+3k_1^2\right) - G_2\left(k_0^2-5k_1^2\right)\right]\cos^2\alpha \right. \\
& \qquad \left. + k_0^2\left(k_0^2-2G_2\right) + 4G_1\left(k_0^2-G_2\right) + 2\left(k_0^2-2G_1-2G_2\right)\frac{G_2k_1^2}{k_0^2}\right\} q^4 \\
& - 8\left(k_0^2-2G_2\right)\left[\left(k_0^2-k_1^2\right)\left(G_1+\frac{G_2k_1^2}{k_0^2}\right)\cos^2\alpha \right. \\
& \qquad \left. - G_1k_0^2 - \left(k_0^2-2G_1-2G_2\right)\frac{G_2k_1^2}{k_0^2}\right] q^2 , \\
b_1 = & \, q^4 + 4\left[\left(k_0^2-k_1^2\right)\cos^2\alpha + 2\left(G_1+G_2\right)\right] q^2 + 16\left(k_0^2-2G_2\right)\left(k_0^2-k_1^2\right)\frac{G_2}{k_0^2} , \\
b_2 = & -\frac{q^4}{2} - 2\left[\left(k_0^2-3k_1^2\right)\cos^2\alpha + k_0^2 + G_1 - G_2\right] q^2 - 4\left(k_0^2-2G_2\right)\left(k_0^2-\frac{2G_2k_1^2}{k_0^2}\right) ,
\end{aligned}
$$

with k_1 given by (2.23). In phase III:

$$
\begin{aligned}
a = & -\frac{q^4}{4} - \left(\Omega - k_0^2\cos^2\alpha + 2G_2\right) q^2 - \Omega\left[\Omega - 2\left(k_0^2\cos^2\alpha - 2G_2\right)\right] , \\
b_0 = & \frac{q^8}{16} + \left[\Omega - 2\left(k_0^2\cos^2\alpha - G_1 - G_2\right)\right]\frac{q^6}{4} \\
& + \left[\Omega^2 - 4\left(k_0^2\cos^2\alpha - 2G_1 - G_2\right)\Omega + 4\left(k_0^2\cos^2\alpha - 2G_1\right)\left(k_0^2\cos^2\alpha - 2G_2\right)\right]\frac{q^4}{4} \\
& + 2G_1\Omega\left[\Omega - 2\left(k_0^2\cos^2\alpha - 2G_2\right)\right] q^2 , \\
b_1 = & \, 0 , \\
b_2 = & -\frac{q^4}{2} - \left[\Omega + 2\left(k_0^2\cos^2\alpha + G_1 + G_2\right)\right] q^2 - \Omega\left(\Omega + 4G_2\right) .
\end{aligned}
$$

Bibliography

[1] K. von Klitzing, Rev. Mod. Phys. **58**, 519 (1986).

[2] M. Z. Hasan and C. L. Kane, Rev. Mod. Phys. **82**, 3045 (2010).

[3] X.-L. Qi and S.-C. Zhang, Rev. Mod. Phys. **83**, 1057 (2011).

[4] F. Wilczek, Nat. Phys. **5**, 614 (2009).

[5] J. D. Koralek, C. P. Weber, J. Orenstein, B. A. Bernevig, S.-C. Zhang, S. Mack, and D. D. Awschalom, Nature **458**, 610 (2009).

[6] M. H. Anderson, J. R. Ensher, M. R. Matthews, C. E. Wieman, and E. A. Cornell, Science **269**, 198 (1995).

[7] K. Davis, M.-O. Mewes, M. Joffe, M. Andrews, and W. Ketterle, Phys. Rev. Lett. **74**, 5202 (1995).

[8] C. Bradley, C. Sackett, J. Tollett, and R. Hulet, Phys. Rev. Lett. **75**, 1687 (1995).

[9] C. J. Pethick and H. Smith, *Bose-Einstein Condensation in Dilute Gases*, 2 ed. (Cambridge University Press, New York, 2003).

[10] C. Chin, R. Grimm, P. Julienne, and E. Tiesinga, Rev. Mod. Phys. **82**, 1225 (2010).

[11] B. Paredes, A. Widera, V. Murg, O. Mandel, S. Folling, I. Cirac, G. V. Shlyapnikov, T. W. Hansch, and I. Bloch, Nature **429**, 277 (2004).

[12] T. Kinoshita, T. Wenger, and D. S. Weiss, Science **305**, 1125 (2004).

[13] Z. Hadzibabic, P. Kruger, M. Cheneau, B. Battelier, and J. Dalibard, Nature **441**, 1118 (2006).

[14] J. Dalibard, F. Gerbier, G. Juzeliūnas, and P. Öhberg, Rev. Mod. Phys. **83**, 1523 (2011).

[15] M. Matthews, B. Anderson, P. Haljan, D. Hall, C. Wieman, and E. Cornell, Phys. Rev. Lett. **83**, 2498 (1999).

[16] K. Madison, F. Chevy, W. Wohlleben, and J. Dalibard, Phys. Rev. Lett. **84**, 806 (2000).

[17] J. R. Abo-Shaeer, C. Raman, J. M. Vogels, and W. Ketterle, Science **292**, 476 (2001).

[18] M. V. Berry, Proc. R. Soc. A **392**, 45 (1984).

[19] J. Ruseckas, G. Juzeliūnas, P. Öhberg, and M. Fleischhauer, Phys. Rev. Lett. **95**, 010404 (2005).

[20] S.-L. Zhu, H. Fu, C.-J. Wu, S.-C. Zhang, and L.-M. Duan, Phys. Rev. Lett. **97**, 240401 (2006).

[21] K. J. Günter, M. Cheneau, T. Yefsah, S. P. Rath, and J. Dalibard, Phys. Rev. A **79**, 011604 (2009).

[22] N. R. Cooper and Z. Hadzibabic, Phys. Rev. Lett. **104**, 030401 (2010).

[23] P. Hauke, O. Tieleman, A. Celi, C. Ölschläger, J. Simonet, J. Struck, M. Weinberg, P. Windpassinger, K. Sengstock, M. Lewenstein, and A. Eckardt, Phys. Rev. Lett. **109**, 145301 (2012).

[24] I. B. Spielman, Phys. Rev. A **79**, 063613 (2009).

[25] Y.-J. Lin, R. L. Compton, A. R. Perry, W. D. Phillips, J. V. Porto, and I. B. Spielman, Phys. Rev. Lett. **102**, 130401 (2009).

[26] Y.-J. Lin, R. L. Compton, K. Jimenez-Garcia, J. V. Porto, and I. B. Spielman, Nature **462**, 628 (2009).

[27] J. Struck, C. Ölschläger, R. Le Targat, P. Soltan-Panahi, A. Eckardt, M. Lewenstein, P. Windpassinger, and K. Sengstock, Science **333**, 996 (2011).

[28] C. V. Parker, L.-C. Ha, and C. Chin, Nat. Phys. **9**, 769 (2013).

[29] Y.-J. Lin, K. Jimenez-Garcia, and I. B. Spielman, Nature **471**, 83 (2011).

[30] Y. A. Bychkov and E. I. Rashba, J. Phys. C: Solid State Phys. **17**, 6039 (1984).

[31] G. Dresselhaus, Phys. Rev. **100**, 580 (1955).

[32] P. Wang, Z.-Q. Yu, Z. Fu, J. Miao, L. Huang, S. Chai, H. Zhai, and J. Zhang, Phys. Rev. Lett. **109**, 095301 (2012).

[33] L. W. Cheuk, A. T. Sommer, Z. Hadzibabic, T. Yefsah, W. S. Bakr, and M. W. Zwierlein, Phys. Rev. Lett. **109**, 095302 (2012).

[34] V. Galitski and I. B. Spielman, Nature **494**, 49 (2013).

[35] N. Goldman, G. Juzeliūnas, P. Öhberg, and I. B. Spielman, arXiv:1308.6533 (2013).

[36] H. Zhai, arXiv:1403.8021 (2014).

[37] F. Dalfovo, S. Giorgini, L. P. Pitaevskii, and S. Stringari, Rev. Mod. Phys. **71**, 463 (1999).

[38] L. P. Pitaevskii and S. Stringari, *Bose-Einstein Condensation* (Oxford University Press, New York, 2003).

[39] J. T. M. Walraven, Quantum Gases - Collisions and Statistics, Lecture course at master level, University of Vienna, 2013.

[40] E. Gross, Il Nuovo Cimento **20**, 454 (1961).

[41] L. P. Pitaevskii, Sov. Phys. JETP **13**, 451 (1961).

[42] A. Griffin, *Excitations in a Bose-condensed Liquid* (Cambridge University Press, New York, 1993).

[43] A. L. Fetter, Ann. Phys. **70**, 67 (1972).

[44] A. L. Fetter, Phys. Rev. A **53**, 4245 (1996).

[45] N. N. Bogoliubov, J. Phys. (USSR) **11**, 23 (1947).

[46] J. Stenger, S. Inouye, A. P. Chikkatur, D. M. Stamper-Kurn, D. E. Pritchard, and W. Ketterle, Phys. Rev. Lett. **82**, 4569 (1999).

[47] D. M. Stamper-Kurn, A. P. Chikkatur, A. Görlitz, S. Inouye, S. Gupta, D. E. Pritchard, and W. Ketterle, Phys. Rev. Lett. **83**, 2876 (1999).

[48] J. Steinhauer, R. Ozeri, N. Katz, and N. Davidson, Phys. Rev. Lett. **88**, 120407 (2002).

[49] R. Ozeri, N. Katz, J. Steinhauer, and N. Davidson, Rev. Mod. Phys. **77**, 187 (2005).

[50] S. Stringari, Phys. Rev. Lett. **77**, 2360 (1996).

[51] M. Fliesser, A. Csordás, P. Szépfalusy, and R. Graham, Phys. Rev. A **56**, R2533 (1997).

[52] S. Stringari, Phys. Rev. A **58**, 2385 (1998).

[53] R. Kubo, Can. J. Phys. **34**, 1274 (1956).

[54] R. Kubo, J. Phys. Soc. Japan **12**, 570 (1957).

[55] G. Placzek, Phys. Rev. **86**, 377 (1952).

[56] P. Nozières and D. Pines, Phys. Rev. **109**, 741 (1958).

[57] R. P. Feynman, Phys. Rev. **94**, 262 (1954).

[58] Y. Li, L. P. Pitaevskii, and S. Stringari, Phys. Rev. Lett. **108**, 225301 (2012).

[59] Y. Li, G. I. Martone, and S. Stringari, EPL **99**, 56008 (2012).

[60] G. I. Martone, submitted to EPJ Special Topics (2014).

[61] W. Zheng, Z.-Q. Yu, X. Cui, and H. Zhai, J. Phys. B: At. Mol. Opt. Phys. **46**, 134007 (2013).

[62] W. Zheng, B. Liu, J. Miao, C. Chin, and H. Zhai, Phys. Rev. Lett. **113**, 155303 (2014).

[63] M. Boninsegni and N. V. Prokof'ev, Rev. Mod. Phys. **84**, 759 (2012).

[64] T.-L. Ho and S. Zhang, Phys. Rev. Lett. **107**, 150403 (2011).

[65] L. D. Landau and E. M. Lifshitz, *Statistical Physics, Part 1*, 3rd ed. (Oxford, Pergamon, 1980).

[66] J.-Y. Zhang, S.-C. Ji, Z. Chen, L. Zhang, Z.-D. Du, B. Yan, G.-S. Pan, B. Zhao, Y.-J. Deng, H. Zhai, S. Chen, and J.-W. Pan, Phys. Rev. Lett. **109**, 115301 (2012).

[67] G. I. Martone, Y. Li, L. P. Pitaevskii, and S. Stringari, Phys. Rev. A **86**, 063621 (2012).

[68] W. Zheng and Z. Li, Phys. Rev. A **85**, 053607 (2012).

[69] L. Santos, G. V. Shlyapnikov, and M. Lewenstein, Phys. Rev. Lett. **90**, 250403 (2003).

[70] T. Macrì, F. Maucher, F. Cinti, and T. Pohl, Phys. Rev. A **87**, 061602 (2013).

[71] S. Saccani, S. Moroni, and M. Boninsegni, Phys. Rev. Lett. **108**, 175301 (2012).

[72] S.-C. J. Ji, L. Zhang, X.-T. Xu, Z. Wu, Y. Deng, S. Chen, and J.-W. Pan, arXiv:1408.1755 (2014).

[73] M. A. Khamehchi, Y. Zhang, C. Hamner, T. Busch, and P. Engels, arXiv:1409.5387 (2014).

[74] L.-C. Ha, L. W. Clark, C. V. Parker, B. M. Anderson, and C. Chin, arXiv:1407.7157 (2014).

[75] M. Klawunn, A. Recati, L. P. Pitaevskii, and S. Stringari, Phys. Rev. A **84**, 033612 (2011).

[76] S. Hoinka, M. Lingham, M. Delehaye, and C. J. Vale, Phys. Rev. Lett. **109**, 050403 (2012).

[77] L. P. Pitaevskii and S. Stringari, J. Low Temp. Phys. **85**, 377 (1991).

[78] L. P. Pitaevskii and S. Stringari, Phys. Rev. B **47**, 10915 (1993).

[79] D. M. Stamper-Kurn, H.-J. Miesner, S. Inouye, M. R. Andrews, and W. Ketterle, Phys. Rev. Lett. **81**, 500 (1998).

[80] T. Ozawa, L. P. Pitaevskii, and S. Stringari, Phys. Rev. A **87**, 063610 (2013).

[81] C. Wang, C. Gao, C.-M. Jian, and H. Zhai, Phys. Rev. Lett. **105**, 160403 (2010).

[82] C.-J. Wu, I. Mondragon-Shem, and X.-F. Zhou, Chin. Phys. Lett. **28**, 97102 (2011).

[83] S. Sinha, R. Nath, and L. Santos, Phys. Rev. Lett. **107**, 270401 (2011).

[84] T. Ozawa and G. Baym, Phys. Rev. A **85**, 063623 (2012).

[85] Y. Li, G. I. Martone, L. P. Pitaevskii, and S. Stringari, Phys. Rev. Lett. **110**, 235302 (2013).

[86] D. A. Zezyulin, R. Driben, V. V. Konotop, and B. A. Malomed, Phys. Rev. A **88**, 013607 (2013).

[87] Z. Lan and P. Öhberg, Phys. Rev. A **89**, 023630 (2014).

[88] Q. Sun, L. Wen, W.-M. Liu, G. Juzeliūnas, and A.-C. Ji, arXiv:1403.4338 (2014).

[89] W. Han, G. Juzeliūnas, W. Zhang, and W.-M. Liu, arXiv:1407.2972 (2014).

[90] C. Hickey and A. Paramekanti, arXiv:1409.1216 (2014).

[91] A. F. Andreev and I. M. Lifshitz, JETP **29**, 1107 (1969).

[92] A. J. Leggett, Phys. Rev. Lett. **25**, 1543 (1970).

[93] G. V. Chester, Phys. Rev. A **2**, 256 (1970).

[94] G. I. Martone, Y. Li, and S. Stringari, Phys. Rev. A **90**, 041604 (2014).

[95] N. Ashcroft and N. Mermin, *Solid State Physics* (Saunders College, Philadelphia, 1976).

[96] M. Kunimi and Y. Kato, Phys. Rev. B **86**, 060510 (2012).

[97] R. Barnett, S. Powell, T. Graß, M. Lewenstein, and S. Das Sarma, Phys. Rev. A **85**, 023615 (2012).

[98] X.-Q. Xu and J. H. Han, Phys. Rev. Lett. **108**, 185301 (2012).

[99] R. Liao, Z.-G. Huang, X.-M. Lin, and W.-M. Liu, Phys. Rev. A **87**, 043605 (2013).

[100] N. N. Bogoliubov, Phys. Abh. SU **6**, 1 (1962).

List of publications

A large fraction of the material presented in this thesis has been published on scientific journals in the following papers by the author and his collaborators:

1. Y. Li, **G. I. Martone**, and S. Stringari,
   Sum rules, dipole oscillation and spin polarizability of a spin-orbit coupled quantum gas,
   EPL **99**, 56008 (2012);

2. **G. I. Martone**, Y. Li, L. P. Pitaevskii, and S. Stringari,
   Anisotropic dynamics of a spin-orbit-coupled Bose-Einstein condensate,
   Phys. Rev. A **86**, 063621 (2012);

3. Y. Li, **G. I. Martone**, L. P. Pitaevskii, and S. Stringari,
   Superstripes and the Excitation Spectrum of a Spin-Orbit-Coupled Bose-Einstein Condensate,
   Phys. Rev. Lett. **110**, 235302 (2013);

4. **G. I. Martone**, Y. Li, and S. Stringari,
   Approach for making visible and stable stripes in a spin-orbit-coupled Bose-Einstein superfluid,
   Phys. Rev. A **90**, 041604(R) (2014).

A few results have been reported in the following preprint:

5. **G. I. Martone**,
   Optimization of superstripes in a spin-orbit-coupled Bose-Einstein condensate,
   submitted to EPJ Special Topics (2014).

A review paper, covering most of the topics discussed in the thesis, is also available:

6. Y. Li, **G. I. Martone**, and S. Stringari,
   Bose-Einstein condensation with spin-orbit coupling,
   arXiv:1410.5526, book chapter to appear on Volume III of the Annual Review of Cold Atoms and Molecules (World Scientific).